Change detection and deformation analysis using Terrestrial Laser Scanning

Case study of the metro tunnel at Rotterdam central station

B. van Goor

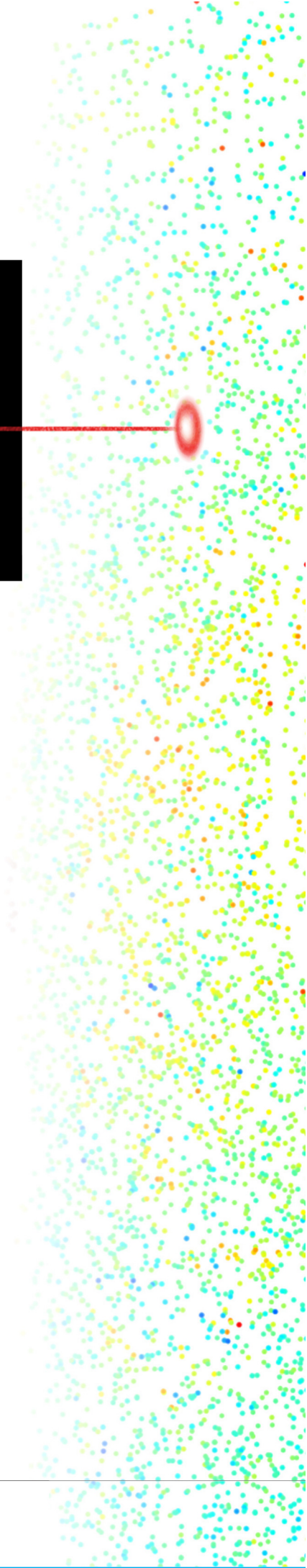

TU Delft
Delft University of Technology

Change detection and deformation analysis using Terrestrial Laser Scanning

Case study of the metro tunnel at Rotterdam central station

Master of Science Thesis

To obtain the degree of Master of Science in Geomatics at Delft University of Technology

Bas van Goor

February, 2011

Graduation Professor:	prof.dr.ir. R.F. Hanssen	(DUT)
Supervisors:	dr. R.C. Lindenbergh	(DUT)
	S.S. Soudarissanane, MSc.	(DUT)
	ir. R van Gosliga	(RPW)
Co-reader:	dr. H. Ledoux	(DUT)

contact email address: b.vangoor@gmail.com

Delft Institute for Earth-Oriented Space research
Faculty of Aerospace Engineering
Mathematical Geodesy and Positioning

Rotterdam Public Works
Buitenruimte
Department Surveying

Abstract

The project *Rotterdam Centraal* concerns the construction of a new metro station next to the existing metro station, located at Rotterdam central station. The area is excavated and new foundations are placed below the existing metro station, which may lead to deformations. Furthermore, many people make use of the station area and the metros are operated according to their normal schedule during the construction works. A robust deformation monitoring program is required, to guarantee a safe environment.

A dense network of measurements is required to detect small deformations at an early stage. The current deformation monitoring consists of total station and joint meter measurements. These instruments measure the deformation at single locations and a dense network of measurement points is difficult to realise. A Terrestrial Laser Scanning (TLS) measures its surrounding with a high point density and high accuracy and is therefore a potentially suited surveying technique to monitor the deformations. However, processing the TLS data is challenging task.

The objective of this graduation project is to develop a method to detect changes and analyse deformations from repeated TLS point clouds. Changes are either new objects a in scene or removed objects, whereas deformations are small variations in the surface of an object. For the latter, stochastic methods are required to investigate the surfaces in detail, while there is no need to use these methods for changed objects. Therefore, a key step in the processing chain is to distinguish surfaces that are changed between two acquisitions from unchanged surfaces.

The presented method consists of five steps. The first step is the registration process, where all acquired point clouds are transformed to one common coordinate system. To analyse deformations over time, this coordinate system must be an absolute system, in this project the Dutch *Rijksdriehoeksstelsel* and NAP (RDNAP) system. The next step is the segmentation of the point clouds, where points are grouped based on a homogeneity property. For this project, the resulting segments are planar, but curved segments can also be considered.

The distinction between changed and unchanged surfaces is based on an identification of corresponding segments. If the location of two segments is similar, and if the segments intersect, the two segments represent the same surface and are used for further inspection during the deformation analysis. If there is no matching segment, the surface is considered to be changed, or it was occluded during the acquisition.

During the deformation analysis, the distance between two point clouds is computed. For every point in a point cloud, the distance to a local surface representation of the local neighbourhood in other point cloud is computed. The resulting distance is a combination of among others the registration error, deformation and measurement errors.

The presented method is applied to three case studies from the metro station and tunnel. In the first case, the method is used to analyse the registration accuracy of a wall, by processing two scans from one epoch. The registration accuracy corresponds well with the reported accuracy by the software Cyclone. A slight rotation was detected. Furthermore, occluded areas are correctly identified.

In a part of the metro tunnel below the *Nationale Nederlanden* building, changes were expected, but no deformations. In the second case study, the presented method detected the changes correctly, although small, curved objects led to false changes. In addition to that, unexpected deformations of the tunnel wall are seen, which are likely caused by the injection of water outside the tunnel.

The third case study concerns a tunnel joint. In this area, deformations were expected, but no significant changes. The deformation analysis shows an uplift of 9 mm on the tunnel side and 18 mm on the station sides of the joint. These results are validated using total station and joint meter measurements. The relative deformation of both parts corresponds well, however the absolute deformation as measured with TLS is smaller than the one measured with total stations. It is likely that this difference is caused by the registration process. Furthermore, small changes are detected in this area, for example new pipes.

With the method presented in this project, it is possible to detect changes and analyse deformations in repeated point clouds of the metro tunnel. It is expected that the methods also works for other (industrial) scenes. Furthermore, the presented method can be used to map occlusions in scans from one epoch and analyse the registration accuracy.

Table of Contents

List of Figures

List of Tables

Glossary

List of Acronyms

ALS	Airborne Laser Scanning
BRDF	Bidirectional Reflectance Distribution Function
DTM	Digital Terrain Model
DUT	Delft University of Technology (Technische Universiteit Delft)
GPS	Global Positioning System
HSL	Hogesnelheidslijn (high speed train)
ICP	Iterative Closest Point
IMU	Integrated Measurement Unit
kNN	k-nearest neighbours
LS3D	Least Squares 3D surface matching
LS	Least Squares
MAD	Median Absolute Deviation
NAP	Normaal Amsterdams Peil (height reference datum in the Netherlands)
NURBS	Non-Uniform B-Spline
PCA	Principle Component Analysis
PDF	Probability Density Function
RDNAP	*Rijksdriehoeksstelsel* and NAP (The Dutch national coordinate system, RD, and and the vertical reference level, NAP)
RPW	Rotterdam Public Works (Gemeentewerken)

SNR Signal-to-Noise Ratio

TLS Terrestrial Laser Scanning

TIN Triangulated Irregular Network

List of Symbols

α	Angle between two (normal) vectors
δ	Shortest distance between a point and a plane
$\delta(S_k^I, S_l^{II})$	Approximated distance between two segments
δ_D	Distance due to deformation
δ_M	Distance due to measurement errors
δ_N	Distance due to unmodelled errors
δ_P	Distance due to the plane fitting error
δ_R	Distance due to the registration error
δ_{th}	Distance threshold, used by the planar segmentation algorithm
δ_T	Total distance between two point clouds
ω	Angular frequency of a harmonic wave
θ	Phase difference of a phase-based laser system
$\mathbf{b}_{tls}$	Baseline from the terrestrial laser scanner measurements
$\mathbf{b}_{ts}$	Baseline from the total station measurements
$\mathbf{n}$	Normal vector
b_{tls}	Length of the baseline from the terrestrial laser scanner measurements
b_{ts}	Length of the baseline from the total station measurements
c	Speed of light
d	Distance from the origin to the plane
R_{phase}	Range of a phase-based laser system
R_{pulse}	Range of a pulse-based laser system
t	Two-way travel time of a signal

Preface

With this graduation thesis, the end of my student days in Delft is a fact. It has been a number of years in which a learned a lot, of course about the field of geodesy and not in the last place about myself. This graduation contributed to it, but many of my side activities in the tempting and bright student life of Delft did as well.

In the first year of the MSc Geomatics I noticed an announcement in which a graduation student was sought. The topic was 'Deformation analysis of the metro tunnel below Rotterdam CS' and it immediately had my attention. During my BSc Geodesy in Delft, my interest towards the application of mathematics in geodetic methods grew and this graduation topic fitted really well. Therefore I was surprised that a few years later, when I had to decide on my graduation project, this project was still unfulfilled. Apparently, no other student dared or wanted to take up this challenge. Now, at the end of the project, I have time to look back and read the initial assignment again. Honestly, I am surprised how close the final result is to the announcement. Two goals were set: detect deformations in the order of magnitude of 1-2 cm and find deformations that are not detected with total station measurements. While during the project the focus shifted from deformation analysis towards structuring the processing of laser scanner data, I ended up reaching the set goals after all.

As a result of the small world that the MSc Geomatics is, I had numerous supervisors, who I want to thank for their help during my graduation project. First of all, Roderik Lindenbergh, the creator of the announcement which got me in to this project in the first place. We had good discussions on small mathematical details and he was always enthusiastic with the smallest results, sometimes to my surprise. Sylvie Soudarissanane helped me out a lot with practical issues in Cyclone and Matlab and always managed to find gaps in my methods. She made me focus on the bigger story when I got lost in small details. I hope she did not have any nightmares because of my occasional Dunglish writing. Peter Teunissen and later on in the project Ramon Hanssen showed sincere interest in my project, although it is not directly in their field of research. At *Gemeentewerken Rotterdam* I was intensively supported as well. Rinske van Gosliga allowed me to work on the project in my own way and somehow arranged it when I needed something. Theo Koster knew a lot about the available laser scanning data and the project area and was a great help during the surveying campaign. Finally, Robert Berkelaar was always willing to answer my questions concerning the construction works and provided me with lots of surveying measurements.

I want to thank my parents for their support and believe in the decisions I have made over the last years. My route towards graduation did not always follow its geodetic line, but luckily for me they also believe in personal development. I had many valuable discussions with friends about my graduation project and they encouraged me to finish it. And finally, Evelinde always listened to many of the problems and ideas patiently and came up with very useful suggestions. Thanks!

Bas van Goor,

Rijswijk, February 2011

Chapter 1

Introduction

1.1 Problem definition

Large infrastructural projects in densely populated urban areas carry a high risk. The chance on an accident is minimal, but if it happens, the damage can be large. An example in the Netherlands is the construction of the *Noord/Zuidlijn*, an underground metro line in Amsterdam. A small leak in a sheet pile wall caused a change in the ground water level, resulting in subsidence of buildings around the construction pit. These type of larger accidents are often preceded by smaller deformations in the construction. Monitoring during the construction works by using accurate measurements and real-time analysis is a useful tool to minimise the risk of accidents.

As part of the project *Rotterdam Centraal*, a new metro station is built in the Rotterdam central station area, while the old metro station is still in use. This requires a solid deformation monitoring. The combination of underground construction works and high buildings near by are a potential risk. It is a challenging task to build a new metro station while 'normal life' at street level should continue as much as possible, and metro trains should run their normal schedule.

An intensive monitoring program was set up, consisting of automatic processing and analysing of measurements. These measurements include the horizontal and vertical displacements measured with a total station or a joint meter, water levels and pressure, strains on the constructions and temperatures. Real-time analysis of the measurements enables a continuous control of the possible deformations. If the maximum accepted values are exceeded, the responsible parties are automatically warned, so precautions can be taken. A disadvantage of these instruments is that measurements are only made at a single location, which requires careful selection of the most important measurement locations. Furthermore, the measurement locations are usually located several meters apart. Dense measurements are required to indicate possibly dangerous deformations in an earlier stage. However, a total station is not a suitable instrument to create a dense network of measurement points, i.e. one point per 10 cm^2.

A Terrestrial Laser Scanning (TLS) acquires a high density point cloud and is therefore a suitable instrument for this task. Further advantages are the high accuracy of the point cloud

and the short time span in which it is acquired. The point clouds consist of tens of millions of points per standpoint. All the points that are visible from the standpoint of the laser scanner are sampled, not just the areas of interest. Two point clouds of the construction, captured at different epochs, can be used for a deformation analysis, by doing a detailed analysis of the two surfaces using stochastic methods. Furthermore, changes can be detected, i.e. detect objects that are placed in or removed from a scene, ranging from new walls or pillars to smaller objects such as litter bins or lamps.

However, TLS data processing is time consuming and requires trained processors. The processing steps towards a change detection and deformation analysis should be automated as much as possible, to minimise the manual work and save time and money.

The starting point of this graduation project was deformation analysis using TLS. All currently available methods use a uniform point quality. This assumption simplifies the deformation analysis, but in reality the point quality differs within a point cloud. The first formulated research question was how to use individual point quality in the deformation analysis and to verify whether the analysis is improved by this approach. However, throughout the project, various problems arose with the processing steps that have to be done before the deformation analysis can be done. Furthermore, handling the large amounts of data during the processing appeared to be a problem on its own. Therefore, the focus of the project shifted towards the processing chain and the handling of the data.

1.2 Research objective and methodology

A metro tunnel consists of various objects that vary in size and complexity. The largest objects are the walls, which are cylindrical for bored tunnels and approximately planar for immersed tunnels. Furthermore, trains tracks, sleepers, ventilation pipes, emergency facilities and smaller objects such as lamps are often present in the scene. During the construction works on the metro station, installations for freezing the ground and the controlling of the ground water level are placed in the tunnel.

All there objects together form a rather complex scene and they should all be sampled during the acquisition of the TLS data. The acquired point clouds require further processing steps to arrive at a change detection or deformation analysis. Part of this processing is for example the registration process, where all point clouds are transformed to the same coordinate system, or the segmentation process, to group points that belong to the same object. As mentioned in Section 1.1, the large amount of data proved to be problematic. All this data should be handled in an efficient way, so all the available information can be used and to limit the time required for the processing.

Between two acquisitions, objects can be placed in or removed from the tunnel. For these objects it is not necessary to use stochastic methods to find deformations, since these objects are only sampled once. Therefore, surfaces that changed should be distinguished from surfaces that are unchanged during the processing.

These conditions lead to the following research objective:

Present a method to detect changes and deformations in repeated TLS point clouds of a complex infrastructural scene.

The presented method should be able to detect changes in the metro tunnel, as well as deformations that occur on the unchanged surfaces. Although the method focusses on the metro tunnel, it should also be applicable in similar scenes, such as industrial sites or outdoor infrastructural constructions.

To fulfil the research objective, a set of key questions is formulated:

1. What is the difference between a change and a deformation?
2. What methods are already available for change detection and deformation analysis and how can they be used in the method proposed in this project?
3. How can changed surfaces be distinguished from unchanged surfaces?
4. What are the limitations of each step of the proposed method?

The first question is answered to have a clear definition of changes and deformations. Outside the field of geomatics, the two terms are often considered to be the same phenomenon. Therefore it is important to define them to avoid confusions. The definitions are based on a literature study.

Currently available methods for change detection and deformation analysis follow from literature study. For promising methods is investigated which parts are useful for this project.

A solution to distinguish between changed and unchanged surfaces is based on the results of the preceding processing steps.

During the processing of the data, various problems are encountered. These problems give insight in the requirements on the input data, as well as the limitations of each processing step.

Finally, the proposed method is tested on TLS data sets of the metro tunnel at Rotterdam central station acquired during four different epochs. The results of the deformation analysis are validated using the available deformation monitoring measurements.

1.3 Structure of the report

Chapter 2 describes the construction works of the project *Rotterdam Centraal*, with focus on the works at the metro station and in the tunnel. An intensive deformation monitoring is set up and the measurements relevant for the metro station are discussed. Expected deformations in the station and tunnel are presented based on these measurements. The chapter concludes with a description of Rotterdam Public Works (RPW), where this research is partly conducted. Their organisation is described, as well as their role in the project. Finally, the use of TLS at RPW is explained, together with a perspective for the near future.

Chapter 3 provides a theoretical overview of the acquisition and processing of TLS data. Basic principles of a laser scanner are presented: range and intensity measurements, error sources and more. Methods for the registration and segmentation process are discussed in more detail. The chapter concludes with possible approaches for the change detection and the deformation analysis.

Chapter 4 presents the proposed processing steps for a change detection and deformation analysis. Each step of the workflow is explained in detail.

Chapter 5 presents the implementation of the proposed workflow. A description of the available TLS data is given. The acquisition and registration of the TLS data acquired during this project is described in detail. For each processing step, practical aspects are discussed, such as the used software, software limitations and selection of the best input parameters.

Chapter 6 introduces three case studies to demonstrate the workflow. The first case study illustrates the use of the presented method to get more insight in the accuracy of the registration process. The second case study demonstrates change detection, but also incorporates interesting results for the deformation analysis. Finally, the third case study illustrates the change detection and deformation analysis on a part of the tunnel where deformations are expected.

Chapter 7 presents the conclusions of the research. The questions posed in Section 1.2 are answered. Finally, recommendations for further research are given.

Chapter 2

Rotterdam Centraal: structural monitoring

In this chapter, background information is given. First, an overview of the project *Rotterdam Centraal* is provided. Next, the construction works for the old and new metro station and tunnel are described. All these works are intensively monitored to prevent deformations. The used measurement techniques are described and the results of the deformation monitoring program are used to quantify what deformations can be expected from the laser scanning data. The chapter finishes with a description of Rotterdam Public Works and the use of Terrestrial Laser Scanning at the surveying section.

2.1 The project Rotterdam Centraal

The municipality of Rotterdam aims at improving the connectivity and the appearance of its city centre. The project named *Rotterdam Centraal* is among the urban development projects that are executed to achieve this goal. The aim of the project is to create an appealing, dynamic and well functioning junction for public transport. Fig. 2.1 gives an impression of the new central station.

At the moment, more than one hundred thousand people a day use Rotterdam central station. With a connection to the new high speed train network, the Hogesnelheidslijn (HSL), and the light rail network RandstadRail, the amount of travellers is expected to triple the coming decades (RotterdamCentraal, 2010). To facilitate all these passengers, a new junction for public transport will be built. The railway and metro station will have a completely new appearance. Different kinds of public transport will arrive and depart from this public transport junction, such as trains, buses, trams and metros.

The surrounding area will also be restructured. The new gateway to the city centre will be formed by the boulevard for pedestrians with subsurface parking facilities for cars and bicycles. Multi-storey buildings will form a business district for new and existing companies.

Figure 2.1: Impression of the new central station.

All the projects have to be executed while trains, trams and buses should run on time and passengers should be able to move around in the area (RotterdamCentraal, 2010).

2.2 Works on the metro station

The metro tunnel in Rotterdam was built in the sixties of the last century. The tunnel is built up from tunnel segments, each with a length of approximately 100 m. These segments were created at two dry docks along the route, that were excavated at street level with the use of sheet pile walls. The docks and the route were filled with water, so the tunnel segments started to float and could be moved through the canals towards their final position in the route. At that point, the tunnel segments were immersed. Along the route, piles were placed to fund the tunnel. At the final stage, the canals were filled with sand (Hannink and Thumann, 2007). Fig. 2.2a shows how the old metro station was built with the segments. The tunnel segments are connected at the extension joints, where some space is preserved for deformations.

The RandstadRail is a new light rail connection between The Hague, Zoetermeer and Rotterdam. During the last years, a 2.5 km bored tunnel was built to connect the Rotterdam metro network to The Hague. Since the summer of 2010 the connection is ready and the light rail RandstadRail metros are able to ride from Rotterdam central station to The Hague. The old metro station needed extensive upgrading, since it had only two tracks and served as an end station with only one travelling direction. The new station is located on the western side of the old station, compare Fig. 2.2b and (c). It has three tracks with two platforms and gives the RandstadRail trains the opportunity to continue their route on the existing network.

Since the construction works are radical and complex, it was decided to make use of a large building pit. The outline of this building pit is at the same time the outline of the new metro station, see Fig. 2.2c and (d). In January 2005 the construction works started.

The building pit was created with diaphragm walls. These walls were constructed by excavating small trenches to a depth of 38 m below Normaal Amsterdams Peil (NAP) (Rijkswaterstaat, 2010), where NAP is approximately at ground level in this area. The trenches are filled with reinforcing bars and concrete. At this depth an impermeable layer of clay and loam is located, called the Kedichem layer, see Fig. 2.3. The construction of the walls to this depth ensures that the surrounding ground water level is not affected by the groundwater extraction from within the building pit and the later excavation of the building pit. Moreover, the building pit remains dry since the ground water cannot leak into the pit.

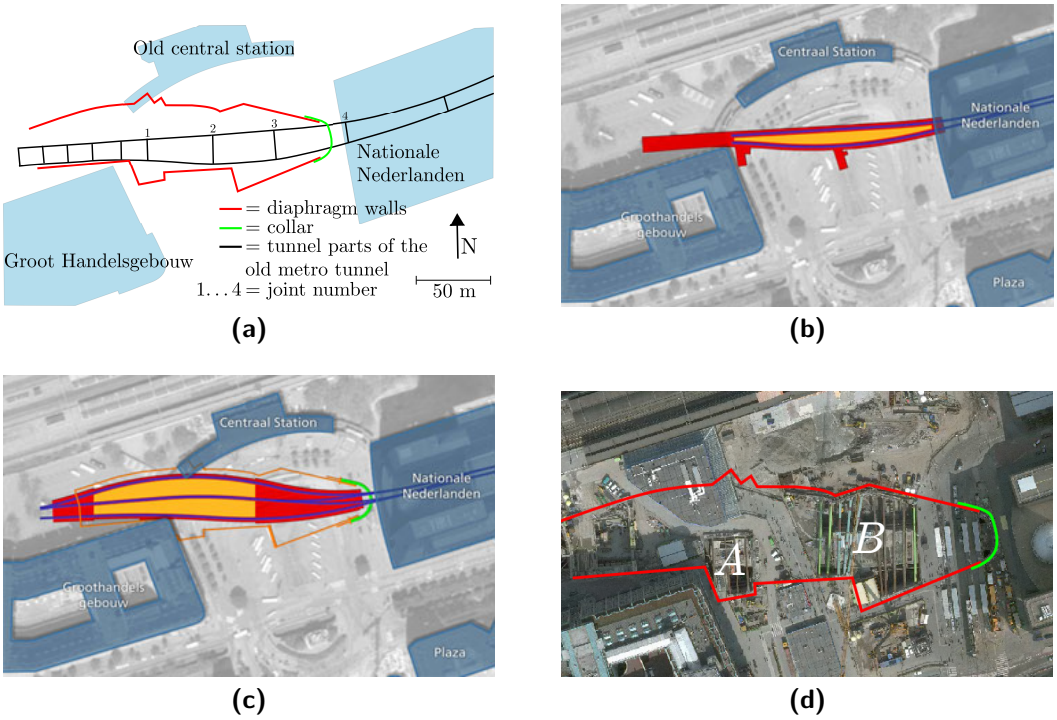

Figure 2.2: Overview of the Rotterdam central station area. (a) The outline of the new metro station and the tunnel segments of the old tunnel. (b) Schematic representation of the old metro station (yellow), the tunnel (red) and the tracks (blue). (Source: www.randstadrail.nl) (c) Schematic representation of the new metro station (yellow), the tunnel (red) and the tracks (blue). (Source: www.randstadrail.nl) (d) Aerial image of the Rotterdam central station area, with the outline of the building pit (red) and the collar (green). This image is acquired in 2009. The regions indicates with A and B are not covered during the excavation of the building pit.

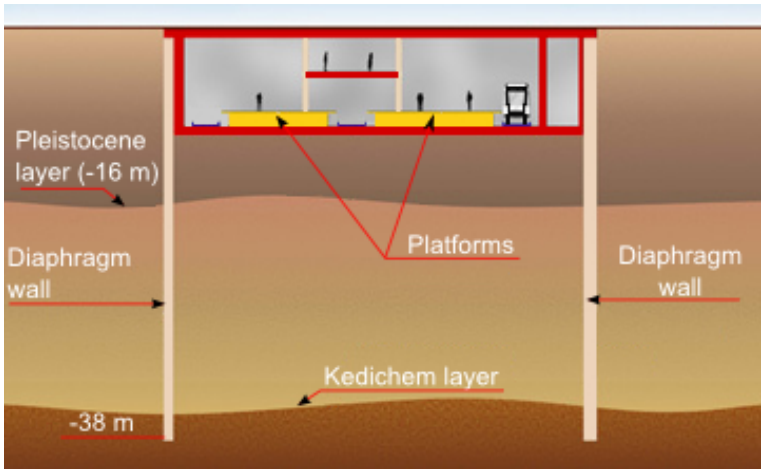

Figure 2.3: Schematic overview of the diaphragm walls and the layers in the subsurface. (Source: www.randstadrail.nl)

At the east side of the building pit, it was not possible to construct a diaphragm wall due to the presence of the metro tunnel and parts of ancient constructions. This problem was solved by freezing the soil to create a collar, using liquid nitrogen and brine freezing technique. This freezing was done between March 2007 and February 2009. The building pit is partly covered with the new roof of the metro station. Normal life at street level can continue as much as possible and the nuisance to the travellers is minimised. An aerial photograph, Fig. 2.2d, shows that only the regions indicated with A or B of the building pit are not covered. With the roof placed on the building pit, the pit is excavated (Hannink and Thumann, 2007). To finalise the building pit, a concrete wall was constructed next to the collar. In March 2009 the freezing of the collar stopped. Almost a year was needed for the ground to completely thaw.

The building pit was excavated to a depth of 14 m below NAP, exposing the old metro tunnel. The pile foundation was expanded. New piles were drilled in the ground to serve as an additional foundation. A new large concrete plate of 2 m thickness was created under the tunnel parts, so that they form one rigid element (Hannink and Thumann, 2007). This plate ends at the collar. The result is that the part of the tunnel between the collar and the joint is hovering.

Since September 2009, the new metro station is in use. The first RandstadRail trains arrived at the new station in August 2010. In 2012 the project Rotterdam Centraal should be completely finished.

2.3 Surveying measurements for deformation monitoring

With the numberous people that make use of the station area every day and the hard condition that the metro line must continue to operate during all the construction works, it is very important to monitor the metro tunnel and the tracks. Deformations can result in dangerous situations for the trains, passengers and surrounding people. The construction of the diaphragm walls which are located close to existing buildings, the driving of the piles for the funding and the excavation of the building pit can lead to deformations of the surroundings. All the risks should be monitored well. Therefore a robust deformation monitoring program is set up.

The deformation monitoring in the project *Rotterdam Centraal* is the responsibility of the building contractor, who subcontracted the engineering company Fugro to take care of the monitoring. Their monitoring program consists of several measurements (Fugro, 2006), including:

- vibration measurements,
- sound measurements,
- ground water level measurements,
- strains on constructions,
- horizontal and vertical deformation measurements,
- temperature measurements.

Most of these measurements are not needed to monitor the deformation of the tunnel, but are useful to monitor the diaphragm walls or the frozen ground. The deformation measurements

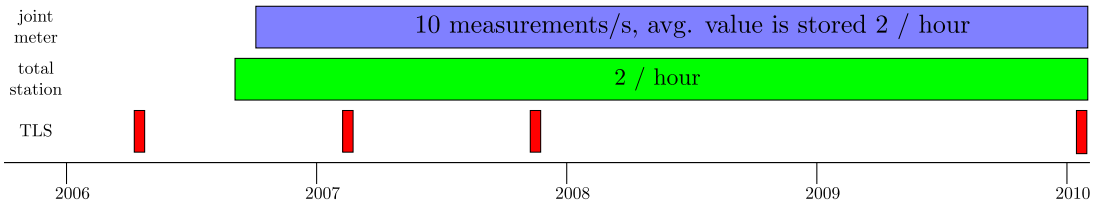

Figure 2.4: Overview of the measurements for the deformation monitoring and the TLS acquisitions, with their time span and the measurement frequency.

of the metro tunnel include the tracks, walls and floor of the tunnel. The measurements are performed using total stations, joint meters and tilt meters.

Fig. 2.4 gives an overview of the measurement frequency and the time span of the total station, joint meter and Terrestrial Laser Scanning (TLS) measurements.

2.3.1 Total station measurements

A traditional geodetic method to measure deformations is by means of a total station. A total station measures the horizontal and vertical angle to a point, together with the distance to that point, which results in the polar coordinates of the measured point. With triangulation these coordinates can be transformed to a local Cartesian coordinate system. When also known points are measured, for example points with coordinates in a known coordinate system, the measured points can be transformed to that known coordinate system.

The distance is based on the travel time of infrared light. Angles are derived from scanning an internal reference drive on which regular interval marks are placed. The accuracy of the distance measurement of a total station is 1 mm + 1 ppm and the accuracy of the angles is 0.15 mgon (Leica, 2004).

For deformation monitoring, artificial points (prisms) are measured at a regular interval. Comparing the coordinates of the points with previous measurements gives information on movements of the points.

In the tunnel, prisms are placed on various objects. There are four categories of deformation measurements:

- points on the train tracks,
- points in the tunnel,
- points on the floor of the metro station close to the collar,
- the horizontal distance between the walls of the tunnel.

Two robotic total stations are placed in the tunnel. Most of the points can be seen from these locations. Most measurements are taken automatically by the robotic total station, with a frequency of twice per hour. Each total station has a data processing unit, that determines the absolute coordinates of the measured points, which are uploaded to a database. Points that are not visible are manually measured, once a month (Fugro, 2006). Fig. 2.5a shows the location of the measurement points and the total stations.

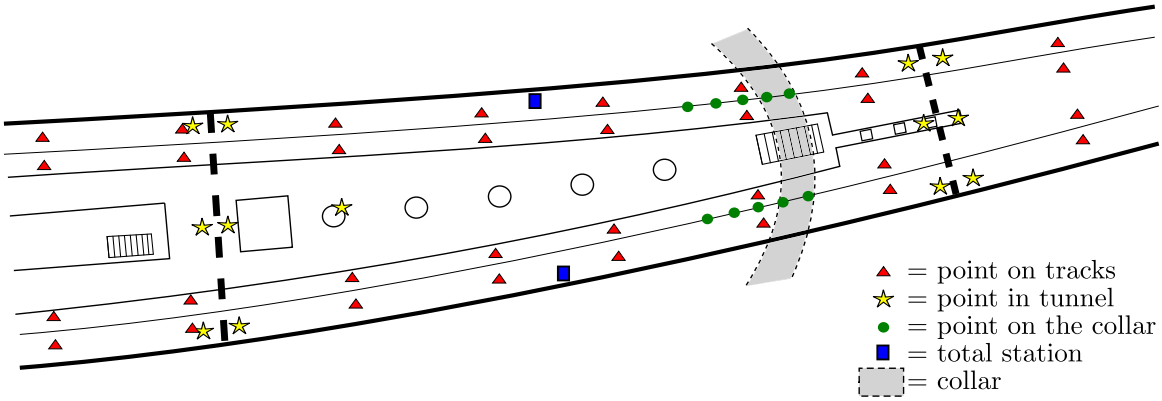

(a)

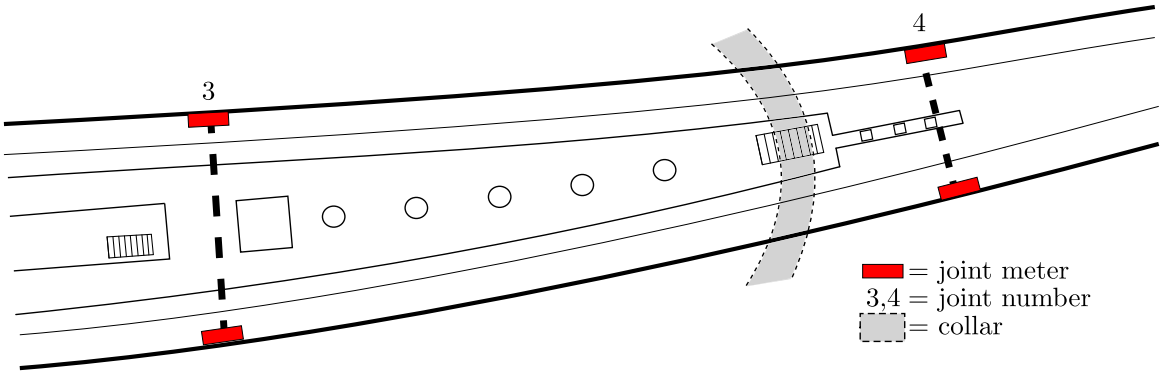

(b)

Figure 2.5: (a) The location of the total stations and the points that are measured for the deformation monitoring. (b) The location of the joint meters with the number of the joint.

With the use of reference points, the measured points can be transformed to a common coordinate system, in this case *Rijksdriehoeksstelsel* and NAP (RDNAP) (Kadaster, 2010). The reference points are located inside and outside of the tunnel, on locations that are assumed to be stable. The reference points are measured every month to verify their stability. Additionally, a local coordinate system is defined, with the x-axis in the direction along the tunnel, positive from west to east. The y-axis is perpendicular to the x-axis, positive from south to north. The z-axis is defined as the vertical axis, orthogonal to the xy-plane, with the positive direction upwards.

All the measurements are stored in a database. The measurements are tested with hazard warning levels, which gives an almost immediate warning to the responsible people when deformations exceed a predefined threshold. Furthermore, the measurements are accessible

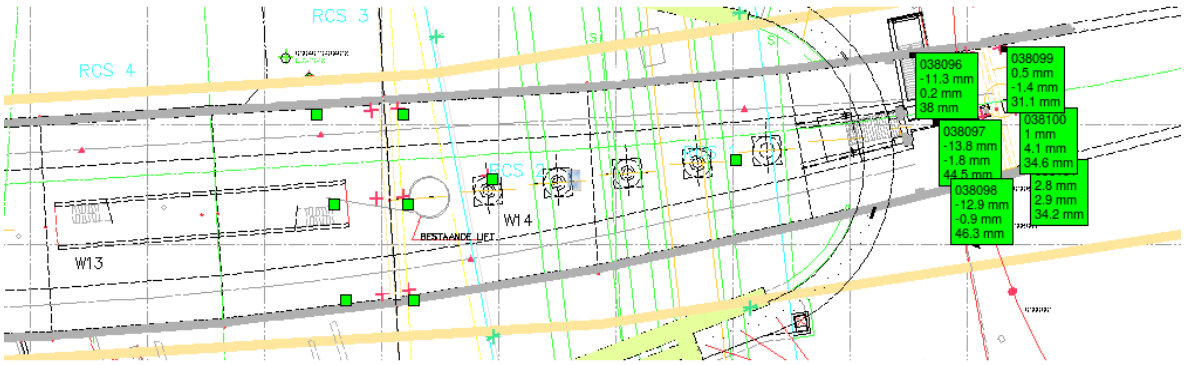

Figure 2.6: Example of the web application where the real time measurements can be visualised. The green boxes indicate the measurement points. The first number in a box is the point number. The other three numbers give the deformation in mm, w.r.t. the reference measurements. The green colour indicates that the measured deformation is below the signalling threshold. (Viewed on May 6$^{\text{th}}$, 2010)

via an Internet application. Graphs and tables show the measurements real time. Fig. 2.6 depicts an example of the web application visualisation. Colours indicate whether a threshold is exceeded. In this application it is also possible to visualise time-series for the measurement points.

The large green boxes show the most recent measurements, in this case of January 22$^{\text{nd}}$, 2010. The first number in a box is the point number. The next three numbers show the deformations in the x, y and z-direction, in mm, w.r.t. the reference measurements. The small green squares show other measurement points. The green colour indicates that the measured deformation is below the signalling threshold.

2.3.2 Joint meter measurements

While the tacheometric measurements result in absolute deformations, the joint meters measure the relative deformations in three dimensions. The joint meters are placed at the northern and southern sides of each joint, at two different heights, see Fig. 2.5b. On one side of the joint, the meter is anchored in the wall, on the other side, the relative movements are measured with linear potentiometers, which relates the mechanical movement of the sensor to a voltage output sent to a data logger.

The measurement accuracy of the joint meter is 0.1 mm. The measurement frequency is very high: 10 measurements per second. The measurements are filtered so that the effects of passing trains are removed. Per 30 minutes, the minimum, maximum and average values are uploaded to the database.

Fig. 2.7a shows a photograph of joint 4, with the joint meter installation, and Fig. 2.7b shows the locations of the joint meters in a cross-section of the tunnel at joint 4.

Examples of data acquired with joint meters are shown in Fig. 2.9.

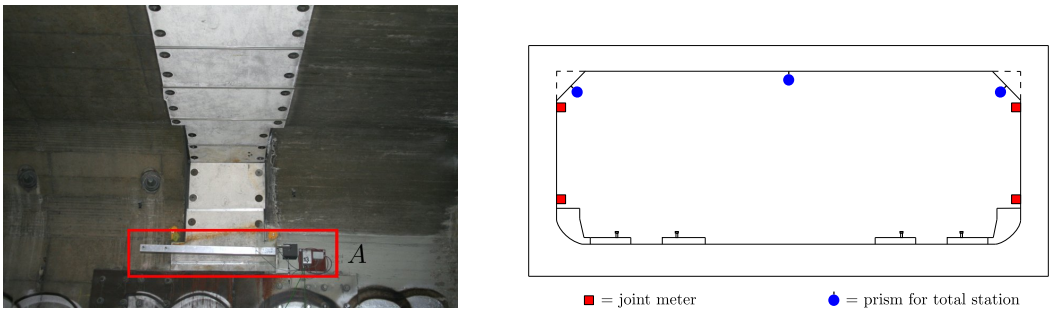

(a) (b)

Figure 2.7: (a) Joint 4, with the joint meter installation, marked by A. (b) The cross-section of the tunnel at joint 4, with the locations of the joint meters and the prisms for the total station measurements.

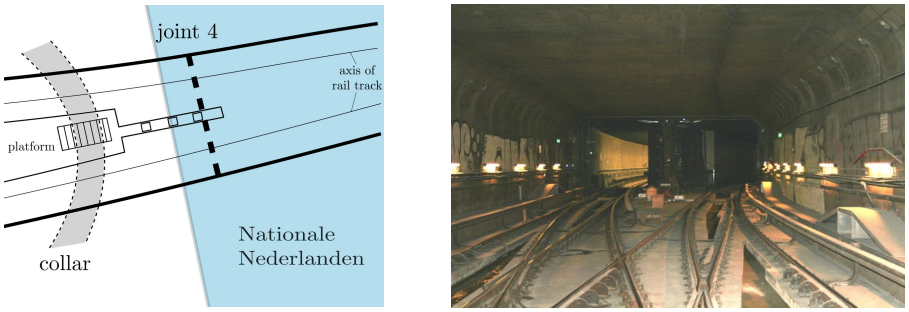

(a) (b)

Figure 2.8: (a) Map of the area of interest. (b) A photograph of the area of interest, as seen from the tunnel towards the metro station.

2.4 Expected deformations

The area of interest is mainly joint 4, below the building of the *Nationale Nederlanden*, which is close to the collar, as shown in Fig. 2.8.

This joint is the only place where the tunnel has space to move after the construction of the concrete plate. The part of the tunnel below the building is fixed to the building and can be regarded as stable. The weakest point is expected to be the joint, where the tunnel can extend or shrink. Furthermore, the end part of the station is hovering, since it is not supported by the new concrete plate and is therefore not as well founded as the other parts of the station.

To estimate the deformation that can be expected in the laser scans, the total station and joint meter data are used.

2.4.1 Relative deformations

A data set is available with joint meter measurements starting from October 10, 2006 until January 22, 2010. The measurements are averaged over one day. Fig. 2.9a and (b) show the measurements of the joint below the *Nationale Nederlanden* building. Only the joint

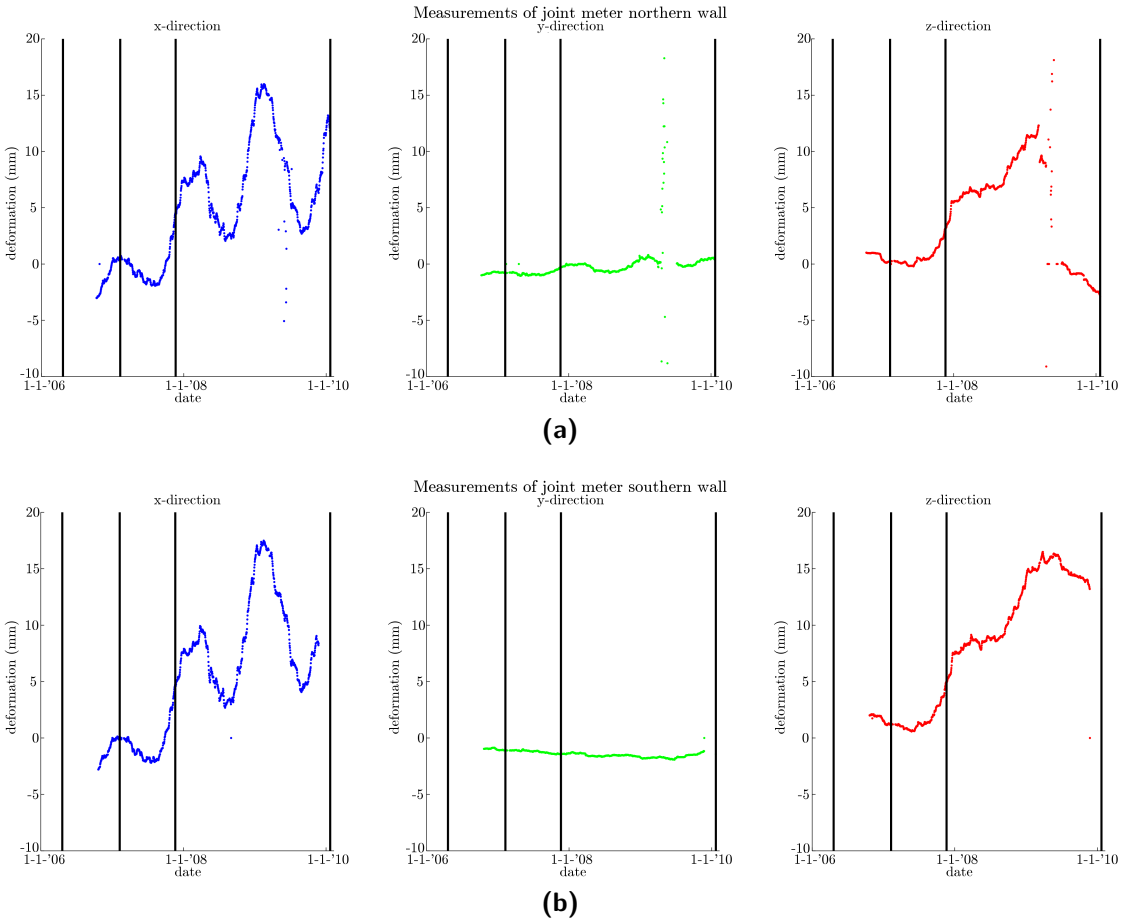

Figure 2.9: Relative deformations of the joint meters at joint 4. The four vertical black lines indicate the moments of TLS data acquisition. (a) The deformations at the northern side. (b) The deformations at the southern side.

meters that are placed high on the wall are used, since the lower ones are more disturbed by the construction works. The four vertical black lines indicate the moments of TLS data acquisition. Joint 4 shows deformations in the x and z-direction of almost 2 cm with respect to the start of the measurements, whereas there is a negligible small movement in the y-direction.

2.4.2 Absolute deformations

To assess the absolute deformation, the measurement points located on both sides of the joint are used. These measurement points are depicted in Fig. 2.5a, and in Fig. 2.7b. The points were measured with a total station between September 15, 2006 and December 2009. The measurement frequency differs in the data set. For the first two weeks, there are tens of observations during one day. For December 2006, there are a lot of observations in one day as well. For some other months, there are no measurements at all, or only once per month. To present the results, the observations are averaged for one day. Nevertheless there is still is large difference in the measurement density over the whole period. Fig. 2.10 shows the absolute deformations in mm, for both sides of the joint. For each side of the joint, three

measurement points are used.

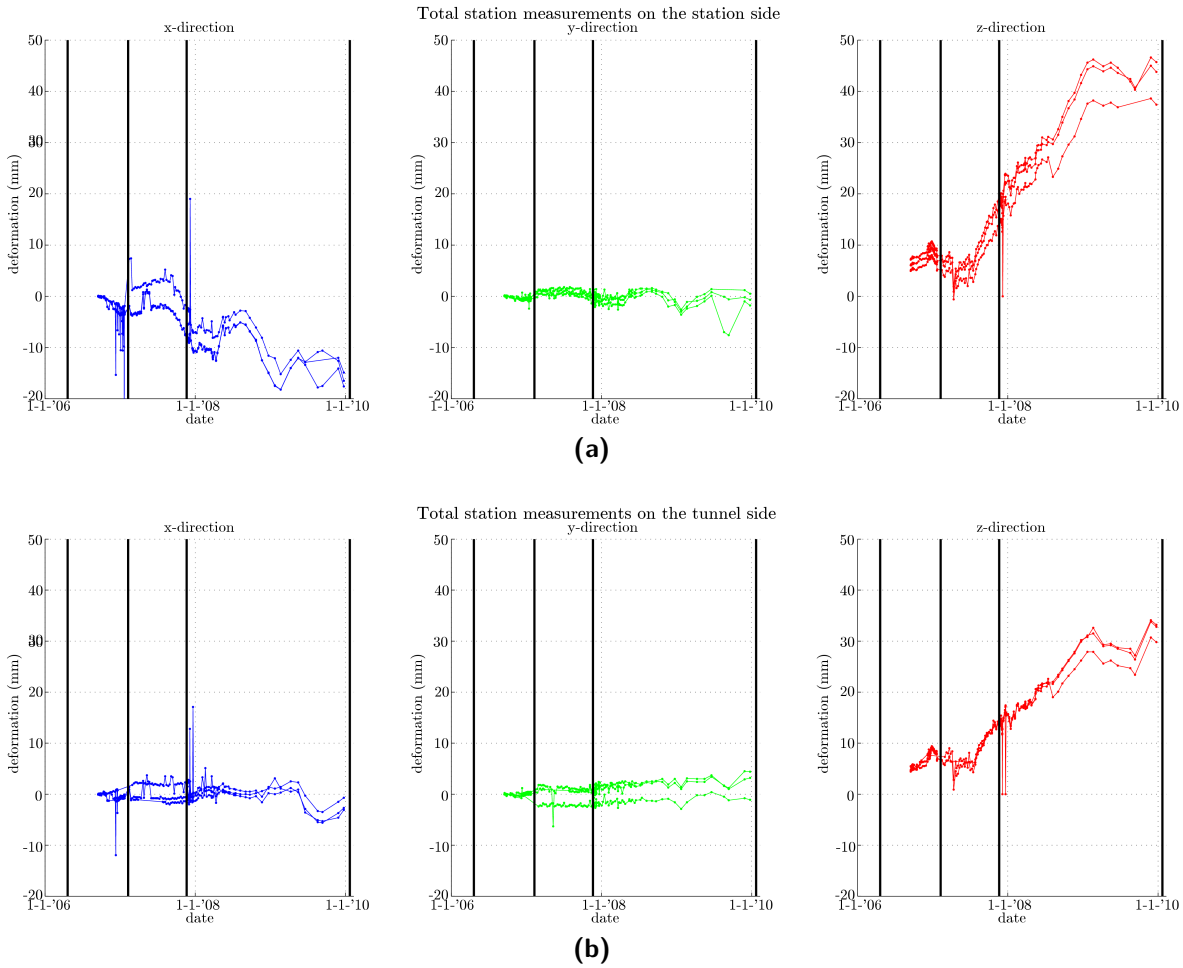

Figure 2.10: Deformations of the measurement points near the joint, measured with a total station. The four vertical black lines indicate the moments of TLS data acquisition. (a) The deformation of the three measurement points on the station side of the tunnel, in x, y and z-direction. (b) The deformation of the three measurement points on the tunnel side of the tunnel, in x, y and z-direction.

The data contains some incidental large values. It is not likely that these deformations occurred, since that would mean that a measurement point deformed back and forth 5 cm or more. More likely, these measurements are errors or outliers. These errors could be caused by distortions of the measurement points, e.g. prisms that are rotated or removed. Another possible reason for the errors is that the position of the total station was not correctly calculated. This could explain why the errors occur for all directions at the same time. Furthermore, it is not likely that all the measurement points are disturbed, as it is the case near the end of the time-series.

Points located on the same side of the joint show a similar trend. Again, there is only slight deformation in the y-direction (across tunnel direction), but in the direction along the tunnel and in the vertical direction more deformation are observed. For the z-direction at the station side of the joint, the absolute deformation goes up to 4 cm.

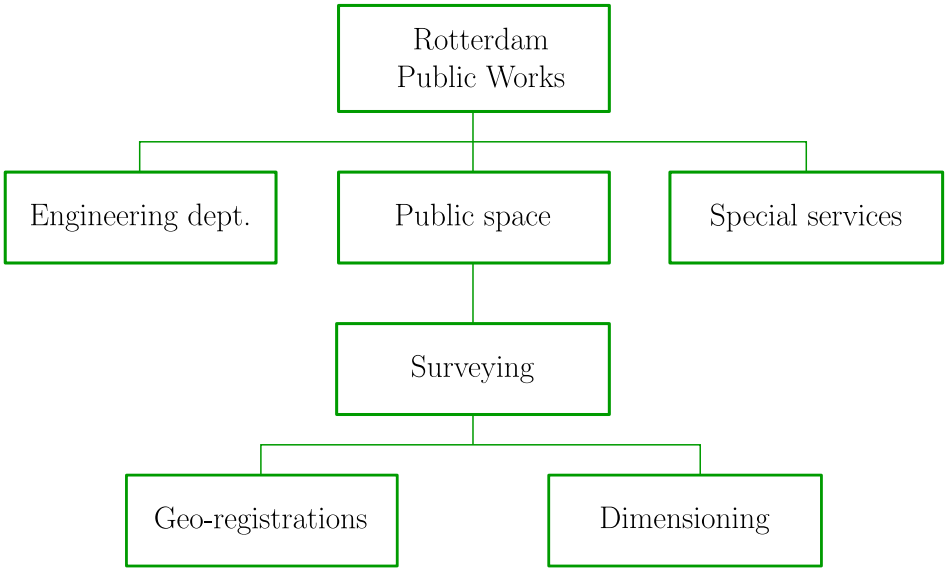

Figure 2.11: Organisation chart of Public Works

2.5 Surveying department of the Rotterdam Public Works

2.5.1 General information

This research is executed partly at the surveying section (*Landmeten*) of the Rotterdam Public Works (RPW) department of the municipality of Rotterdam. RPW is responsible for the management and maintenance of the facilities in the public space, for example infrastructure and green areas. Furthermore, they manage the spatial planning and restructuring of urban areas. Public Works is divided in three departments: the engineering department (*Ingenieursbureau*), for the design and realisation of infrastructure and environment, public space (*Buitenruimte*), for the management and maintenance of the facilities in the public space and special services (*Bijzondere Diensten*). An organogram of the organisation is given in Fig. 2.11.

The surveying section is part of the department public space and is responsible for the basic administration of geo-information in Rotterdam. The section is divided in two subsections: geo-registrations and dimensioning. The first subsection is responsible for the acquisition, processing, maintenance and distribution of geo-information in the municipality of Rotterdam. The second subsection carries out the surveying campaigns, measuring infrastructure, buildings and utilities for the engineering department. Furthermore, deformation measurements are performed. Recurring deformation measurements concern quays and infrastructural works.

The engineering department needs geo-information for the design of infrastructure and the management of projects. The surveying section delivers this information. Height profiles, Digital Terrain Models (DTMs) or 3D models are examples of end-products. The acquisition of the data is done with traditional geodetic techniques like (robotic) total stations, leveling or Global Positioning System (GPS).

2.5.2 The role of Rotterdam Public Works in the project Rotterdam Centraal

RPW is involved in managing the project Rotterdam Centraal and is responsible for the 'city side' (RotterdamCentraal, 2010). The city side involves the design and building of the new train station, the underground parking facilities and the restructuring of the roads in the station area. For the new metro station a management team is put together under the name *Projectbureau RandstadRail*, with specialists from the different departments of RPW. This project not only deals with the new metro station, but also with other parts of the route of the RandstadRail within Rotterdam, such as the new tunnel.

For the deformation monitoring, the surveying department performs a deformation monitoring campaign every month, to control the results of the building contractor. The surveying section also delivers the reference coordinate system, by means of known reference points close to the metro station.

2.5.3 The current and future use of Terrestrial Laser Scanning at the surveying department

Resources for this section are taken from Van Gosliga and Berkelaar (2008) and Van Gosliga (2008).

The surveying section has gained some experience with TLS technology over the last five years. For some of the larger surveying projects, TLS has been used instead of standard total station GPS measurements. Examples of projects where TLS is used are the junction and square in front of the central station, several metro stations and more recent a large conveyor belt at the dry bulk terminal in the harbour of Rotterdam. Since the section does not own a laser scanner, an engineering company is hired to perform the measurements and to deliver the desired end product. For the surveying section the desired end product is often the registered point cloud.

The size of the project is an important factor in the decision to use TLS. For smaller projects, where the desired point density is low or the area of interest is small, TLS is not cost-effective because an engineering company is hired. Standard geodetic techniques are usually faster and cheaper. For larger projects or complex scenes, TLS is very interesting, especially because of the huge amount of data that is captured in a short time, also data that is not directly needed.

The engineering department is the client for many of the projects at the surveying department. Their specifications on the deliverable product play a role in the decision for the acquisition technique. Most of the modelling work is done in 2D design software, like AutoCAD or Microstation. If the desired end-product is a 2D model, TLS is not always a suited technique. If the interest is towards 3D models, TLS is very interesting since detailed models can be created from the data. Some sections of the engineering department work more and more with 3D models. When the required geo-information is delivered in a 3D format, a large amount of time can be saved.

The fact that the TLS also acquires data that is not directly needed is a great advantage. With a traditional measurement technique, a surveyor needs to return to the area and carry out new measurements for an area not already measured. With TLS the information can

already be present in the scans. Within an infrastructural project, the geo-information that is required can concern utilities, objects in the public space, detailed height profiles or a DTM. Each time, a surveying team has to go outside to acquire the necessary data. It is more convenient to have all the data of an area at once, which saves time and money for both the engineering as the surveying department. With the software suit Cyclone from Leica it is possible to create TruView files. These files can be viewed in a web browser with this plug-in installed. In these TruView files anyone can measure distances between points in the acquired point cloud. The web viewer makes it easy for a designer or constructor to extract additional information from the point clouds.

Other than with total station measurements, the location of the laser reflection is not exactly known. For deformation analysis or construction measurements, it is necessary to have a point cloud in one common coordinate system. The registration process brings all the point clouds into one reference coordinate frame. In the past, the engineering companies took care of the processing, but if the surveying section wants to have their own laser scanner, they should also be capable of processing the data themselves. At the moment this knowledge is very limited within the section.

Since laser scanning has proven to be suitable for surveying, it is likely that the surveying section wants to increase the use of this technique in the future. It would be a great help if the engineering department is convinced of all the advantages of laser scanning, e.g. 3D modelling or the data archive. Without the request for TLS data, it is not interesting to use this technique for surveying. Demonstrations of the advantages of TLS can increase the interest of the engineering department towards TLS data. Only with their interest it is efficient to buy a laser scanner and to train employees how to work with the hard- and software. However, with the savings in the coming years, it is not likely that the section will buy a laser scanner within the next years.

Chapter 3

Acquisition and processing of laser scanning data

3.1 Introduction

After the acquisition of the Terrestrial Laser Scanning (TLS) data, several processing steps are required before a change detection or deformation analysis can be done. These processing steps notably consist of registration and segmentation of the data. The registration process has a large influence on the final quality of the point cloud. In this chapter, the theory of the acquisition and the processing is described.

In the first section, the acquisition of TLS data is explained. The second section describes the error sources of the laser scanner. In the remaining of the chapter, the focus is put on the registration and segmentation processes and finally to change detection and deformation analysis.

3.2 Data acquisition using Terrestrial Laser Scanning

The distance measurement capability of laser light has been recognised already a few decades ago when it was implemented in total stations. In the last decade, TLS became more popular and it has proven to be suitable for many applications. The engineering applications of TLS range from cultural heritage documentation to crime scene investigation, but also traditional land surveying tasks such as the construction of as-built models and deformation monitoring can be conducted. (Shan and Toth, 2009).

Laser scanning instruments can be placed on a tripod for static measurements or on a moving platform for dynamic measurements, known as mobile mapping. The advantages of a laser scanning system are the large amounts of points, tens of millions, that can be measured from one standpoint, the high accuracy, systematic measurement errors below 5 mm, and the short acquisition time span, up to 500,000 points per second (Faro, 2009; Leica, 2005). A more

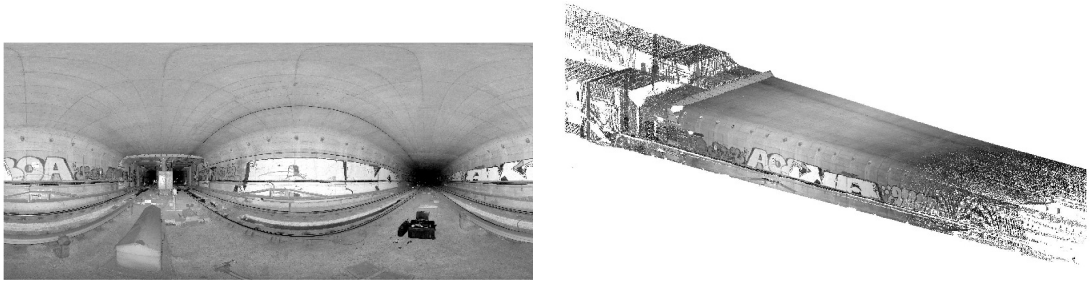

(a) **(b)**

Figure 3.1: Two visualisations of the point cloud of the tunnel. The points are coloured with the reflected intensities in gray-values. (a) The structured 2.5D image. (b) The unstructured 3D point cloud.

practical advantage is that no access to the area of interest is necessary, which is very useful for surveying hazardous locations, such as railroads or busy traffic junctions (Lindenbergh, 2010; Shan and Toth, 2009).

A laser scanner measures the distance to an object that reflects the laser beam, with a field-of-view of 360° in the horizontal and up to 320° in the vertical direction. The scene is sampled with an angular resolution of 0.01-0.02° (Faro, 2009; Leica, 2005). For some systems the horizontal resolution differs from the vertical resolution, e.g. the Faro systems used in this project have a horizontal resolution which is ten times higher than in the vertical direction (Faro, 2009). It should be noted that a high angular resolution does not results in a more accurate point cloud. If the beamwidth is larger than the object that is sensed, its angular position can be biased (Lichti, 2004). A full resolution scan made with the Faro LS880 laser scanner contains 470,000×35,556 points (Faro, 2009). Depending on the purpose of the survey and the required point density, the scanning resolution can be set by the user.

For each point in the point cloud, two angles are recorded together with a range measurement. Additionally, the intensity of the reflection is recorded and for some types of scanners the RGB-value of the reflection is captured. The intensity is not a calibrated value. The original intensity values are rescaled such that the final values resemble a black and white photo of the scanned scene (Soudarissanane et al., 2007).

The 2.5D image is the intuitive representation of the measured points. Each pixel represents a position in a spherical coordinate system. The rows and columns of the image represent the horizontal and vertical lines of the scans. The measured range or the reflected intensity is used as the pixel value. When the measured range is used, the 2.5D image is called the range image. Transformation of the spherical coordinates to Cartesian coordinates results in an unstructured point cloud, with for each point x, y and z-coordinates and an intensity value. If the point cloud is georeferenced, the Cartesian representation enables to directly retrieve the coordinates of the points in an absolute coordinate system. Fig. 3.1a and (b) depict an example of a spherical and a Cartesian representation of a point cloud.

Three techniques are commonly used to measure the distance between the scanner and an object: triangulation-based, pulse-based and phase-based measurements. Most of the used laser scanning systems are pulse-based or phase-based (Wehr, 2008).

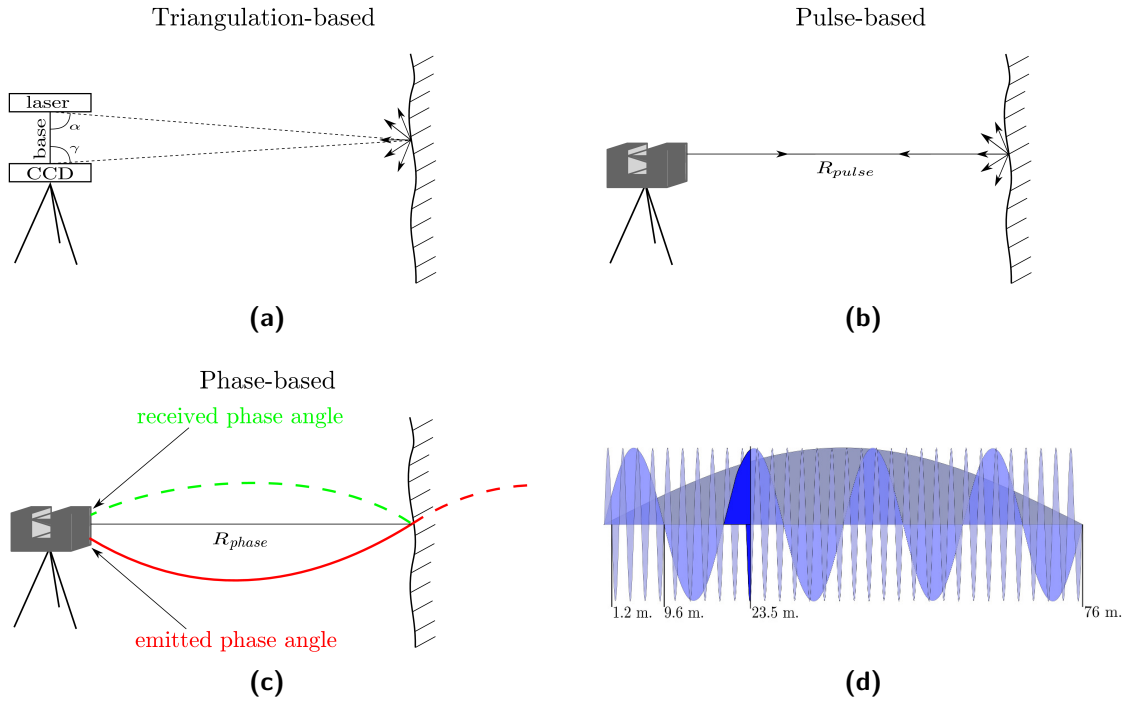

Figure 3.2: The principle of laser range measurement. (a) Triangulation measurements, after Boehler and Marbs (2002). (b) Pulse distance measurements, after Boehler and Marbs (2002). (c) Phase difference distance measurements, after Van Ree (2006). (d) The three signals that are used for the modulation of the phase-based systems (Faro, 2005).

Triangulation-based TLS The distance between the laser and the recording unit, a CCD camera, and two angles α and γ, formed by laser, camera and object, are used to calculate the distance between instrument and object, see Fig. 3.2a. Within this triangle, the base and the angles α and γ are known. The range is computed using this triangle (Boehler and Marbs, 2002).
Triangulation-based systems are suitable for small ranges (below 10 m), since the length of the base is limited. The accuracy achieved with these systems is high, e.g. 0.5 mm at 2 m, but decreases with the square of the range (Boehler and Marbs, 2002).

Pulse-based TLS This distance measurement is based on the two-way travel time t of the signal. With known speed of light c, the distance R_{pulse} is calculated:

$$R_{pulse} = \frac{1}{2}\, c\, t, \tag{3.1}$$

see also Fig. 3.2b. The maximum range of the pulse-based systems is several hundreds of meters and depends on the emitted amount of energy. For the Leica ScanStation C10, the maximum range is 300 m for 90% reflectivity (Leica, 2010b).

Phase-based TLS The instrument measures the phase shift between the emitted and returned signal, see Fig. 3.2c. The emitted laser signal is modulated with two or three

harmonic waves. The measured phase difference θ is proportional to the the travelling time t,

$$t = \frac{\theta}{\omega}, \tag{3.2}$$

with ω the angular frequency of the harmonic wave that is used to modulate the signal (Wehr, 2008).
Combining Eq. (3.1) and Eq. (3.2) leads to the phase-based range R_{phase} (Wehr, 2008):

$$R_{phase} = \frac{c}{2}\,\frac{\theta}{\omega}, \tag{3.3}$$

Using the propagation law of variances (Teunissen, 2000a), the accuracy of the phase-based range measurement is

$$\sigma^2_{R_{phase}} = \left(\frac{c}{2\omega}\right)^2 \sigma^2_\theta. \tag{3.4}$$

From Eq. (3.4), it follows that the variance of the range measurement depends on the variance of the phase difference measurement, provided that c and ω are constant. The smaller the angular frequency ω is, the higher the accuracy. Therefore the signal with the highest frequency determines the accuracy of the range measurement.
For example, the FARO LS880 laser scanner uses three wavelengths for the laser signal modulation: 2.4 m, 19.2 m and 152 m (Faro, 2005). As mentioned, for each wavelength the maximum range that can be measured equals half the wavelength. A phase difference of 90 degrees for the smallest wavelength can occur in any cycle, which is known as ambiguity. When it is known in which cycle this phase difference occurs, the range is measured. To identify the cycle the larger wavelengths are used, as shown in Fig. 3.2d. With the measurement on the 152 m wave, it is first identified in which cycle of the second wave the measurement is. This 19.2 m wave is used to identify the cycle of the 2.4 m wave. The phase difference of the 2.4 m. wave results in the final range measurement of 23.5 m. Using Eq. (3.4), with $\sigma_\theta = 0.5°$, the variance of the range measurement is 1.6 mm.

The accuracy achieved with pulse-based and phase-based systems is similar, but the measurement frequency differs. For pulse-based systems, the next pulse can only be emitted when the previous signal has returned. For phase-based systems, the measurements are taken continuously resulting in a higher measurement frequency, e.g. ten times as high as for pulse-based systems. Depending on the goals of the survey the most suitable scanner can be chosen.

3.3 Error sources of laser scanning points

Measurements are subject to errors. Each measurement has a unique standard deviation, depending on various factors. For a laser scanner, four categories of errors are defined that contribute to the individual point quality (Soudarissanane et al., 2008):

Scanning geometry The range and the incidence angle are determined by the scanning geometry, which results from the standpoint of the laser scanner with respect to the

scene. For pulse and phase-based scanners, the accuracy decreases with increasing range, as the returned signal is weaker and the footprint is larger for larger distances. The incidence angle is the angle between the incoming laser beam and the normal of the surface. If the incidence angle is larger, the footprint of the beam on the object is larger, which makes the precise determination of the phase difference more difficult. For good results, the incidence angle should not exceed 75° (Soudarissanane et al., 2007).

Surface properties The signal interacts with the surface depending on the Bidirectional Reflectance Distribution Function (BRDF). The BRDF of a surface gives the ratio of the incoming to the outgoing radiance for a certain wavelength (Rees, 2001), i.e. it describes the scattering properties of the surface.

Clark and Robson (2004) show that the colour of the surface influences the range measurement. The effect of the surface colour on the signal depends on the wavelength of the laser. The roughness of the surface determines the type of the reflection. Smooth surfaces result in specular reflections, where the signal is reflected away from the laser scanner for larger angle of incidences. Rough surfaces result in diffuse reflections, where the signal is scattered in many directions and only limited amount of the signal returns to the laser scanner.

Instrument calibration and properties Mechanical instrument errors contribute to the errors in the measurements. Small offsets of the mirror centre propagate in the measurements, as well as aberrations in the rotation mechanism, which influences the angular increments and thus the angular measurements (Lichti, 2007). Calibration of the instrument gives insight in these errors. Furthermore, the properties of the instrument are important, for example the wavelength of the laser signal.

Environmental conditions The emitted signal is affected by environmental conditions such as temperature, atmosphere and illumination. The instrument performs best within a certain temperature range. Furthermore, systematic errors can be present in the data due to internal heating of the instrument. The atmospheric conditions, for example humidity or air pressure, influence the propagation speed of light, but this can be neglected for short ranges. Steam and/or dust can cause additional refraction of the signal, which results in erroneous measurements. Illumination is an influencing factor as well if the frequency the light is in the same band as the laser signal's frequency band and if the radiation is strong compared to the laser signal (Boehler and Marbs, 2003).

3.4 Registration of Terrestrial Laser Scanning data

3.4.1 The goal of the registation process

Since the laser scanner only measures the line-of-sight, the back side of an object and occluded objects are not measured. To sample the surface of an object completely and to be able to reconstruct the entire scene, it is needed to acquire scans from different standpoints. All the scans are then transformed to one common coordinate system, which process is called the registration. It is a rigid body transformation, so that the geometry as captured with the laser scanner is not changed. For each point cloud, seven transformation parameters are defined: a 3D translation, a 3D rotation and a scaling factor. The scaling factor is often assumed to be the same for all point clouds.

The reference coordinate system can be set to the system of one of the scans or to a known coordinate system, in this project the *Rijksdriehoeksstelsel* and NAP (RDNAP). In the latter case, the coordinates of some ground truth points have to be known in the RDNAP-system. These points can be acquired using other techniques, for example total stations measurements or Global Positioning System (GPS).

The registration of a set of point clouds is an important processing step before a change detection and the deformation analysis can be achieved. All the scans are combined to one large point cloud and point clouds from different epochs are transformed to the same coordinate system. Errors in the registration process propagate in the final point cloud and influence the ability to detect deformations. A registration with an accuracy in the order of magnitude of a few millimeters is therefore required.

3.4.2 Overview of registration methods

Pfeifer and Böhm (2008) categorise the available approaches for the registration process as follows:

- marker-based registration methods,
- sensor-based registration methods,
- data-driven registration methods.

Marker-based registration methods

A basic method in the geodesy to find the registration parameters is based on markers, also known as control points, and is used for various applications, for example combining surveying networks or georeferencing in photogrammetry. For most applications, artificial control points are placed in the scene. Registration based on control points is discussed in detail in Section 3.4.3.

Sensor-based registration methods

Registration methods can also be based on additional measurements. For Airborne Laser Scanning (ALS) systems and airborne photogrammetry, the position and orientation of the scanner is determined with GPS and an Integrated Measurement Unit (IMU). It enables to determine the trajectory of the scanner and to find its absolute orientation. No gound control points are needed (El-Sheimy, 2008). For mobile mapping systems, sensor-based registration is useful as well. For TLS, sensor-based approaches can be used to directly measure the position and orientation of the laser scanner. Schuhmacher and Böhm (2005) demonstrate the registration of TLS data with GPS measurements. However, they show that marker-based registration is still superior in terms of registration accuracy.

Data-driven registration methods

The data-driven approaches use the geometry and other properties of the point clouds to find the registration parameters. Most of these methods origin from computer vision technology

(Pfeifer and Böhm, 2008). A widely used algorithm is the Iterative Closest Point (ICP) algorithm proposed by Besl and McKay (1992). In short, the aim of the algorithm is to minimise the distance between corresponding points in the point clouds. This algorithm is described in detail in Section 3.4.4. In the years after their publication many improvements of the algorithm were proposed. An extended overview of these algorithms and other data-driven registration methods is given by Salvi et al. (2007).

Gruen and Akca (2005b) use an approach related to ICP. Their Least Squares 3D surface matching (LS3D) algorithm is based on the observations that the point cloud represents a surface. Therefore, the registration process is a surface matching process Non-ridigly deformed data sets should also be matched and it is desired that there is more control of the internal quality of the registration. All these requirements are incorporated in the LS3D algorithm. The aim is to minimise the distance between the two surfaces. A surface can be represented by a point cloud but also by any geometrical model. With the Least Squares (LS) approach, the quality of the estimated registration parameters can easily be checked.

3.4.3 Registration with control points

Often used method to combine two sets of points are marked-based methods, for example in photogrammetry, where ground control points are used to retrieve the orientation of the photographs. Another example is found in the field of surveying, where surveying networks are merged using points measured in multiple networks. The methodology of the registration of two point clouds is similar. The point clouds are registered based on clearly identifiable points that are sampled in both point clouds. One of the point clouds is transformed in such a way that the distance between the tie points is minimised. Traditionally, this error minimalisation is done in a network adjustment, using LS. To solve the seven unknown parameters of the registration, at least three tie points are required. Equivalently to a network adjustment, it is possible to use the stochastic properties of the tie points to find the registration parameters.

The drawback of the TLS system is that it is not exactly known which point on an object causes the reflection. With the diverging laser beam, the area of the footprint increases with the range. At larger distances, it is difficult to exactly identify a point in the point cloud as a tie point. Registration based on clearly identifiable points will introduce an error in the point clouds. A solution is to use artificial objects placed in the scenery for the registration, called targets. The high point density of the TLS acquisition of the targets is used to determine the coordinates of a tie point. A simple, often used method is to use an easy-to-recognise pattern on a paper sheet, such as a checkerboard target as given in Fig. 3.3a. With a pattern recognition algorithm, the centre of this type of target is calculated with high accuracy. Fig. 3.3b shows another type of planar paper sheet target. The centre of the circle can also be calculated from the sampled points. Since the inner circle has a uniform colour, there is less difference in the point quality of the sampled points, as is the case for the checkerboard target.

Other types of planar targets can also be placed in the scene, see for an example Fig. 3.3c. Depending on the mounting system, the target can be rotated or tilted in such a way that the centre of the target remains in the same location but the visibility towards the scanner improves. Another possibility is to use spherical targets, which always have the same incidence angle of the incoming signal. However, the points towards the sides of the sphere have a bad

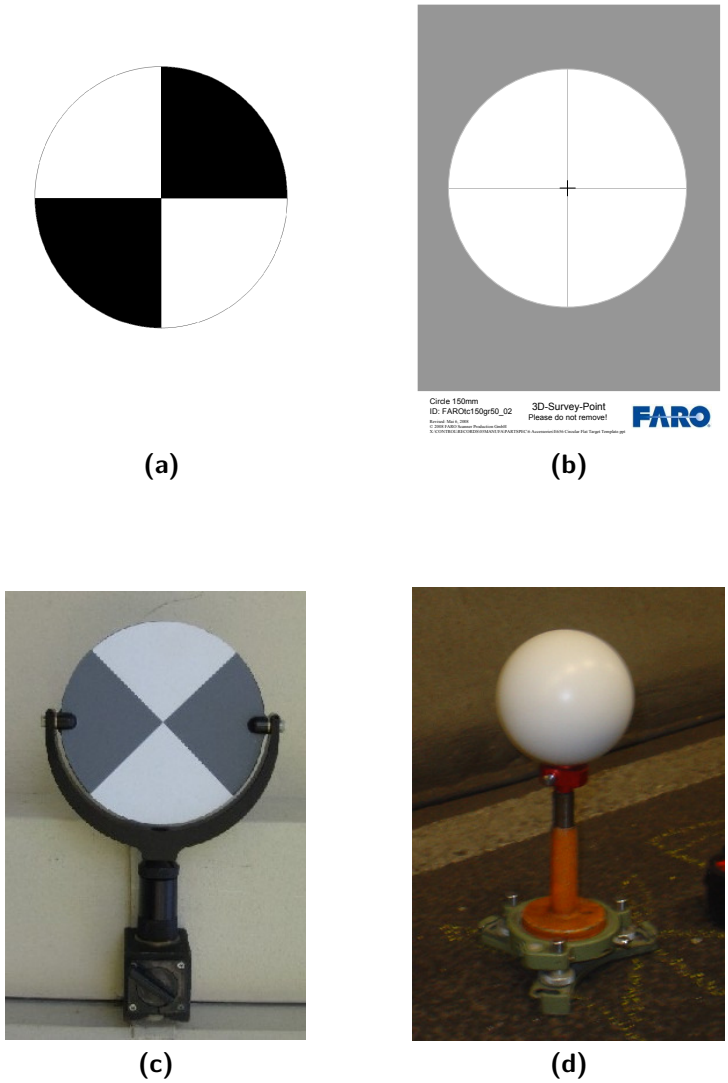

Figure 3.3: Examples of registration targets. (a) A planar paper sheet target. (b) A circular planar target. (c) A more advanced planar target that can rotate. (d) A spherical target.

incidence angle. A spherical target is illustrated in Fig. 3.3d. Using the provided registration software, the centre of the target is calculated. Since many points are measured on the target, the accuracy of the target is high.

3.4.4 Registration with the Iterative Closest Point method

The ICP method by Besl and McKay (1992) was one of the first methods to register two data sets and is still widely used. Originally, the aim of the algorithm is to register a data set of an object with its geometric model, which is useful for industrial applications, for example shape inspection of industrial equipment. For deformation monitoring, this algorithm is appropriate as well, for example when a point cloud of a scene is registered to a 3D model of that scene.

Algorithm 1: The ICP algorithm.

Data: point clouds P^I and P^{II}
Result: transformation parameters to transform P^I to the coordinate system of P^{II}

Initialisation of transformation parameters $\mathbf{R}$ and $\mathbf{t}$ and threshold ϵ
maximum number of iterations j_{max}

while $e_j - e_{j-1} > \epsilon$ or $j < j_{max}$ **do**
  calculate for every point in P^I the distance to the closest point in P^{II}
  calculate $\mathbf{R}$ and $\mathbf{t}$ using Least Squares from the set of correspondences
  apply the rotation and transformation to P^I
  calculate mean square distance error e_j

In that case, there is no need for a global coordinate system.

Let P^I and P^{II} be two scans of the same scene, taken from two different standpoints. The algorithm finds for every point $\mathbf{p}_i^I$ from P^I the closest point in P^{II}, i.e. find the point $\mathbf{p}_i^{II}$ for which the distance between $\mathbf{p}_i^I$ and $\mathbf{p}_i^{II}$ is the minimum distance:

$$d(\mathbf{p}_i^I, P^{II}) = \min_{\mathbf{p}^{II} \in \{P^{II}\}} \|\mathbf{p}^{II} - \mathbf{p}_i^I\|. \tag{3.5}$$

Point $\mathbf{p}_i^I$ and its closest point $\mathbf{p}_i^{II}$ form a correspondence. The goal of the ICP algorithm is to find registration parameters $\mathbf{R}$ and $\mathbf{t}$ for which the sum of the mean square distance errors between the correspondences is minimised.

The transformation is applied to the first point cloud, P^I. With the updated point cloud, the algorithm is run again. This process continues until the difference between the mean square distance error of the current step, e_j, and the previous step, e_{j-1}, is smaller than threshold value ϵ or a predefined number of steps is performed.

An overview of the algorithm is given in Alg. 1. Mathematical details of the ICP algorithm are presented in Appendix A.

This method is straightforward and has the advantage that only initial values of the transformation parameter are needed. It can be used to register the point clouds with the use of all the points, or with the use of only a select group of points, like targets (which is similar to the use of control points). The quality of the registration then depends on the choice of the points (Gruen and Akca, 2005a).

One of the disadvantages of this method is that it cannot deal with non-overlapping areas (Salvi et al., 2007). These non-overlapping areas cause large distances for the corresponding points. Outliers have the same effect on the correspondences. In the algorithm, there is no threshold for a maximum distance (Salvi et al., 2007). Different point densities have a similar influence. For elongated objects like tunnels, where the point density decreases towards the end of the scanned area, this can result in a misalignment.

Furthermore, the processing time is high, since for every point in point cloud P^I the closest point in P^{II} has to be found. The distance between two corresponding points is minimised by minimisation of a distance cost function. The algorithm converges monotonically to a local minimum. To assure that this minimum is also the global minimum, which is required to arrive

at the best solution, good a priori registration parameters are necessary. The convergence might take up to fifty iterations (Besl and McKay, 1992).

The algorithm assumes that all the points in the point cloud have the same quality, which is generally not the case. This assumption may lead to larger registration errors.

In the years after the publication of this algorithm, various improvements have been suggested by various authors. Most of these improvements deal with the processing time, since finding the correspondences takes the majority of the time. Using a different method to find the closest point, for example point-to-tangent distance, nearest neighbourhood searches or using search structures like kd-trees, reduces the computation time (Eggert et al., 1998). By using only a limited amount of points, the time needed to calculate the correspondences is lower. In further iterations more points can be used. The computation time is reduced when the number of iterations is low as well.

Another type of improvement to the algorithm concerns the matching of features present in the data, such as normal vectors, curvature or colours. This information is added to the distance function and is subject to the minimisation (Salvi et al., 2007).

3.5 Segmentation of Terrestrial Laser Scanning data

3.5.1 The principle of the segmentation process

If all objects of interest are sampled, one usually wants to group the points that belong to the same surface. This processing step is called segmentation and can be done before or after the registration process. Subsets of the point cloud are formed by grouping points with similar properties under a given homogeneity criterion.

The segmentation of TLS based on 2.5D images has a similarity with the image segmentation of images used in photogrammetry. Several algorithms origin from traditional photogrammetry, computer vision and signal processing fields (Belton and Lichti, 2006). Most of these algorithms segment the data into smooth surfaces. However, many man-made objects can be modelled with simple geometrical objects like planes, spheres and cylinders. Only few parameters are needed to describe these objects. Direct extraction of the objects from the data is possible using the parameter space, for example with a Hough transform (Vosselman et al., 2004).

3.5.2 Extraction of smooth surfaces

Smooth surfaces are often extracted by grouping nearby points that share a similar property. A smooth surface can be part of an object in the scene or form the complete object. Grouping nearby points is done using region growing. A seed point, which is a point from the data set, is selected and nearby points are added to the segment while the similarity property is not exceeding a threshold and a spatial connection (Vosselman et al., 2004).

According to Rabbani et al. (2006), the available segmentation methods can be divided in three categories:

Edge-based Edge-based segmentation consists of two steps. First, edge detection outlines the borders of the regions and distinguishes points that form the edges of the objects and points that form the surface of an object. Grouping of the points inside the boundaries results in the segments. Examples of surfaces properties used to find the edges are the local surface normal, gradients or principal curvatures. An example of an edge-based segmentation is the algorithm proposed by Belton and Lichti (2006). Their algorithm first classifies the points based on the local variance as a surface point, an edge point or a boundary point. The segmentation is finished with region growing using the points belonging to a surface.

Surface-based Local surfaces properties, for example the normal or the intensity, are used as a measure of similarity. Points that are spatially close and have similar surface properties are merged to one segment. There are two approaches for these algorithms: bottom-up or top-down. The bottom-up approach uses one seed point and adds point while the similarity criterion is still met and the new point is spatially close. The top-down approach starts with one segment for the whole point cloud and fits a surface to these points. As long as the residual is greater than a threshold, the segment is subdivided. Most surface-based segmentation algorithms are bottom-up. A detailed description of such algorithm is given in Sec. 3.5.3.

Scanline-based These algorithms can be used to segment planar or curved features in a range image. Each row in the range image is regarded as a scanline. Every scanline on a 3D plane results in a 3D line. First, each scanline is divided into line or curve segments. The method to create a line segment is similar to the region growing. Points are added to the line as long as the distance from that point to the line does not exceed a threshold value. Next, line segments from adjacent scanlines are investigated. The line segments are merged to planar segments if the properties are similar.

3.5.3 Segmentation using smoothness constraint

The similarity with image segmentation only holds for the 2.5D representation of the point cloud, where the data is stored in a regular grid. This representation cannot be used for the registered point clouds; in general only a full 3D unstructured point cloud representation is suitable. Furthermore many segmentation algorithms only work for planar features. In this section a segmentation method is presented that works with 3D unstructured point clouds and is not limited to planar surfaces.

The segmentation using a smoothness constraint algorithm presented by Rabbani et al. (2006) is a bottom-up surface-based algorithm. It uses the surface normal based on the local neighbourhood as a measure for the similarity, followed by a region growing method. The algorithms performs good for industrial installations, where there are many planar and non-planar objects.

The first step of the algorithm is to calculate surface normals for each point. A plane is fitted through a set of k neighbouring points. As long as enough points are used, the method is not sensitive to outliers. As an alternative to the k-nearest neighbours (kNN) method, a fixed distance neighbourhood can be used. The kNN method is preferred in the case of large differences in point density in a point cloud, since it is guarantees enough points are used to estimate a plane. For tunnels, this is a useful property, since the point density is

Algorithm 2: Algorithm of the segmentation using smoothness constraint.

Data: Point cloud P with xyz points
Input: normals of the points: $\{\mathbf{n}\}$
residuals of the normal calculation: {r}
angular threshold: α_{th}
residual threshold: r_{th}

R_c is the current region
S_c is the list of potential seed points

while $P \neq \emptyset$ **do**
  select point from P with minimum residual: p_{min}
  add p_{min} to R_c and S_c
  remove p_{min} from P
  for $i = 0$ to size S_c **do**
    B_c is the set with the nearest neighbours of $S_c(i)$
    calculate $\mathbf{n_{S_{c(i)}}}$
    for $j = 0$ to size B_c **do**
      current neighbour point is p_j
      if $p_n \in P$ and $\angle(\mathbf{n_{S_{c_i}}}, \mathbf{n_{p_n}}) < \alpha_{th}$ **then**
        add p_n to R_c
        remove p_n from P
        if $r(p_n) < r_{th}$ **then**
          add p_n to S_c

sort R_c according to the size of the region
Result: R_c

influenced by the tunnel geometry. Besides the surface normal for each point, the residual of the plane fitting is stored. The residual is given by the mean distance of all the points to the fitted plane. This residual gives information on edges and high curvatures as well, where the residual is larger. All points are sorted based on their plane fitting residual, which will be used during the region growing step.

The second part of the algorithm deals with the region growing. The smoothness constraint is fulfilled by assuring local connectivity. Therefore, only neighbouring points are used and a maximum deviation in the surface normal is allowed. The point with the minimum plane fitting residual is used as the first seed point. Next step is the selectino of the points in the neighbourhood. Every neighbouring point is tested on the angle between the normal vectors. If this angle is smaller than the maximum angle, α_{th}, the point is added to the current region. Points for which also holds that the residual is smaller than the residual threshold r_{th} are added to the list of current seed points. The next seed point is selected and its neighbouring points are found. This process is repeated for all the points in the list with seeds. When the list with potential seed points is empty, the region is returned as one segment and the process starts again with the next point with the smallest plane fitting residual. An overview of the algorithm is given in Alg. 2.

Under segmentation is occurring when an object is divided in too few segments, e.g. where a non-continuous surface results in one segment. Over segmentation results in too many segments, e.g. where a continuous surface is divided in multiple segments. By adjusting the value of the residual threshold, under or over segmentation, is influenced. The setting of the

residual threshold is thus a trade-off between under and over segmentation.

3.6 Change detection

Change detection is the process of identifying differences in the state of an object or phenomenon by observing it at different times (Singh, 1989). It is widely researched in the remote sensing field. Automatic detection of changes with airborne photogrammetry or ALS is a useful addition for topographic map makers. These changes can be caused by human activities or natural processes.

For ALS data, there are different approaches to detect changes. One method is to subtract two Digital Terrain Models (DTMs). Subtracting is the easiest is if the DTM has a regular grid, but it also works for Triangulated Irregular Networks (TINs) or other surface representations. Another approach is to compare a base map with the acquired ALS data set. With object detection, first a map is created of the area with the buildings, which is compared with the base map in a later stage.

In the optical remote sensing, 2.5D images are acquired. The pixels represent the reflected light, either in a specific part of the visible electro-magnetic spectrum or in RGB-values. Therefore it is very important that two pixels describe the same location on an object. Changes in optical remote sensing data are detected by looking at changes of the pixel values.

For TLS data sets, the approaches for change detection are not so straight forward. The main reason is that TLS data is often represented in 3D, whereas ALS data is regarded 2.5D. Similar to the segmentation process, many of existing change detection methods work on 2.5D data sets. Once the TLS data is registered, the unstructured 3D representation is necessary for the point cloud. Pixel comparison or surface comparison is more complicated. In the remaining of this section, two methods are described to detect changes in TLS point clouds. The first method uses the 2.5D representation, but its main principle will proof useful within this project. The second method is an extension of the first method to 3D point clouds.

3.6.1 Change detection using a range image

Zeibak and Filin (2007) propose a method where range images are used to detect changes between two scans. The two scans are acquired in the same scene, but at a different time and not necessarily from the same standpoint.

The different scanning geometry leads to various problems. First, the point density varies within and between scans. Objects that are further away from the scanner have a lower point density. It results in an object that can be scanned with two different point densities, which affects the size of the change that can be detected. A second problem is occlusions. Since the standpoints of the two scans are not necessarily the same, some areas of the scene are sampled in the first scan but not in the second. The problem of occlusions arises as well in case an object is sampled from two sides. The third problems concerns areas with no reflectance or noise.

The algorithm proposed by Zeibak and Filin obviates these problems. Their formulated question is whether a point that is seen in the reference scan is also sampled in the second scan. There are three possible answers to this question:

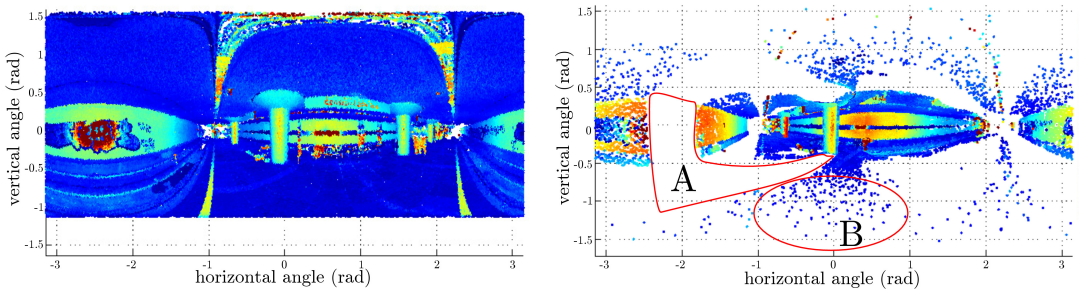

(a) (b)

Figure 3.4: Two 2.5D images, coloured with intensity, with (a) the reference scan and (b) the second scan in the coordinate system of the reference scan. In the second scan, the regions with no data are clearly visible. Region A was occluded and in region B the point density is lower.

- Yes, but there is no object in the reference scan. This yields a change.
- Yes, and it is located on the same object. There is no change.
- No, the object is hidden. The point is marked as changed, but it can also be caused by occlusion of the point.

The algorithm aims at finding the right answer to the question.

To investigate if a point is sampled in the second scan, the range images are used. The second scan is transformed to the position of the reference standpoint during a registration process, see also Section 3.4. It is not necessary to georeference the scans. After the transformation, it can be seen which points from the second scan are visible from the reference standpoint and the change detection is more or less reduced to an image subtraction, see Fig. 3.4.

After the registration, occluded areas in the second scan are clearly visible as regions with no data. Therefore, the occluded points are not marked as a change. Another possibility is that points are occluded in the reference scan but are sampled in the second scan. The range measurement for these points will be larger in the second scan and their is change or occlusion. For points that are sampled in both scans, a distance threshold ϵ is applied to detect the changes in the range R. The threshold is chosen in such a way that measurement and registration errors are taken into account, e.g. 5 cm. To summarise, the options are:

$$\begin{aligned} \text{change} \quad & R_{ref} - R_{new} \quad > \epsilon \\ \text{no change} \quad & |R_{ref} - R_{new}| \quad \leq \epsilon \\ \text{occlusion} \quad & R_{ref} - R_{new} \quad < -\epsilon \end{aligned}$$

The required processing is limited. The small regions in the second scan without data are filled, for example with the value of neighbouring points. Some image processing is used to reduce the presence of noise and edge effects. Edge effects occur when the laser is partly reflected by the edge of an object and partly by some other object.

One of the advantages of the algorithm is its computation speed, since only two images are to be subtracted. With this method, Zeibak and Filin show that major as well as minor changes

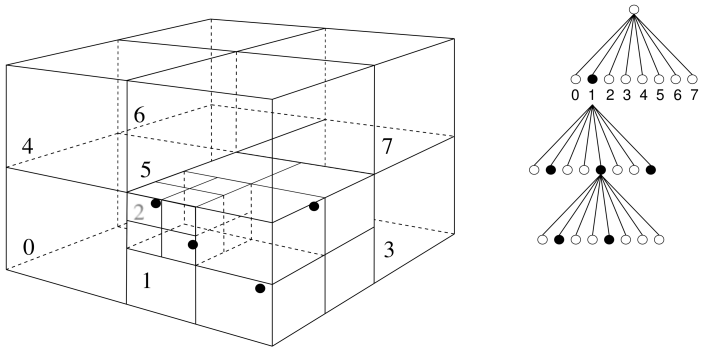

Figure 3.5: The division of a 3D space with an octree. On the right the decision tree to locate the points (after Girardeau-Montaut et al. (2005)).

are detected in a scene. One of the drawbacks is that only two scans can be compared at a time. More complex scenes need multiple scans to be completely sampled, which requires registration. Transforming a complex 3D scene to a 2.5D range image will result in multiple range measurements per pixel. To arrive at one range measurement per pixel, the second scan can be interpolated to a regular grid, which is the same grid as for the reference scan. Without these additional steps, the image subtraction of registered point clouds is not possible.

3.6.2 Change detection using an octree subdivision

The change detection method proposed by Girardeau-Montaut et al. (2005) also acknowledges the 3D nature of the TLS data. The goal of their algorithm is to compare two point clouds directly, which means that the point clouds are not modelled in advance.

The algorithm proposed uses an octree subdivision of the 3D space. The registered point clouds are enclosed in a cubical bounding box. The bounding box is divided into 8 equivalent cubes. Each cube is then divided in 8 more cubes. This process continues until there is only one point in a cube or when the size of the new cubes are below a preset value. The location of a point in the octree is represented by a number or by a subdivision tree. An illustration of an octree is given in Fig. 3.5.

An important aspect for the comparison of two point clouds with octrees is that the octrees are identical. This is achieved by using the same bounding cube for all point clouds. Points that lie in corresponding octree cells are assumed to be sampled on the same object.

With this principle, various cell comparison strategies are defined by Girardeau-Montaut et al.. One possibility is to calculate the average distance between the points in the reference cell to their closest neighbour in the corresponding cell. A second option is to calculate the best fitting plane using all the points in one cell. If the orientation of the normal vectors in the corresponding cells differ, it can indicate a change for that cell. For both methods there is a problem when one of the cells is empty. As an alternative, Girardeau-Montaut et al.

(2005) suggest to use the Hausdorff distance. For all the points in one cell, the distance to their nearest neighbour is calculated. The Hausdorff distance is the maximum of all those distances. It is used as a measure for the correspondence between two point sets (Aspert et al., 2002). Where the first method only considers points that are in the corresponding octree cell, the Hausdorff distance also considers points in other cells, so that for every point a distance is calculated. However, drawbacks of the Hausdorff distance are the sensitivity to the point density and it does not necessarily mean that there is a change, for example when objects are occluded in one of the scans and different points are sampled.

Girardeau-Montaut et al. also propose a solution to overcome these problems. The first problem is easy to solve. Modelling the surface, for example by fitting a plane, followed by calculating the distance between a point and the plane, reduces the error. To identify occluded areas, the 2.5D representation is used. The scans are transformed to a 2.5D image as seen from the standpoint of the reference scan, similar to Zeibak and Filin's method. For every pixel the visibility is determined by comparing the range for that pixel with a buffer value. This buffer value stores the current range that is associated with the pixel. If a second range measurement for the pixel is available, is is compared with the buffer value. When a point is closer than the buffer value, the point is labeled as visible. For these points the Hausdorff distance is calculated. If a range value is greater than the buffer value, there is already a point available which is closer to the scanner. These points are marked as invisible. Points that are invisible can be either out of range, moved away from the sensor in the second epoch or unveiled in the second epoch because an object disappeared. To make a distinction between the last two cases, a third scan is necessary to provide more information. Finally, for the points of this third scan the distance can be calculated as well, either in the same way as for the visible points or in some other way.

3.7 Deformation analysis

During the change detection, objects or areas in the point cloud are identified where changes occurred. In a deformation analysis, the unchanged surfaces in a scene are investigated in more detail. The deformations that are to be found are in the order of magnitude of the point accuracy, but also in the same order as the noise. The registration of the point clouds influence the accuracy of the point clouds and therefore the possibility to detect deformations. An accurate registration is thus an important step.

The available deformation methods can be divided in three different categories:

- point-to-point-based methods,
- point-to-surface-based methods,
- surface-to-surface-based methods.

In this section, a short overview of some of the available methods in these categories is presented.

3.7.1 Point-to-point-based deformations

When monitoring deformations with total stations, fixed points are measured at different epochs. The coordinates of these points are compared to find deformations. With a laser

scanner, it is uncertain that the exact same point is sampled at two different epochs. Furthermore, the point density on an object can vary as it is scanned from multiple standpoints. A direct point-to-point comparison is therefore not favourable.

An approach of a pointwise comparison of the points for a deformation analysis is to use the range images, similar as for the change detection as described in Section 3.6. If the scans are taken from different standpoints, the scans are transformed to the same standpoint. Per point, represented by a pixel in the range image, the distance is calculated by subtracting the range value of that pixel in the other range image. Instead of the question whether a change occurred, the range difference is now used to quantify the deformation. Problems arise when the point density varies or when areas are occluded.

Little (2006) uses a pointwise comparison to monitor mining excavation. Two laser scanners are permanently installed on the sides of the mining pit. On the slope that is investigated, a regular grid with intervals of 5 m is created. Only these points are measured, twice a day. A pointwise comparison is carried out to monitor the volume changes.

Tsakiri et al. (2002) use retro-reflective targets that are placed on the object. These targets are scanned during multiple epochs and for each target the centre is calculated. Results show that deformations below 0.5 mm can be detected using TLS and targets. However, the accuracy achieved by traditional surveying is even higher (Tsakiri et al., 2006).

3.7.2 Point-to-surface-based deformations

One of the great advantages of the TLS is the high point density. Point-to-point approaches do not use this high point density. Surrounding points can give information on the deformations. This information is used in the point-to-surface-based methods. One of the point clouds is represented by a surface (usually the reference point cloud) and for a point in the second point cloud the distance to the surface is calculated.

According to Remondino (2003), the aim of the surface reconstruction is to find a surface model Q' that represents the surface Q. The model is based on the sampled points and these points are assumed to lay on the unknown surface Q. Additional information, such as break lines, can be used to improve the model. Since the number of sampled points is limited, the model will not exactly represent the original surface. If the point density increases, the model will converge to the original surface.

There are some possibilities to represent a surface (Remondino, 2003):

Tessellation A surface representation by means of a mesh is a common approach (Tsakiri et al., 2006). The point cloud is partitioned in simplexes and the surface is represented by vertices, edges and faces. A common representation is a TIN and is used in 2D and 3D. A TIN uses all the available points. Furthermore, it is possible to use break lines, for example to define edges in the point cloud.

Implicit functions These functions are defined by an implicit relation between the variables, for example in the form of $f(x, y) = 0$ (Stewart, 1999). Examples of implicit functions are planes, spheres or cylinders. These functions are not exact, which means the data points are not necessarily on the surface.

Explicit functions The outcome of an explicit function depends on the input variables, for example $y = f(x)$ (Stewart, 1999). Examples of these surface representations are splines or Non-Uniform B-Spline (NURBS).

An example of a point-to-surface method is proposed by Van Gosliga et al. (2006), where a tunnel is subject to a deformation analysis. Since the tunnel is bored, it can be represented by a cylinder, which is fitted to the data using LS. The point clouds are converted to a local spherical coordinate system, using the estimated cylinder, so that deformations are perpendicular to the tunnel axis. All the data points are interpolated to a regular grid, assuming that the tunnel is locally flat. Between the two acquisitions, artificial deformations are placed in the tunnel. The difference in the range for a grid point is tested on deformation.

3.7.3 Surface-to-surface-based deformations

The third category of methods consists of computing the distance between two surfaces. Both point clouds are represented by a surface representation as mentioned in Section 3.7.2. Lindenbergh and Pfeifer (2005) use a surface-to-surface-based method to detect deformations on a lock. The lock is scanned twice from the same standpoint. Their first attempt was to directly compare the observed points, since the surface was sampled from the same standpoint and therefore the sampled points represent more or less the same point on an object. This 2.5D approach is point-to-point-based. However, the comparison turned out to be difficult, possible due to small movements of the instrument. The next step was to segment the point cloud into homogeneous areas. For each of the segments, a plane is fitted and the residuals of the plane fitting are visualised. At this stage, the method is point-to-surface-based, as for every point the residual to the plane is investigated. The residuals show different deformation regimes for the inner and outer areas. This weakens the choice to use one plane for the entire segment. Therefore the segment is divided in grid cells of 5×5 cm. For each grid cell, a plane is fitted to all the points contained in that cell. The plane parameters and their covariance are used for the deformation analysis, resulting in a surface-to-surface method.

Chapter 4

Segmentation matching for change detection and deformation analysis

4.1 Introduction

While the acquisition of Terrestrial Laser Scanning (TLS) data takes relatively short time, the processing steps are often time consuming. Depending on the desired end product, the processing requires several steps. In this project, the required processing steps are organised in a processing workflow. This chapter describes the proposed workflow and the subsequent processing steps for the purpose of change detection and deformation analysis. Chapter 5 describes the practical implementation of this workflow.

4.2 The proposed workflow for the processing of Terrestrial Laser Scanning data

In the proposed workflow, all the processing steps are ordered to arrive at the change detection or the deformation analysis. There are two ways to use the workflow. In both methods, the steps are identical, but the input data for some of the steps differs. The first possibility is to try to find changes and deformations over time. At least two point clouds, captured at two different epochs are required to achieve this. The second possibility is to deal with a point cloud of one epoch. The individual scans of that point cloud are processed. In that case, it is impossible to perform a change detection and a deformation analysis, since there is no time difference. However, the results can give information on the occluded areas and the registration error of the scans. An overview of all the steps is given in Fig. 4.1. During this chapter, the focus is on processing of two point clouds to detect changes and analyse deformation.

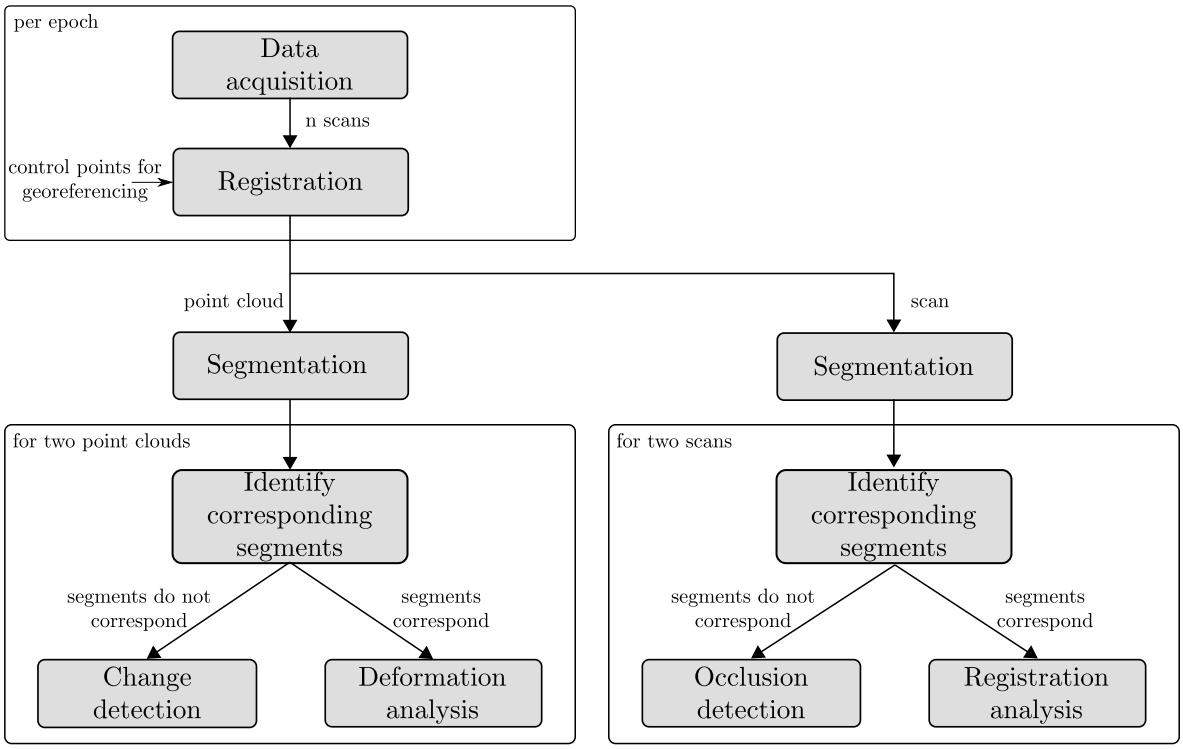

Figure 4.1: Overview of the workflow, from the acquisition of the laser scan data to the change detection or deformation analysis. After the registration can be chosen to continue the processing either towards a change detection and a deformation analysis or towards an occlusion detection and a registration analysis. The steps are identical, but the input data differs.

Acquisition of TLS data

The starting point of the proposed workflow is the acquisition of the TLS data. In most cases, multiple scans are required to sample the complete scene. For more details on the acquisition process, see Section 3.2.

Registration of the acquired scans

The first processing step is the registration of the data. As described in Section 3.4, the registration process transforms all the scans to one common coordinate system. The result is one point cloud per epoch, which consists of multiple scans. When processing towards change detection and deformation analysis, the registered point clouds are used. During the processing towards occlusion mapping and registered analysis, registered individual scans are used.

The registration is done per epoch, since the control points are randomly distributed in the scene, not at the same position and perhaps subject to deformation.

Segmentation of the registered data

The next step is the segmentation of the individual scans or point clouds. This processing step groups points based on a homogeneity property, see also Section 3.5. The results are used in the next step of the workflow.

Difference between change detection and deformation analysis

For people outside the field of geomatics, change and deformation seem to represent be a similar phenomena. However, in the remote sensing field, there is a clear distinction between those two. In this project, changes are defined as differences in the state of an object, see Section 3.6. Deformations are small differences at an object's surface. However, the two are closely related: a large deformation can be considered as a change.

4.3 Identification of the corresponding segments

The step after the segmentation process is to use the segmentation results in such a way that surfaces that appear in multiple epochs are identified. A deformation analysis only makes sense if the surfaces that are compared belong to the same object. If a surface changed significantly between the acquisitions, the segmentation results will be different. By looking at the geometry of the segments, a distinction between changed and unchanged surafaces is made. This step in the workflow is named the identification of corresponding segments.

Ideally, when a wall is scanned twice from the same standpoint and under the same conditions, the segmentation results should be very similar, i.e. the segments have the same orientation, position and size. Small differences are caused by the fact that the laser scanner does not sample the exact same points. Even if the standpoint is different and there is a clear line-of-sight to the wall, the segmentation results should be similar. Differences are caused by occlusions or changes. When a wall is sampled at least twice and the segments correspond, the segments can be compared using a deformation analysis. If segments without a correspondence exist, it indicates that a possible change occurred. For these areas, a detailed analysis of the surface is not necessary. Section 4.4 deals with change detection in more detail, Section 4.5 describes the comparison of the segments for a deformation analysis.

The starting point of the segmentation matching is two segmented point clouds, acquired during two different epochs. Let the set of all segments from the first epoch be S^I and the set of all segments from the second epoch be S^{II}. The segment k from epoch I is notated as S^I_k and segment l from epoch II is notated as S^{II}_l. The main interest of this project are the walls of the tunnel. These walls should result in (more or less) planar segments. The next described steps are suitable and valid for planar segments.

Two planar segments from two epochs correspond if the following two conditions are valid:

Condition I The segments are in the same plane.
Condition II The segments intersect.

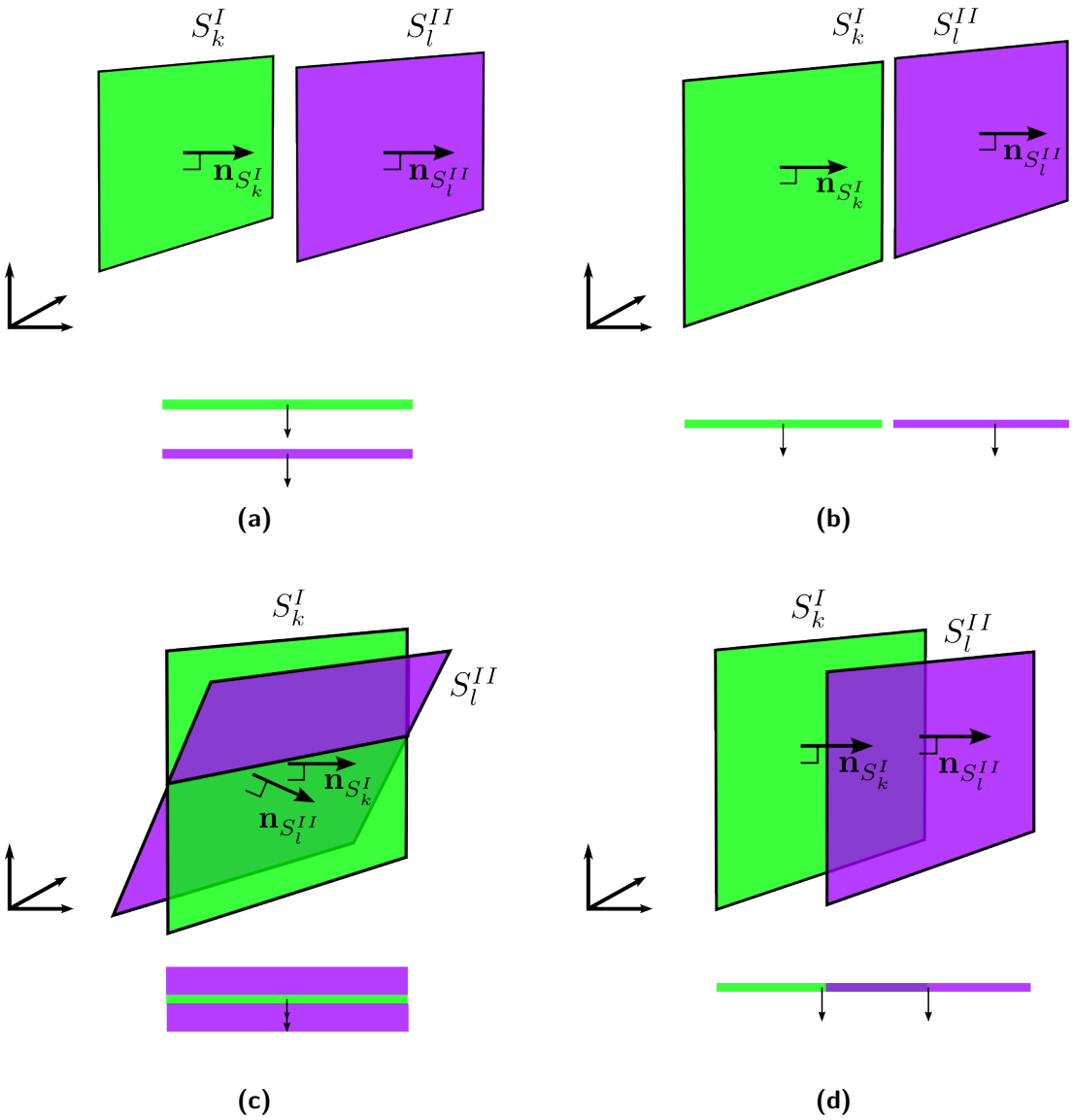

Figure 4.2: Four possible orientations and locations of two planar segments, with their top view. (a) The orientation of the segments is similar, but the segments do not intersect. (b) The segments have the same orientation, but there is no intersection. (c) There is an intersection between the two segments, but the orientation is different. (d) The segments have the same orientation and intersect.

The two conditions are illustrated in Fig. 4.2. Since a plane is not bounded in space, two segments that lie in the same plane do not necessarily intersect. Moreover, two segments that intersect do not necessarily lie in the same plane. Therefore, both conditions need to be fulfilled. The order in which the conditions are checked is not important. The presented order is based on the computational efforts needed.

4.3.1 Condition I: segments are in the same plane

Two segments are in the same plane if for both segments:

- the orientation is the same, thus the segments have the same normal vector $\mathbf{n}$,
- the distance d between the segment plane and the origin is the same.

Note that measurement noise influences both the normal vector and the distance. Therefore small deviations are allowed, by means of threshold values.

Orientation of the segments

To compare the orientation of the segments, the normal vector is calculated for both segments by fitting a plane through the points, see Section 4.5.2. This results in two unit normals, $\mathbf{n}_{S_k^I}$ and $\mathbf{n}_{S_l^{II}}$. The angle α between the two normals is calculated with

$$\alpha = \cos^{-1}\left(\frac{\mathbf{n}_{S_k^I} \cdot \mathbf{n}_{S_l^{II}}}{\left|\mathbf{n}_{S_k^I}\right| \left|\mathbf{n}_{S_l^{II}}\right|}\right). \tag{4.1}$$

Since $\mathbf{n}_{S_k^I}$ and $\mathbf{n}_{S_l^{II}}$ are unit normal vectors, Eq. (4.1) can be reduced to

$$\alpha = \cos^{-1}\left(\mathbf{n}_{S_k^I} \cdot \mathbf{n}_{S_l^{II}}\right). \tag{4.2}$$

Distance between two segments

A plane in 3D is completely defined by $\mathbf{n}$ and d. The distance to the plane can be calculated using any point that is located in the plane, for example the centre of gravity, see Section 4.5.2.

For two segments, the distance d is only similar if the orientation is similar and if they are approximately in the same plane, see Fig. 4.3a. Furthermore, the distance also depends on the location of the plane in the coordinate system, compare Fig. 4.3a and (b). Therefore, using d to quantify the distance between planar segments is not satisfying. Another approach to calculate the distance between two segments is required.

Formally, the distance between two points is the length of the path connecting them (Weisstein, 2010b). Since there are infinite paths connecting two points, generally the shortest path is used as the distance. The Euclidean distance between two segments is the shortest distance between the two segments and is symmetric. However, determining the Euclidean distance is a computational intensive task, since the minimum of all the distances between the two

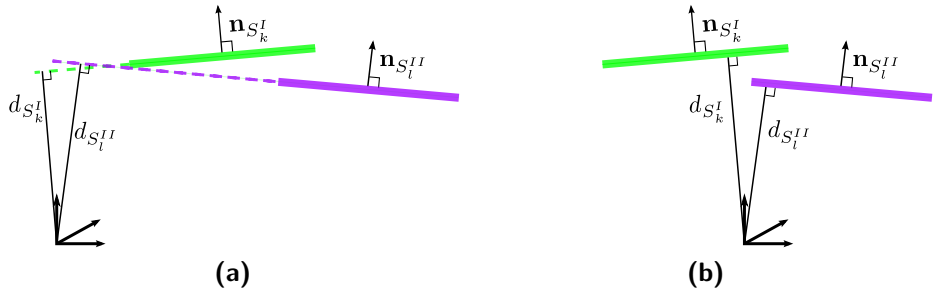

Figure 4.3: The distance d to the plane. The distance depends on the orientation of the planes and on the location of the segments with relation to the origin of the coordinate system.

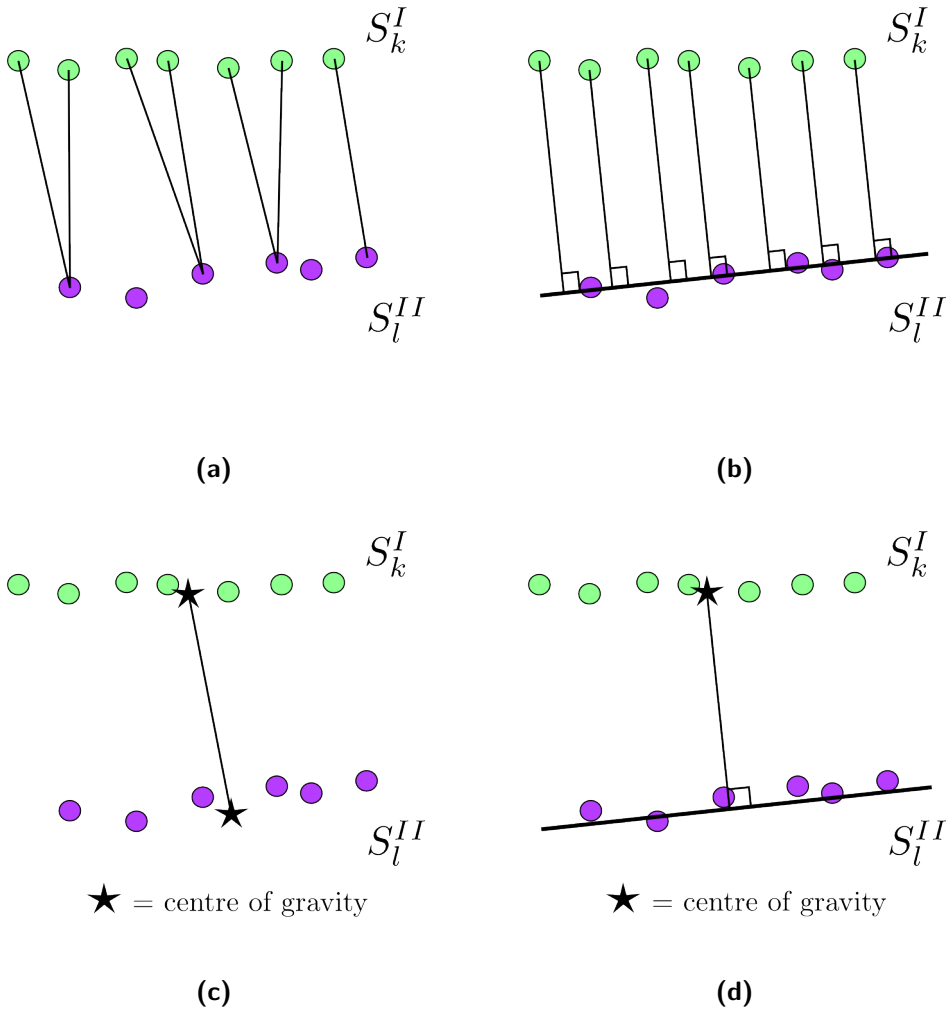

Figure 4.4: Four methods to approximate the distance between two segments. (a) Distance calculation between each point and its closest point in the other segment. (b) Distance between each point in epoch I and the fitted plane in epoch II. (c) The distance between the two centre of gravities. (d) The distance between the centre of gravity in epoch I and the fitted plane in epoch II.

segments needs to be computed. Other approaches are defined, which do not all follow the definition of a distance, but provide an approximation for the distance between two segments. Four methods are discussed:

1. Calculate for every point in S_k^I the shortest distance to S_l^{II}, which is the distance to its closest point, see Fig. 4.4a. The distance between the two segments is then given by taking the minimum of the shortest distances. A drawback is that for every combination of two points the distance is calculated, resulting in many computations.
2. Calculate for every point in S_k^I the distance to the best fitting plane through the points of segment S_l^{II}, see Fig. 4.4b. The plane is defined by the normal of segment, $\mathbf{n}_{S_l^{II}}$, and the distance $d_{S_l^{II}}$.
   For a point $\mathbf{x}_i$ in S_k^I, the distance δ to the plane of S_l^{II} is calculated by projecting the point on the normal, $\mathbf{n}_{S_j^{II}}$, (Weisstein, 2010c)
   $$\delta = \frac{\mathbf{n}_{S_l^{II}} \cdot \mathbf{x_i}_{S_k^I} + d_{S_l^{II}}}{\left|\mathbf{n}_{S_l^{II}}\right|}. \tag{4.3}$$
3. Calculate the distance between the centre of gravities of the segments. The disadvantage of this approach is that the distance between the centre of gravities depends on the size of the segments and on the overlap, see Fig. 4.4c.
4. Calculate the shortest distance between the centre of gravity of S_k^I to the plane fitted to S_l^{II}, see Fig. 4.4d. This is a combination of the second and the third method. Since the two segments already have a similar orientation, it is not necessary to calculate the distance to the plane for every point in S_k^I. Only calculating the distance from the centre of gravity to the plane of the other segment is sufficient.

In this project, the last method is used as a measure for the distance between two segments. It should be noted that the calculated distance depends on the order of the segments and is not symmetric. One of the reasons for this difference is that the orientation of the segments can differ. However, since this difference in orientation is small, the difference in the distance caused by the order is also small. Furthermore, the results of the identification of the corresponding segments already depends on the order of the epochs. The calculated distance is only used to determine whether two segments are approximately located in the same plane.

The distance between two segments, $\delta(S_k^I, S_l^{II})$, is computed as

$$\delta(S_k^I, S_l^{II}) = \frac{\mathbf{n}_{S_l^{II}} \cdot \bar{\mathbf{x}}_{S_k^I} + d_{S_l^{II}}}{\left|\mathbf{n}_{S_l^{II}}\right|}, \tag{4.4}$$

where $\mathbf{n}_{S_l^{II}}$ is the normal of the plane fitted to S_l^{II}, $\bar{\mathbf{x}}_{S_k^I}$ is the centre of gravity of S_k^I, $d_{S_l^{II}}$ is the orthogonal distance from the origin to the plane of S_l^{II} and $\left|\mathbf{n}_{S_l^{II}}\right|$ is the length of $\mathbf{n}_{S_l^{II}}$.

4.3.2 Condition II: segments must intersect

The second condition that must be fulfilled for two segments to correspond is that there has to be an intersection area. As mentioned before, the two conditions can be checked in any

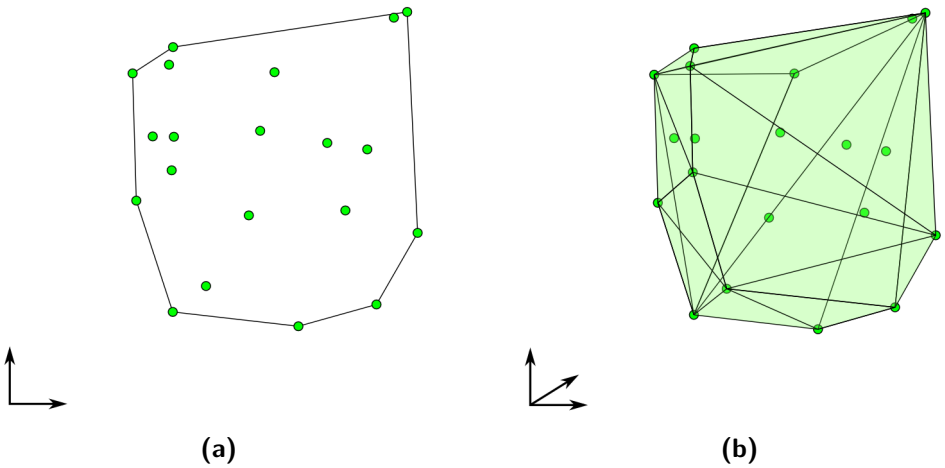

Figure 4.5: The convex hull for (a) a 2D data set and (b) a 3D data set.

order. However, this condition is computationally more intensive than condition I. Therefore the best solution is to make a list of potential correspondences based on condition I, and use this list to check for condition II.

Two segments intersect if the intersection of the two sets is non-empty:

$$S_k^I \cap S_l^{II} \neq \emptyset. \tag{4.5}$$

To find the intersection of the two segments, the convex hull of the points in the segment is computed. The convex hull C of a set of points is defined as the intersection of all convex sets containing the points (Barber et al., 1996). In the convex set C, a straight line between any two points from the set lies completely in the set C (Weisstein, 2010a). In analogy, the convex hull of segment S_k^I is the minimum convex set, containing all the points from the segment S_k^I. The boundary of the convex hull in 3D is given by triangles. Barber et al. (1996) propose an algorithm to find the convex hull of a set of points. The program Qhull (2010) is an implementation of this algorithm and is available in Matlab. Fig. 4.5a shows the convex hull of a 2D data set, consisting of lines. Fig. 4.5b shows the convex hull of a 3D data set, which is formed by triangles.

A problem arises when the segment is concave: it has boundaries that go inward the segment. An example is shown in Fig. 4.6a. The convex hull, as shown in Fig. 4.6b, does not follow this boundary, which also follows from the definition of the convex hull. An alternative is to use alpha shapes. Alpha shapes are a generalisation of the convex hull (Edelsbrunner and Mucke, 1994). It uses polytopes for the geometrical representation of the segments. Only one parameter needs to be set: α. When alpha is infinity, the alpha shape is identical to the convex hull. If α goes towards zero, the alpha shape shrinks and concaves can start to form, which is illustrated in Fig. 4.6c. However, the use of the convex hull is sufficient to demonstrate the algorithm in this project. A solution to overcome concave segments is given later in this section.

The next steps are illustrated with a schematic data set, see Fig. 4.7. The starting point for condition II is two segmented point clouds, S^I and S^{II}. The segmentation labels are

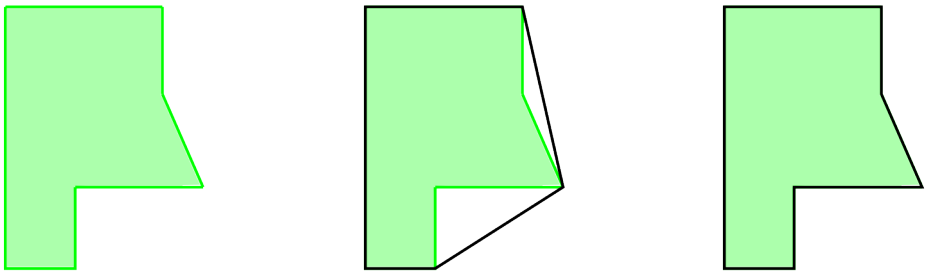

Figure 4.6: The problem of the convex hull with concave segments. (a) A concave segment. (b) The convex hull of the segment. (c) A possible alpha shape for the segment.

given by s^I and s^{II} respectively. Furthermore, the list of possible correspondences L between segments is established, based on condition I. Segments that are not in the same plane are not considered. In this example, all the shown segments satisfy condition I, so the segments are in the same plane.

step 1 The first step uses the list of possible correspondences. For segment S_i^I of the first epoch, see Fig. 4.7a, the possible corresponding segments in S^{II} are identified using the list, see Fig. 4.7b.

step 2 The convex hull of the points in S_i^I is determined, see Fig. 4.7c. All the points of the segments from S^{II} that are in the convex hull of S_i^I, are identified, see Fig. 4.7d. To overcome the problem of the concave segments, for all the selected points in S^{II} the distance to the nearest point in S_i^I is calculated. If this distance is smaller than the specified threshold, the point is in the intersection, see Fig. 4.7e. The other points are no longer considered and receive segmentation label "-2",

step 3 The next step is to find the points of S_i^I that are in the intersection. The convex hull is created using the points of S^{II} that are selected in step 2. All the points of S_i^I that are in the convex hull are selected, see Fig. 4.7f. Again, points in S_i^I that are closer from their nearest point in S^{II} than the distance threshold r_{th} are identified, see Fig. 4.7g. The other points receive the segmentation label "-2".

step 4 From both segments, the points in the intersection area are identified, see Fig. 4.7h and (i). Both sets of points get the same new segmentation label, s_i^I.

step 5 Step 1 to 4 are repeated until all segments in S^I are processed. The points in the point cloud of epoch II that did not receive a new segmentation label and are not an outlier from the segmentation process are also assigned with segmentation label "-2".

The algorithm, including the first condition, is also shown in Alg. 3.

The points from S^I and S^{II} that have been identified are sampled on the same planar surface. These surfaces are compared in a registration or deformation analysis.

During the segmentation matching, the original segmentation results are not lost. For each point a new label is assigned, giving information on the correspondence. A direct identification

Algorithm 3: Algorithm for segmentation matching.

Data: S^I with m segments and S^{II} with n segments
Input: distance threshold r_{th}
angular threshold α_{th}
for $i = 1$ to m **do**
    create the list of possible corresponding segments L_i, containing every segment from S^{II}
    for $j = 1$ to n **do**
        calculate the angle α with between the S_i^I and S_j^{II}
        if $\alpha > \alpha_{th}$ **then**
            remove S_j^{II} from list L_i
    for every S_j^{II} in L_i **do**
        calculate the distance $\delta(S_i^I, S_j^{II}$
        if $\delta(S_i^I, S_j^{II} > \delta_{th}$ **then**
            remove S_j^{II} from list L_i
    create the set of points S_i^{II} containing all the points from the segments in L_i
    calculate the convex hull C_i^I of S_i^I
    remove the points from S_i^{II} that are not in C_i^I
    for every point in S_i^{II} **do**
        calculate distance r to the nearest point in S_i^I
        if $r > r_{th}$ **then**
            remove point from S_i^{II}
            assign segmentation label "-2" to point
    calculate the convex hull C_i^{II} of S_i^{II}
    remove from S_i^I the points that are not in C_i^{II}
    for every point in S_i^I **do**
        calculate distance r to the nearest point in S_i^{II}
        if $r > r_{th}$ **then**
            remove point from S_i^I
            assign segmentation label "-2" to point
    for every point in S_i^{II} **do**
        assign segmentation label s_i of S_i^I

Points in S^I and S^{II} that are not assigned with a new label and were not an outlier during the segmentation process receive the new label "-2" as well.

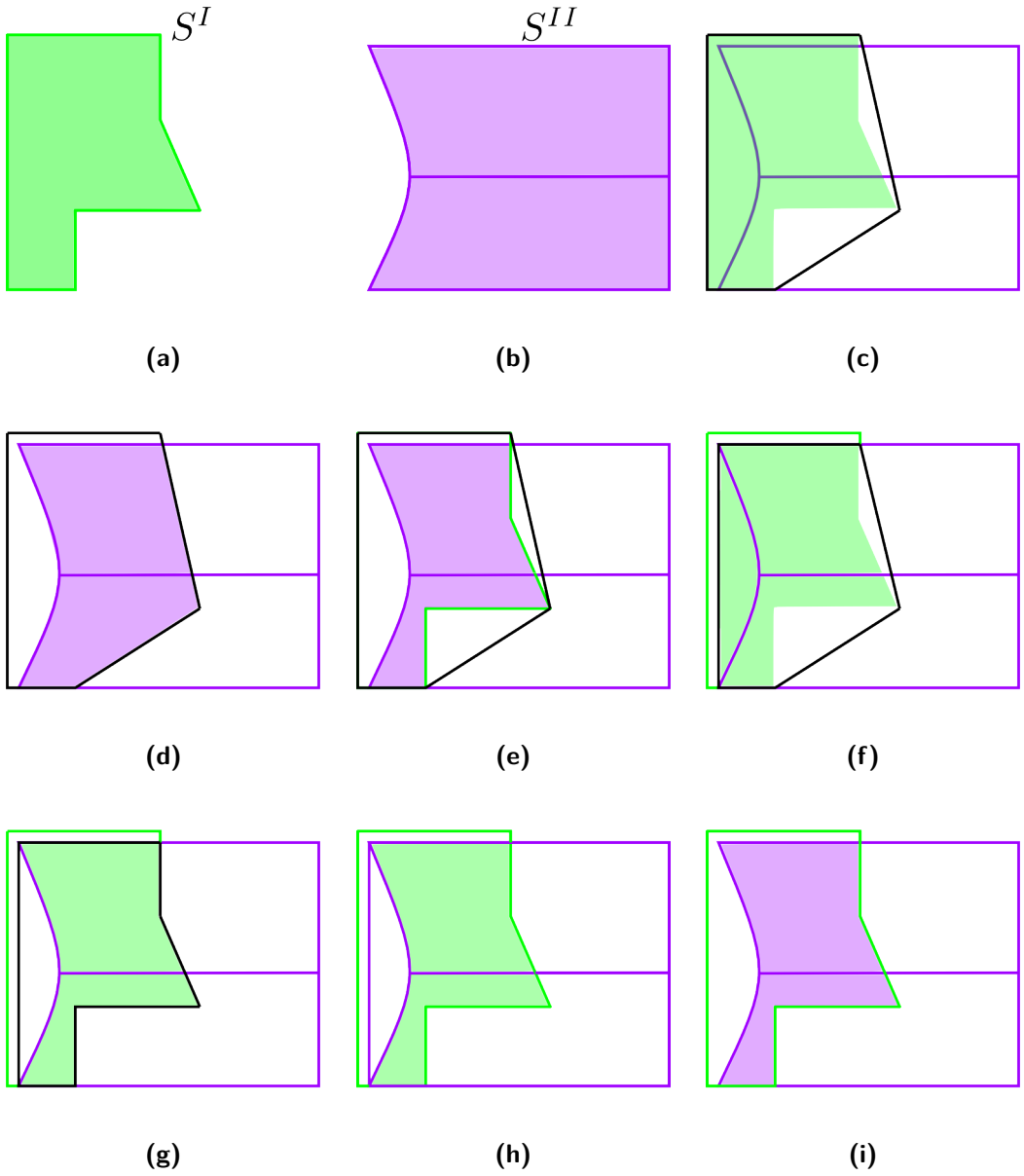

Figure 4.7: An illustration of the steps of the algorithm to find the corresponding segments, for the segmented data sets (a) S^I and (b) S^{II}.
(c) Step 1: calculate the convpnghull of S_i^I.
(d) Step 2: find the points of S^{II} that are in the convex hull of S_i^I. (e) Calculate for all the selected points of S^{II} the distance to the closest point in S_i^I; if larger than threshold, the point is removed.
(f) Step 3: create the convex hull of the points that are still in S^{II}. (g) Calculate for all the selected points of S_i^I the distance to the closest point in S^{II}; if larger than threshold, the point is removed.
(h) The resulting corresponding segment in S^I. (i) Theresulting corresponding segment in S^{II}.

of the segments that have a correspondence is possible with the use of the segmentation labels. Furthermore, it is clear which points can be used for the deformation analysis, since those points have the same segmentation label. At this stage, it is better to speak of a segmentation containing points that are 'likely to be sampled on the same surface'.

4.4 Change detection

The process of finding corresponding segments results in a new label for each point. Corresponding labels in both epochs indicate that these segments can be compared to detect deformations. The detected deformations are small, mostly in the order of magnitude of cm. Besides knowing how a surface deformed, it is also interesting to know whether new objects are placed in or removed from a scene.

The change detection step can also be used to detect 'changes' between scans of one epoch. These 'changes' are no real changes, since the scans are made within a short time span, but they instead represent occlusions. Surfaces that are sampled in one scan but not in the other scan are identified.

The results of the previous processing steps contain information on possible changes. At this stage, there are three possible segmentation labels:

- label > 0: this is a segment that has a corresponding segment.
- label "-1": points that are removed during the segmentation process, because they are considered as an outlier.
- label "-2": points that do not have a corresponding segment, either because there is no corresponding segment or because the points are outside of the intersection of the segments.

For the first category of segmentation labels, the segments are subject to a deformation analysis. The other cases are described below.

Outliers during segmentation process

The segmentation process tries to group points that belong to the same segment. Not all points are assigned to a segment. Points that do not belong to a segment are labelled with the segmentation label "-1".

With the high density point cloud that is produced by a laser scanner, it is not likely that single points represent changes. If an object changed, it will influence more than one single point. Therefore, these points are not considered to represent a change and are not further processed.

Points that are not in a corresponding segment

The third category of points is formed by the points that are not in a corresponding segment after the identification of the corresponding segments. Various reasons can explain such points:

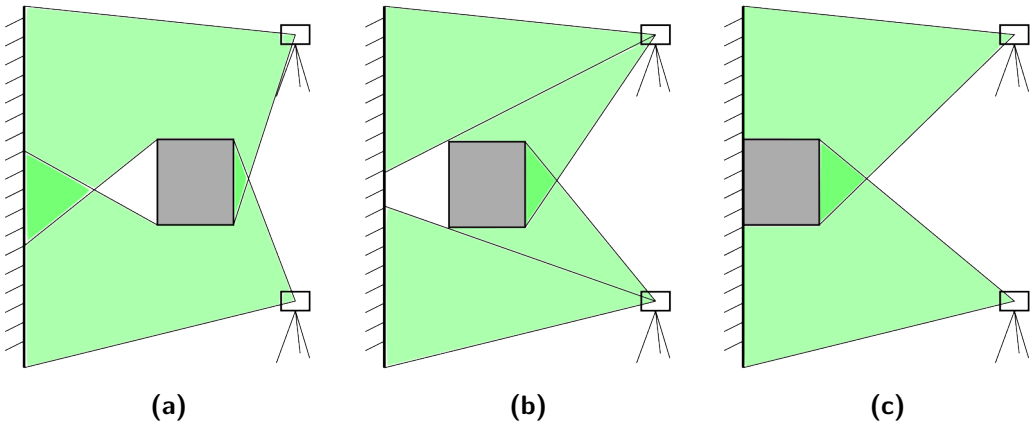

Figure 4.8: Illustration of the similarity between occlusions and changes. (a) There is an object, but the wall is completely sampled. (b) The object is closer to the wall, blocking the view on the wall. (c) The object is adjacent to the wall, again causing occlusion.

- The change of an object results in a difference in the segments. As a result, the segments from the first epoch do not correspond with a segment from the other epoch.
- Due to occlusion of (a part of) the surface, the surface is only sampled in one epoch.
- Edge effect results in points that are not actually sampled on a surface, but near an edge. If such a point is isolated, i.e. the neighbouring points are sampled on an object, it will be not be assigned to a segment during the segmentation process. If nearby points are also influenced by the edges, it is possible that they form a segment.

Points that are not in a corresponding segment are identified as potential changes. The next step is to distinguish between real changes and occlusions or edge effects. Note that edge effects will most likely be assigned as outliers during the segmentation and are therefore not considered.

Distinction between changes and occlusions

The preliminary result of the change detection is a subset of epoch I and a subset of epoch II, containing all the points that do not correspond with a segment in the other epoch. These points are on objects that changed or were occluded in one of the epochs. The distinction between a change and occlusion is difficult to make. Both have the same effect on the segmentation, as illustrated in Fig. 4.8. In Fig. 4.8a, an object is placed in front of the wall. The laser scanner is still able to sample the wall behind the object, so there is no occlusion. In Fig. 4.8b, the object is placed closer to the wall. The line-of-sight of the laser scanner to the wall is blocked by the object, causing an occlusion for that part of the wall. When the object is placed against the wall, see Fig. 4.8c, a part of the wall is still occluded.

The occlusion is also seen in the segmentation results. Possible segmentations of the epoch with the object are shown in Fig. 4.9, following the situations of Fig. 4.8.

In the next epoch, the object is removed. The segmentation of the second epoch results in one planar segment. During the identification of the corresponding segments, the occluded area

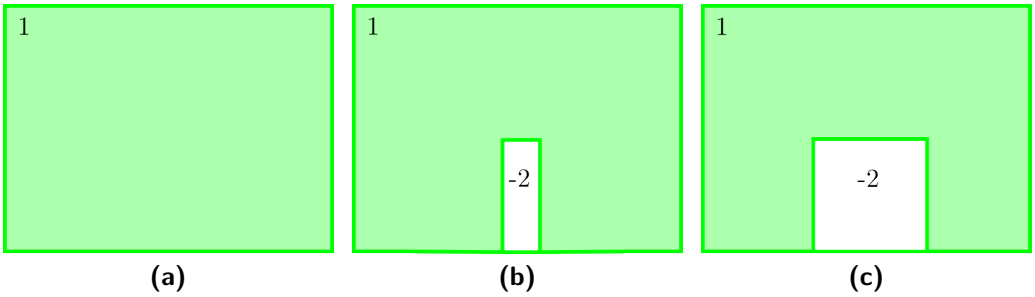

Figure 4.9: Possible segmentations of a wall with an occluded area. (a) There is only one segment. (b) There are two segments and the area of the possible change is identified. However, it is due to occlusion. (c) There are two segments. The area of the possible change is now really where the change is.

is found as a potential change, indicated with label "-2". In the first situation, the change is unnoticed. In the second situation, the change is noticed, since it was possible to sample the points behind the object. In the third situation there is really a change. However, the segments located on the object will not have a correspondence and are therefore identified as a change.

A solution to distinguish between changes and occlusions

Based on the segmentation results and the identification of the corresponding segments, the previous example illustrates the difficulty to determine whether there is a change or an occlusion. Additional information is necessary to distinguish between changes and occlusions, namely information on the scanning geometry.

In both cases there is a surface sampled in one epoch but not in the other epoch. If there is a change between two epochs, there is an object in the scene that is either placed or removed at a certain location. In the case of occlusion, in both epochs there is an object in the scene, but in only one of the two epochs the object blocks the view of the laser scanner. When it is known why a surface is not sampled, the decision between change or occlusion is made. The aim is to find out why points are labelled as a possible change, i.e. why they are sampled in only one epoch.

Zeibak and Filin (2007) use the 2.5D representation of the point cloud to identify the changes between two scans. These scans are either taken at the same standpoint or at different standpoints. When the standpoints are identical, the change detection reduces to image subtraction of the range images, see Section 3.6. If scans are acquired from different standpoints, a transformation to one of the standpoints is required. For every pixel, the line-of-sight is compared. Differences in the range may indicate a change. This approach is also used by Girardeau-Montaut et al. (2005).

A similar approach can be used to distinguish between changes and occlusions. Points that are labelled as potential changes are investigated in more detail. Using the segmentation labels at this stage gives information on which surface the points belong to. Furthermore, the segments represent objects, which is more meaningful than single points, since it is unlikely that single points are changed or occluded.

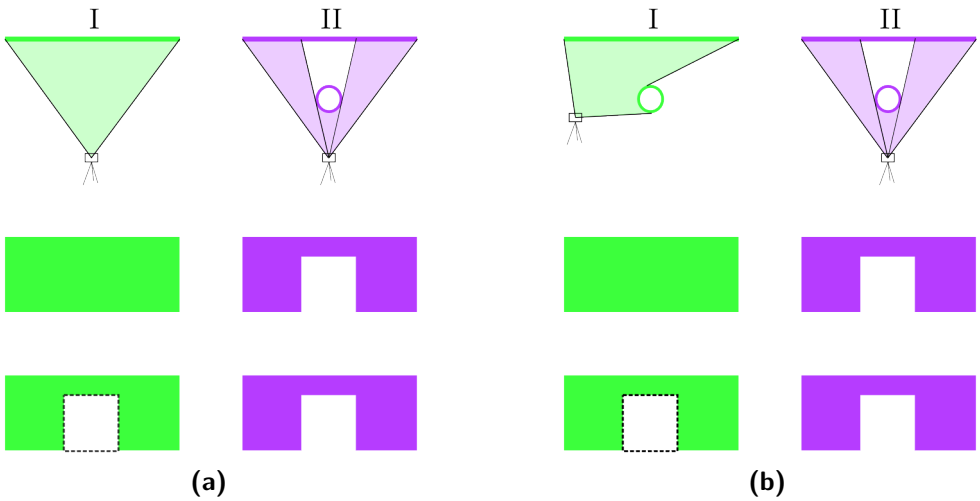

Figure 4.10: Illustration of the distinction between changes and occlusions. (a) In the left column the first epoch is depicted, in the right column the second epoch. The first row shows the location of the scanner and the segment of interest. In the second epoch there is a pillar in the scene. The segmentation results are shown in the second row, the results of the segment comparison in the third row. The dashed region in epoch I are possible changes. When the line-of-sight for these points is investigated, it follows that the pillar blocked the view in epoch II. Since there is no pillar in epoch I, there is a change. (b) The left column shows epoch I, the right column epoch II. The situation is sketched in the first row. In both epochs, there is a pillar. However, the standpoint in epoch I is so that the wall could be sampled. The segmentation results are shown in the second row. The third row shows the results of the segment comparison. Note that the results of this step are the same as in (a), bottom row. Investigating the line-of-sight for these possible changes shows that there is a pillar in both scenes at the same location. Therefore there are no changes but the wall was partly occluded.

For each possibly change, it can be investigated if that segment is seen in both epochs. With the individual scans, it can be seen if the segment is visible, or if an object in the scene is blocking the view. If there is indeed an object blocking the view, and this object is also present in the other epoch at the same location, there is occlusion and no change. If this object is only present in one of the epochs, there is a change.

The process is illustrated in Fig. 4.10. The example is based on one standpoint in a scene. If there are more standpoints, for every scan it should be investigated if the segment is seen.

4.5 Deformation analysis

4.5.1 Introduction

If the surface of an object is sampled in at least two epochs, a deformation analysis is performed. The aim of the deformation analysis is to find deformations in the segments in the order of magnitude of cm.

In Section 3.7, three methods for a deformation analysis are described: point-to-point, point-to-surface and surface-to-surface. For a point-to-point-based comparison corresponding points need to be identified. Besides the fact that the exact origin of the laser reflection is not known, this method does not fully use the high point density. It is possible to use the local neighbourhood of points to estimate points with redundancy. Furthermore, different point densities for the two point clouds influence the results. A surface-to-surface-based comparison requires a surface representation for both point clouds. The deformation is not calculated for the original points, but for points at a fixed interval.

The method used in this project is a point-to-surface-based method. First of all, it uses the full density of the point cloud. Since for only one of the point clouds a surface representation is necessary, computation time is saved. Furthermore, the deformation is calculated for every point in the point cloud.

The deformation analysis of the point clouds is carried out per segment. For each segment, the average deformation can be computed. When a coarse deformation analysis is done for the complete scene, by using a smaller part of the available points, areas of deformation can be identified. These areas can then be subject to a more detailed analysis, for example by using the full point density.

Since the tunnel walls are the main object sampled in the point clouds, a large part of the segments is considered approximately planar. Unfortunately, other surface shapes are also present in the scenery. Fitting one specific geometric model to a segment is therefore not suitable. On the other hand, fitting a suitable model to each segment requires a larger computational effort. Therefore another strategy for a surface representation is necessary.

4.5.2 Plane fitting in 3D

A plane is parameterised by its normal vector $\mathbf{n} = [abc]^T$ and its distance to the origin, d. The relation between the parameters is

$$ax + by + cz + d = 0, \tag{4.6}$$

where $[xyz]^T$ is a point that lies on the plane.

The aim of the commonly used Least Squares (LS) approach is to minimise the sum of the squared orthogonal distances from the points to the fitted plane (Teunissen, 2000a). However, LS is potentially slow for large data sets (Soudarissanane et al., 2008). The problem of plane fitting can be reduced to an eigenvalue problem and can therefore be solved using Principle Component Analysis (PCA) (Rabbani, 2005; Shakarji, 1998).

The PCA is a mathematical procedure that transforms a number of possibly related variables into a smaller number of uncorrelated variables called principal components. The first principal component contains as much of the variability in the data. The succeeding components explain as much of the remaining variability (Wackernagel, 2003).

The axis of the principal components are given by the eigensystem of the experimental variance-covariance matrix of the observations. The experimental variance-covariance matrix, $\mathbf{C_Y}$, is calculated by subtracting the centre of gravity of the observations, $\bar{\mathbf{Y}}$, from the observations $\mathbf{Y}$, resulting in the centralised observations $\mathbf{Y_C}$:

$$\mathbf{Y_C} = \mathbf{Y} - \bar{\mathbf{Y}}. \tag{4.7}$$

The observations form a $m \times p$-matrix, with m the number of points and p the number of parameters, i.e. three columns with x, y and z-coordinates.

Using the centralised observations, the experimental variance-covariance matrix is calculated:

$$\mathbf{C_Y} = \frac{1}{m-1}\mathbf{Y_C}^T\mathbf{Y_C}. \tag{4.8}$$

Alternatively, if the variance of the measured points is available, this can also be used for the variance-covariance matrix.

The eigenvectors and -values are obtained after the eigenvalue decomposition of the variance-covariance matrix:

$$\mathbf{\Lambda} = \mathbf{E}^{-1}\mathbf{C_Y}\mathbf{E}, \tag{4.9}$$

where $\mathbf{\Lambda}$ is the diagonal eigenvalue matrix and $\mathbf{E}$ is the eigenvector.

The eigenvectors form the new 3D orthogonal basis for the observations in the direction of the principal components. The eigenvalues give the length of the principle axes. In the case of plane fitting, the least variability is in the direction normal to the plane. The eigenvector corresponding to the smallest eigenvalue gives the unit normal vector $\mathbf{n}$ to the plane. The distance to the origin from the plane to the origin is calculated as

$$d = \bar{\mathbf{Y}} \cdot \mathbf{n}, \tag{4.10}$$

where $\bar{\mathbf{Y}}$ is the centre of gravity of the points in $\mathbf{Y}$.

4.5.3 Proposed method for the deformation analysis

The walls are approximately planar, especially when considering an area of only a few square cm. Non-planar objects can also be locally represented by small planes if a small area is considered. The high point density results in many points on an object. With a horizontal angular resolution of 0.01° and a distance to the scanner of 10 m, the distance between two adjacent points is 1.7 cm. A point with its 20 nearest neighbours covers then a minimum area of approximately 40 cm^2, assuming that all the points are equally spaced, see also Fig. 4.11. For such a small neighbourhood, the choice for a planar surface representation is justified.

Advantage of a planar surface representation is the simplicity of the model. A 3D plane is defined by only four parameters, see also Eq. (4.6). At least three points are needed to estimate the plane parameters. However, if the point density decreases, the area that is covered by a point and its neighbouring points increases. A planar representation is in that case not always the best solution.

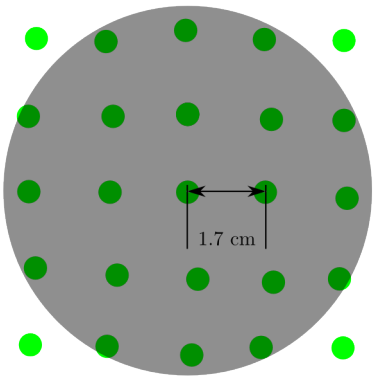

Figure 4.11: The area of a point with its 20 nearest neighbours, at 10 m distance from the scanner.

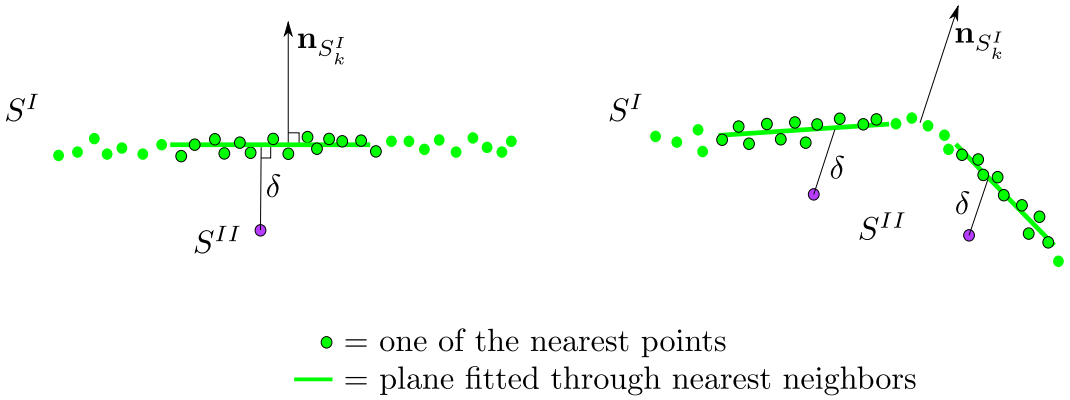

Figure 4.12: Illustration of the deformation analysis perpendicular to a wall. On the left, the wall is represented by a planar segment. On the right, the problem that arises with curved surfaces is illustrated: when the wall is not planar, it is hard to compute the correct orientation of the surface.

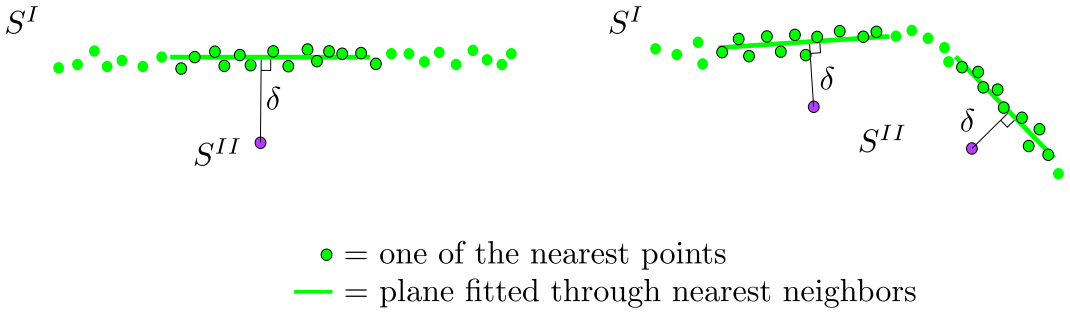

Figure 4.13: Illustration of the deformation analysis perpendicular to the local plane. On the left, the case the surface through points is represented by a planar segment. On the right, the situation with a curved surface is illustrated. The orthogonal distance to the local plane gives in both situations the shortest distance.

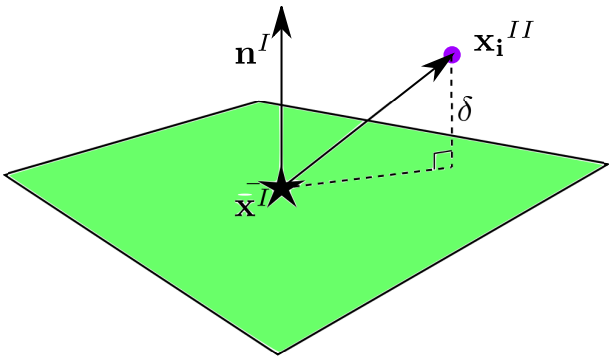

Figure 4.14: Illustration of the point to plane distance calculation.

The proposed algorithm calculates for every point in a segment of epoch II the distance to the plane fitted to the k-nearest neighbours (kNN) in the corresponding segment in epoch I. A possibility is to find the distance perpendicular to the segment, as shown in Fig. 4.12. The orientation is found by computing the normal vector of the whole segment. The distance between the point and the plane is parallel to the normal of the segment. However, not all segments are planar. For a curved surface, the orientation of the surface is harder to define. Fitting a plane through points that represent a curved surface is not justified.

Instead, the algorithm uses the orthogonal distance to a locally fitted plane, which is computed using the 20 nearest neighbours. With this approach, the computed distance is always perpendicular to the local surface, therefore it also holds for curved surfaces, as illustrated in Fig. 4.13.

step 1 For every point in a segment from epoch II, the local neighbourhood in the corresponding segment in epoch I is found. As for the segmentation process, also here can be chosen for a fixed area nearest neighbours or for the k-nearest neighbours (kNN). With differing point densities throughout the point cloud, the kNN method is the best option, since it adapts to the local point density. For a small search window around the point of interest, the k-nearest points are found, based on the Euclidean distance.

step 2 The local neighbourhood is used to fit a plane, as described in Section 4.5.2. The plane represents the surface at that point.

step 3 The next step is to use the parameters of the fitted plane, $\mathbf{n}^I$, and d^I, and the coordinates of the point-of-interest in epoch II, $\mathbf{x}_i^{II}$, to compute the distance to the plane, see Fig. 4.14,

$$\delta = \frac{\mathbf{n}^I \cdot \mathbf{x}_i^{II} + d^I}{\left|\mathbf{n}^I\right|}, \tag{4.11}$$

where δ gives the distance between the two point clouds.

An overview of the algorithm is given in Alg. 4.

Algorithm 4: Algorithm to calculate the deformation between two point clouds.

Data: S^I and S^{II} with m segments
list with corresponding segments
for *i=1 to m* **do**
  for every point $\mathbf{x}_i^{II}$in segment S_i^{II} **do**
    find the k nearest neighbours in S_i^I
    fit a plane to those points using PCA
    calculate the distance δ between $\mathbf{x}_i^{II}$ and the local plane

4.5.4 Quality of the deformation analysis

The deformation analysis of two independent sampled surfaces is only useful if proper error modelling is done. Error modelling allows to distinguish between measurement noise and deformations. Testing theory (Teunissen, 2000b) can be used for this.

An important step in the processing is the registration of the scans, see Section 3.4 and Section 4.2. The registration error propagates in the distance between the point clouds. Furthermore the measurement error also contributes to the total distance, as well as the plane fitting error. The calculated distance δ_T is thus a combination of

$$\delta_T = \delta_R + \delta_D + \delta_M + \delta_P + \delta_N, \tag{4.12}$$

where δ_R is the distance due to the registration error, including the georeferencing, δ_D is the distance due to deformation, δ_M is the measurement error, δ_P is the error due to the plane fitting and δ_N are unmodelled errors, such as errors introduced by the laser scanning system. Finding deformations in the Signal-to-Noise Ratio (SNR) of the laser signal is therefore a challenging task, and only possible if the acquisition and registration of the scans and the plane fitting are done as good as possible.

To eliminate the registration error, corresponding objects in the point clouds can be identified and registered. This involves another transformation of the objects. Surfaces matching algorithms, for example the Iterative Closest Point (ICP) algorithm, can be used for this. This step is suggested after the identification of the corresponding segments, so that each pair of segments is transformed and the distance is dominated by the deformation.

The measurement error is described in detail in Section 3.3. The best strategy to minimise this error is to have a good acquisition plan. With enough standpoints, surfaces are sampled with a small angle of incidence and the distance to the surface is not too large. The residuals of the plane fitting, found by computing the orthogonal distance to the plane, are used. The plane fitting algorithm minimises the sum of the squared residuals. The smaller the sum of the residuals is, the smaller is the error of the plane fitting.

Chapter 5

Implementation of the workflow

In this chapter, the workflow is implemented from the acquisition towards a change detection or a deformation analysis. The theoretical aspects are described in Chapter 4. Practical aspects are discussed, notably acquisition and registration of the fourth epoch are described in great detail.

Since the data involves large data sets with millions of points, the specifications of the computer system are important. In Table 5.1 the specifications of the computer and software used for the processing are given.

5.1 Description of the available Terrestrial Laser Scanning data

The geometry of the old metro station and the tunnel below the building of the *Nationale Nederlanden* was captured with a Terrestrial Laser Scanning (TLS) four times over the last four years. At the beginning of this graduation project, three of the four epochs were already acquired. The first acquisition was in April 2006, by the Delft University of Technology (DUT) in cooperation with the surveying department of Rotterdam Public Works (RPW). It was one of the first experiences of the DUT and RPW with the acquisition of TLS data.

Table 5.1: Computer specifications for the processing of the data.

OS	Kubuntu 10.10
processor	AMD Athlon 64 X2 Dual Core Processor 4600+
RAM	2 GB, +5 GB swap
graphical card	Nvidia GeForce 8500 GT
software	Matlab R2008b
	awk 3.1.6

OS	Windows XP (SP3)
processor	Intel Pentium 4, 3.00 GHz
RAM	3 GB
graphical card	Nvidia Quadro FX 1400
software	Matlab R2007b
	Cyclone 6.0.3
	Faro Scene 4.6
	Qtlaserviewer

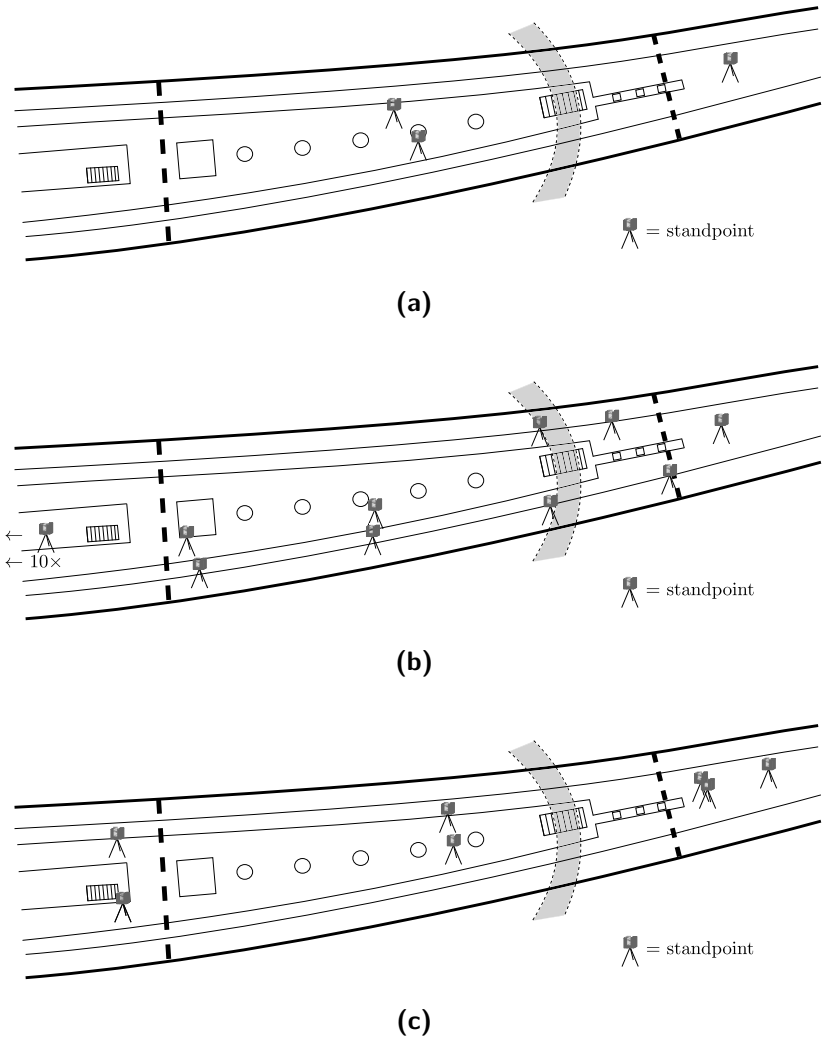

Figure 5.1: Schematic overview of the standpoints of the laser scanner for all the epochs. (a) Epoch I. (b) Epoch II. (c) Epoch III.

The second epoch, in February 2007, was scanned by the engineering company Fugro in order of RPW. The complete metro station and the beginning of the tunnel was scanned. The third epoch, in December 2007, was again acquired by the DUT and RPW. During this graduation project, the fourth epoch is acquired in January 2010.

An overview of the available data and specifications is given in Table 5.2. An explanation of the specifications is given in Section 3.2. In Fig. 5.1, the standpoints of the scans for the first three epochs are shown. The standpoints of the fourth epoch are shown in Fig. 5.2b.

The scans of the tunnel focus on the old platform and the first part of the tunnel below the *Nationale Nederlanden* building. In Section 2.4, it is explained that most of the deformations are expected in this area. In the second epoch, scans in the western direction of the station were acquired additionally. However, it was impossible to scan this area during the fourth epoch, since it was demolished in an early stage of the construction works.

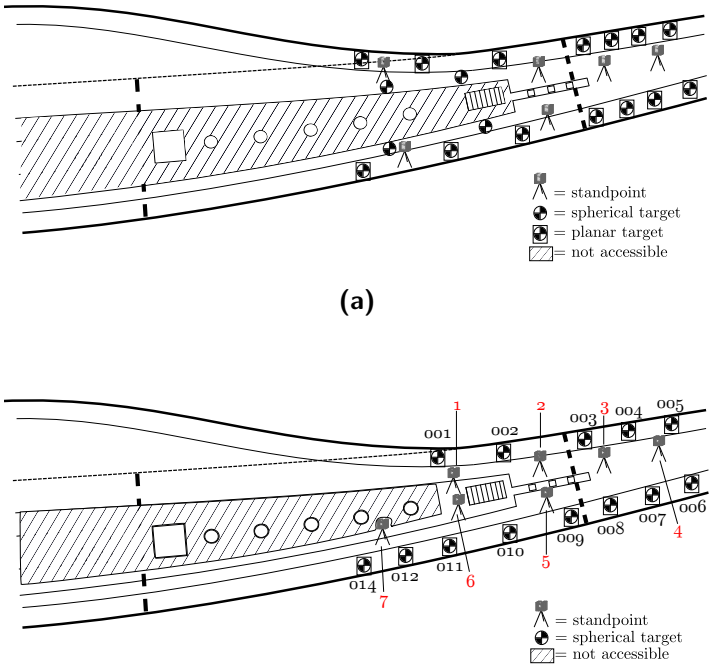

Figure 5.2: Standpoints and targets of the laser scanning survey. (a) As planned in the measurement set-up plan. (b) As placed during the acquisition.

5.1.1 Acquisition of the fourth epoch

In January 2010, in cooperation with the surveying department of the RPW, a laser scanning project was set up to acquire a new data set of the metro tunnel. Based on the previous epochs and information on the progress of the construction works, an acquisition plan is made. This measurement set-up plan describes the standpoints of the laser scanner, the number and the location of the targets. The plan is constructed in such a way that there is enough overlap between acquisitions. This overlap is required for a good registration of the scans. Enough targets should be placed in the overlapping areas. Plenty of targets are used, to avoid any unforeseen circumstances, such as occlusions. The acquisition plan with the proposed standpoints and the location of the targets is shown in Fig. 5.2a.

Even with careful preparations, the scene turned out to be a little different than expected, due to the ongoing construction works. This stresses the importance of knowledge of the scene, to optimise the preparations for the acquisition. During the acquisition, small alterations were made to the planned set-up, resulting in the standpoint locations as shown in Fig. 5.2b.

During the acquisition, three types of planar targets are placed in the scene, see Fig. 5.3. Not all of these targets are used during the registration process, but they were placed to facilitate further research on the registration. Every placed target has a unique four digit number. The first digit indicates the type of planar target, with 1 for the classic checkerboard target in Fig. 5.3a, 2 for the white circular target in Fig. 5.3b and 3 for the square checkerboard target in Fig. 5.3c. The remaining digits are used to identify the location of the target. The three types of targets are always located close to each other at one location, see Fig. 5.4.

Table 5.2: Specifications of the four laser scan acquisitions.

	Epoch I	**Epoch II**	**Epoch III**	**Epoch IV**
Acquisition date	21-04-2006	09-02-2007	20-11-2007	21-01-2010
Company	TU Delft	Fugro	TU Delft	TU Delft
Instrument	Z+F Imager 5003	Leica HDS4500	Faro LS880	Faro Photon 120
Type	Phase	Phase	Phase	Phase
Nr. of scans	3	19	7	13
Nr. points per scan	2153× 5096	2152 × 5042	3444 × 7696	3446 × 7584
Total nr. of points	33 M	206 M	186 M	340 M
Measurement precision	9 mm (20% reflec.)	14 mm (20% reflec.)	3 mm	2 mm
(at 25 m)	3 mm (100% reflec.)	8 mm (100% reflec.)		
Scan area hor.	360°	360°	360°	360°
vert.	310°	310°	320°	320°
Angular resolution	0.02°	0.02°	0.009°	0.009°

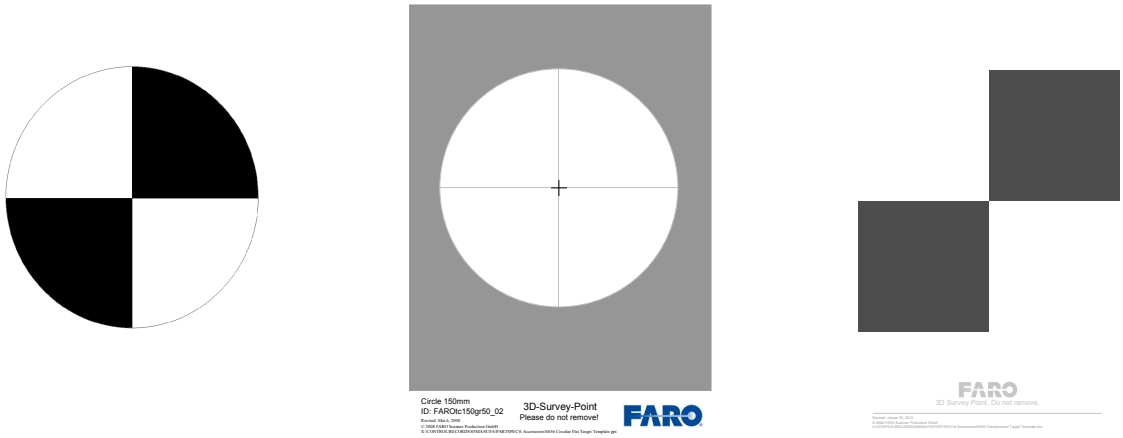

(a) **(b)** **(c)**

Figure 5.3: The three different targets used within this scanning survey. (a) The classic circular checkerboard target. (b) A new type of target, developed by Faro. (c) A square checkerboard target, also developed by Faro.

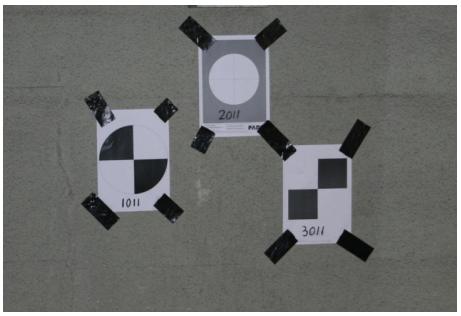

Figure 5.4: A photograph of the three targets as placed in the tunnel. The first digit represents the type of target, the remaining three digits are used to identify the location of the targets.

Table 5.3: Overview of the used registration method per epoch.

	EpochI	**Epoch II**	**Epoch III**	**Epoch IV**
Registration method	control points and object matching	control points and cloud to cloud registration	control points and object matching	control points
Registration accuracy	3 mm	3 mm	6 mm	4 mm
Georeferenced	yes	yes	yes	yes

At each standpoint, two scans were captured, except at the last standpoint. During the first eight scans, one of the metro tracks was still in use. Two trains passed roughly every ten minutes. The scans were mainly captured within two passings. Some of the scans can be influenced by passing trains, since vibrations in the tunnel may have affected the angular precision of the instrument. Moreover, heavy construction works in other parts of the metro station, e.g. drilling, may have affected the measurements as well. For each standpoint, only the first scan is used in this project.

5.2 Registration of the TLS data

During the registration process, the scans are transformed to one common coordinate frame, see Section 3.4. In this project, the registration process is performed with the software Cyclone (Leica, 2010a). For all the epochs, the registration is completed independently of the other epochs.

The software offers some possible registration methods, of which the following three are used:

- control points, i.e. planar or spherical targets,
- matching of modelled geometric objects, e.g. planes or spheres,
- cloud to cloud registration, based on the Iterative Closest Point (ICP) algorithm, see Section 3.4.4. This method requires to identify at least three corresponding points in overlapping areas.

Table 5.3 shows, per epoch, which methods are used and the reported registration accuracies after georeferencing. The registration accuracy is given by the mean squared error between the control points after the registration. The control points are also measured with a total station and the coordinates are available in *Rijksdriehoeksstelsel* and NAP (RDNAP). Therefore, it is possible to georeference the point clouds in the same absolute coordinate system, which is an important step since every scan is acquired in its own local coordinate system.

5.2.1 Registration of the first three epochs

For the first epoch, there was a registration available, performed by RPW, but with relative poor accuracy, i.e. 2.2 cm. To obtain more accurate results, this registration is redone from scratch, resulting in a registration accuracy of 3 mm. For some standpoints, not enough control points were visible, so in addition geometrical objects are matched, planes in this case. These objects are fitted to a part of the ceiling and to the floor. The registration of

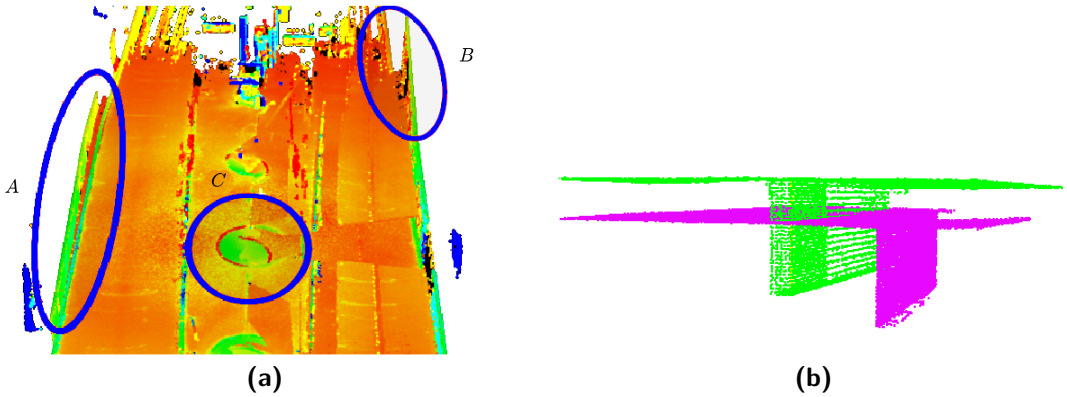

Figure 5.5: Visible registration errors in a previous available registration of the first epoch. (a) A misalignment of the scans at three regions in the scans. (b) An offset at one of the sign boards in the metro station.

the second epoch was done by Fugro. For the third epoch, additional planes were required for the registration. In addition, reference spheres are used as well. The registration of the fourth epoch is described in more detail in Section 5.2.2.

As an example, an erroneous registration is given, depicted in Fig. 5.5a. On the sides of the tunnel, indicated by A and B, the walls are clearly not properly aligned. In the middle of the scan, at location C, a pillar on the platform was scanned from two sides. After registration, the two parts of the pillar should connect but a shift is clearly visible. In Fig. 5.5b, a sign board in the metro station is shown. It was scanned from two sides. Again, it is clearly visible that the initial registration did not align the sign board correctly.

The registration results in parameters for a rigid-body transformation. The parameters obtained from Cyclone are incorporated in a Matlab script to perform the transformation, so that besides the transformed coordinates also the original coordinates, and thus the scanning geometry, of each point are available.

5.2.2 Registration of the fourth epoch

The registration process of the fourth epoch is performed in Cyclone 6.0.3 as well as in Faro Scene 4.6 (Faro, 2010). The Faro software was used because it is the manufacturer software delivered with the laser scanner. Furthermore, some of the targets used are designed by Faro to automatically be detected in their software.

In Faro Scene, it is possible to automatically recognise the checkerboard targets. Targets receive a registration label and the registration process is more or less automated allowing small user interventions if the results are not correct, i.e. if Faro has problems finding the corresponding targets. Even without any experience with the registration process in Faro, the process was completed within a few hours. The achieved accuracy, as reported by the software, is 3 mm, without georeferencing.

In Cyclone, the fitting of the targets and the registration is a manual process. For every target, first a subselection of the point cloud is created, followed by the fitting of the target and adding a registration label to the target. These steps are repeated for every target in

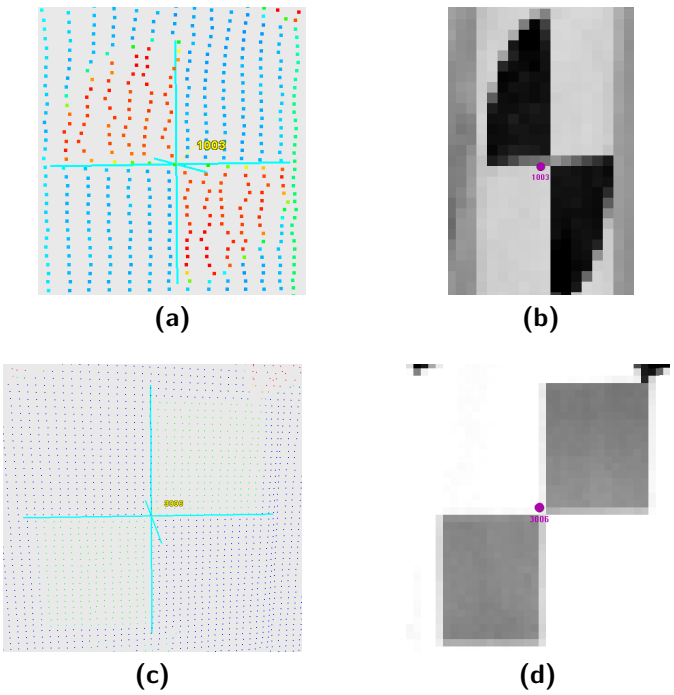

Figure 5.6: The fitted target 1003, (a) in Cyclone and (b) in Faro Scene. Due to the bad scanning geometry, the incidence angle is 64°, the distance between the vertical scan lines is up to 1 cm. This complicates the finding of the target centre for the fitting algorithm. There are approximately 300 points sampled on the target. In Faro, the estimation of the centre is off, while the fitting in Cyclone looks much better. For target 3006, (c) in Cyclone and (d) in Faro Scene, the scanning geometry is good, with an incidence angle of 20°. The result is a high point density on the target, with approximately 900 points sampled on the target. The accuracy of the centre of the target is high.

every scan. The whole registration process takes up to one day. The accuracy of the targets without georeferencing is 3 mm, with georeferencing it is 4 mm.

As said, the Faro software automatically detects the checkerboard targets in the scans. Using the intensity of the reflected laser signal, it is possible to recognise the pattern of the targets. The centre of the target is calculated at subpixel resolution. Unfortunately, this method also finds patterns that are similar to the targets but that are not. Within the acquired scans, this false detection occurred twice, on a total of 26 checkerboard targets. Requirements for the automatic detection of the targets are that there should be at least 81 measurements on the target and that the incidence angle must be smaller than 45° (Gittinger, 2010).

The fitting of the targets in Cyclone is also based on the intensities of the sampled points. A sufficient number of points on the target is required. The centre of the target is calculated from the sampled points (Cerpentier, 2010).

The estimated centre of the target is not the same for Faro and Cyclone, resulting in different coordinates for the same target. This difference can be up to several mm and depends on the scanning geometry. For instance, for the points 1003 and 3006 from scan 7, acquired from standpoint 4, the difference in scanner coordinates is 2 mm for target 3006 and almost 6 mm for target 1003, see also Fig. 5.6.

Table 5.4: The scanning geometry of the targets present in scan 7.

Target nr.	1003	3003	1004	3004	1005	3005	1006	3006	1007	3007	1008	3008
Distance to target (m)	9.56	9.82	6.18	6.04	6.26	6.59	5.86	5.61	5.24	5.54	8.23	8.62
Incidence angle (°)	53	54	29	27	38	42	36	33	36	40	62	64

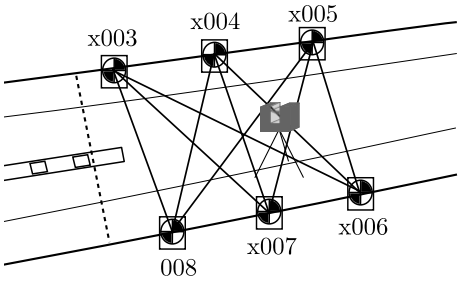

Figure 5.7: The targets visible in scan 7 and the constructed baselines.

5.2.3 Validation of the registration using baselines

To verify the registration in Cyclone, an alternative approach is used. After a initial registration, i.e. a registration without georeferencing, per scan for every target, the distances to all the other targets are calculated. These virtual lines between the targets are called the baselines, notated with $\mathbf{b}_{tls}$. The length of this baseline is given by b_{tls}. The baselines are also calculated with the coordinates that are measured with a total station, $\mathbf{b}_{ts}$, with length b_{ts}. Per scan, for each baseline the difference between the two distances is computed:

$$\Delta b = b_{tls} - b_{ts}. \tag{5.1}$$

A difference in the length of a baseline indicates that something went wrong during the registration process, i.e. the geometry of the scan is not matching with the geometry of the targets as measured with a total station.

Erroneous targets using baselines

With the method proposed above, all the baselines are identified where Δb is larger than 1 cm. In each scan, the targets that are used to construct the baseline are identified. These targets are subject to further inspection.

From the 301 baselines present in the scans, 24 are identified where Δd is larger than 1 cm. The largest error is found in scan 7, which is the first scan acquired at standpoint 4, see Fig. 5.2b. The targets that are seen in scan 7 and the baselines are depicted in Fig. 5.7. Table 5.5 shows the differences of the baselines larger than 1 cm in scan 7.

The largest difference in the length of the baseline is present in the baseline between target 3003 and 3008, 1.6 cm. Target x003 is present in almost every combination. Investigating this target in the scan shows that the point density on the target is low, which affects the ability to calculate the centre of the target, see also Fig. 5.6a. The same holds for targets x008. All four targets have in common that the incidence angle is large, i.e. between 53 and 64°, see Table 5.4.

Table 5.5: Differences in the length of the baseline using the proposed baseline method. Only differences larger than 1 cm are shown.

Target 1	Target 2	b_{tls} (cm)	b_{ts} (cm)	Δd (cm)
3003	3008	1019.0	1020.6	1.6
3003	3007	1121.0	1122.4	1.4
1003	3008	1016.3	1017.6	1.3
3003	1007	1141.7	1143.0	1.3
3003	1008	1022.8	1024.1	1.3
3004	1008	1061.0	1062.1	1.1
1005	1008	1013.4	1014.5	1.1
1003	3007	1108.3	1109.3	1.0
3003	3006	1513.3	1514.3	1.0

Table 5.6: The largest errors as reported by Cyclone, after the initial registration (without georeferencing).

Target ID	Scan 1	Scan 2	Error (mm)
3004	05	07	20
1004	05	07	18
1007	05	07	18
3012	11	13	17
3007	05	07	16
1012	11	13	16
1011	01	13	13
1011	11	13	12
3011	11	13	12
3011	01	13	11

Erroneous targets in Cyclone

Now that possible erroneous targets are identified with the baseline method, it is interesting to investigate which targets are identified as erroneous in Cyclone. Using the registration diagnostics function of Cyclone, a list of erroneous targets is generated. After the registration process, for each target in a scan, the error vector to its corresponding target in another scan is given. This is referred to as the registration error. The overall registration accuracy is the mean of all the error vectors.

The target with the highest error is not the same as the target identified with the baselines method. Therefore, the target reported as 'bad' in Cyclone may not necessarily be 'bad'. For the initial registration, the largest error is for target 3004 in scan 5 and 7, with an error of 20 mm, see Table 5.6. With an overall accuracy of 5 mm, an error of 20 mm is large. It is possible that this target is not well matched in the registration process, i.e. the best transformation is not found.

Scans 5 and 7 are dominant in the top of Table 5.6. With the baselines, these scans also have the largest errors within the scan, but not for the targets as identified with Cyclone. Removing the targets as identified with the baselines, i.e. x003 and x008, from scan 7, and repeating this procedure for the other scans, the overall accuracy of the registration improves from 5 mm to 2 mm. This is a registration without georeferencing.

Based on the numbers in Table 5.5 and Table 5.6, it is concluded that Cyclone did not find the best possible registration between the scans 5 and 7. The largest errors are given to targets that have a good scanning geometry, whereas the targets with a high incidence angle are assumed to be measured equally well. The quality of the target fitting is therefore important for the registration process.

Reproduction of the results

When trying to reproduce the results of this experiment, Cyclone found better registration parameters for the initial registration. The overall registration accuracy is 3 mm, and for none of the points the mean square error is larger than 7 mm. Furthermore, the errors for the targets x003 and x008 are among the largest. The improvement in the registration accuracy is not as spectacular as in the first experiment.

Discussion on the baseline method

The method with the baselines is used to validate the registration results from Cyclone. Furthermore, it also demonstrates a possible approach for the registration process. Cyclone neglects the scanning geometry of a target. It is shown that the incidence angle, amongst others, has an influence on the results. Incorporating this information into the registration process would be useful.

To give a better quantitative description of the differences, it is suggested to use a method from testing theory (Teunissen, 2000b). Data snooping, for example, can help to identity erroneous targets and test if the difference in the distance is significant or due to amongst others the measurement noise.

5.3 Segmentation of the registered data using QtLaserViewer

During the segmentation process, points with homogeneous properties are grouped into a segment, see Section 3.5. The software package Cyclone has a function to segment a point cloud. However, it involves a lot of manual work, since for every segment a seed point needs to be defined. The aim of the workflow is to automate the processing as much as possible. Moreover, the segmentation algorithm used in Cyclone is not made available.

The segmentation process is performed using the software QtLaserViewer, developed by Rabbani (2006), which is a program for interactive viewing, selection, editing, segmentation and fitting of point clouds. The segmentation functionality uses the smoothness constraint algorithm, as described in Section 3.5.3. The advantage of this software is that only a few parameters have to be set. Moreover, it works fully in 3D.

In this section, a small part of 8×3 m of the tunnel is used to demonstrate the segmentation algorithm. Various objects are present in this data set, varying in size, shape and orientation. Therefore, this data set is also used to find the best segmentation parameters for the whole scene. A photograph of the area is shown in Fig. 5.8a, together with a plot of the intensities, Fig. 5.8b, and a cross section of this part, Fig. 5.8c.

(a)

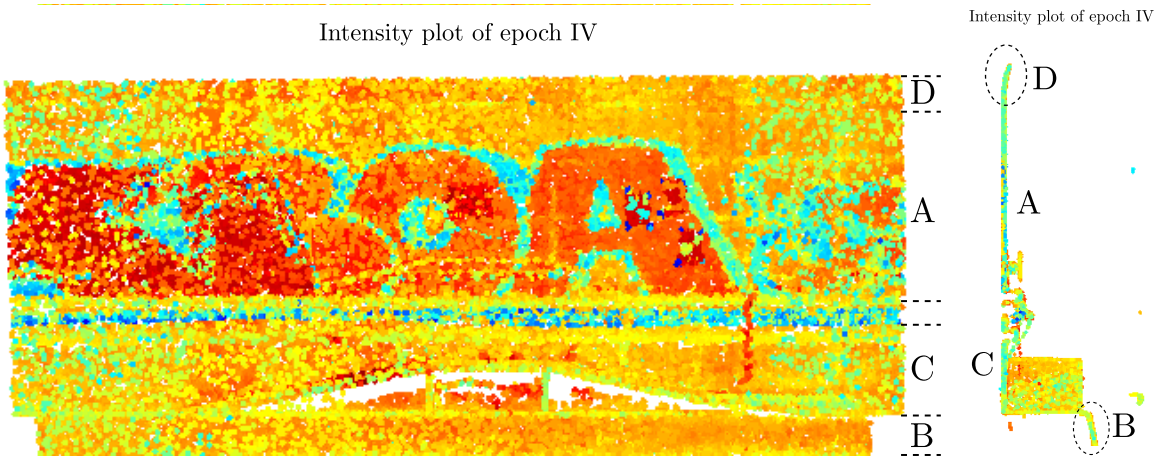

(b) (c)

Figure 5.8: (a) A photograph of a local situation in the tunnel, during the acquisition of the fourth epoch. (b) The point cloud of this part of the tunnel. The sections A to D indicate areas that are interesting for the determination of the segmentation parameters. (c) The cross section of the point cloud. The sections A to D indicate areas that are interesting for the determination of the segmentation parameters.

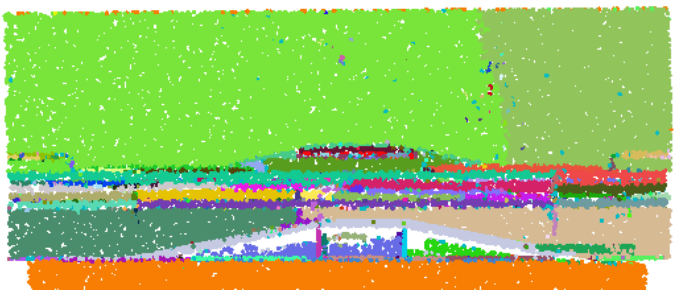

Figure 5.9: The result of a segmentation using smooth patches.

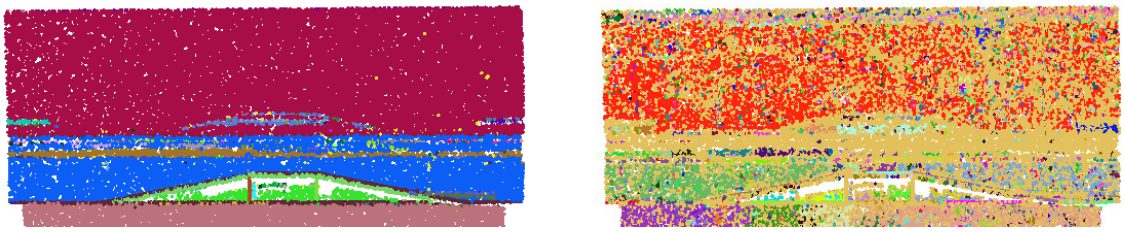

(a) **(b)**

Figure 5.10: Examples of under and over segmentation. (a) Under segmentation. The parameters are k =30, $\alpha_{th} = 50°$ and $\delta_{th} = 25$ cm. There are 122 segments. (b) Over segmentation. The parameters are k =30, $\alpha_{th} = 2°$ and $\delta_{th} = 1$ cm. There are 1750 segments.

5.3.1 Segmentation into smooth patches

The QtLaserViewer program can segment a point cloud into smooth patches. Smooth patches are suitable for curved surfaces and objects, which are present in the tunnel, e.g. the walls have a non-zero curvature. However, the results of the segmentation are not satisfying. There are many segments, 414, and the wall is split into multiple segments, see Fig. 5.9. Relaxing the segmentation parameters does not lead to a more satisfying result either. Therefore this function is not used.

5.3.2 Segmentation into planar patches

The software has a segmentation algorithm dedicated to planar patches as well, which is a modified version of the original smoothness constraint segmentation algorithm. The main difference between the two functions is that for the smooth patches segmentation a seed point is added to the current region of the angle between the seed point and its neighbours point is within the angular threshold. The neighbouring points of a seed point are added to the list of potential seed points if their residual is smaller than the defined residual threshold. In the case of planar segments, a threshold on the maximum distance to the plane of the current region, together with the angular threshold, decides whether the current seed point is added to the current region. If these two requirements are fulfilled, the neighbouring point is always added to this list of potential seed points.

Table 5.7: Overview of the segmentation parameters for various segmentations.

Segmentation nr.	**1**	**2**	**3**	**4**	**5**	**6**	**7**	**8**	**9**	**10**
k	30	30	30	30	30	20	10	20	30	30
α_{th} (°)	20	20	20	10	30	20	20	30	30	10
δ_{th} (m)	5	3	1	1	1	1	1	1	3	3
nr. of segments	414	438	425	635	296	646	1228	419	245	612

Find the segmentation parameters

Three parameters are to be set for the planar patches segmentation:

- k, the number of nearest neighbours,
- α_{th}, the angular threshold,
- δ_{th}, the distance threshold.

Finding the right parameters for the segmentation is a subjective task. It is difficult to decide on what the best parameters are, since it is a trade-off between under and over segmentation. Fig. 5.10a and Fig. 5.10b show cases of under and over segmentation for this example data set. Fig. 5.10a hows under segmentation, because the region located between regions A and C is merged with region C. As is shown in Fig. 5.8a, there are water pipes in this region, which should not result in one single planar segment.

The best parameters are found using experience, i.e. knowledge of suitable parameters for certain cases, and manual inspection of the segmentation results. To find the best parameters, the areas indicated with A to C in Fig. 5.8b and (c) are used. Knowing how these sections are in real life helps finding the best parameters.

Various segmentations are performed, using different segmentation parameters. Table 5.7 shows the number of segments for the used parameters. Visualisations of some of these segmentations are given in Fig. 5.11.

For this scene, the most important requirement is that the upper part of the wall, region A in Fig. 5.8b, is segmented as one segment, which is the case for all the chosen parameters. Further noticeable differences are in the lowest segment, B, which is segmented in one to even three segments, and the upper most segment, C, which differs in height. Setting the nearest neighbours parameter k to 10 results in many segments, compare segmentation 3, Fig. 5.11a, and segmentation 7, Fig. 5.11c. In the latter segmentation, k is set to 10, which results in three times as much segments, if the other parameters are fixed. If k decreases, less neighbouring points are used to calculate the normal, which causes more variation in the orientation. The difference between $k = 20$ or $k = 30$ merely influences the small segments, the larger segments are comparable. The number of segments reduces approximately by 30% if k is set to 30 instead 20.

The angular threshold α_{th} plays a key role in which points are added to the region. If this angle is set too large, points with a deviating orientation are still added to the plane. Setting α_{th} to 10° makes the algorithm sensitive to small variations in the orientation. Values of 20° or 30° affect the total number of segments, which decreases with increasing angular threshold.

Segmentation 3

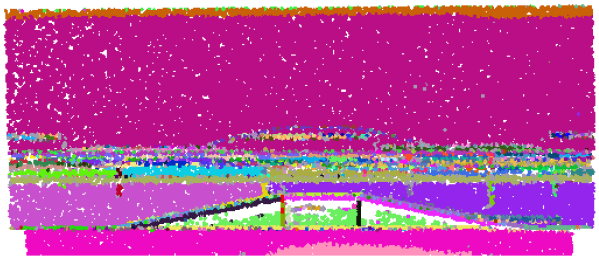

(a)

Segmentation 5

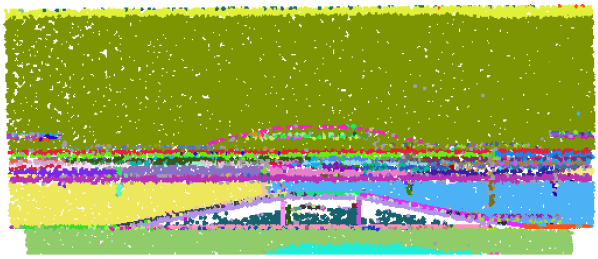

(b)

Segmentation 7

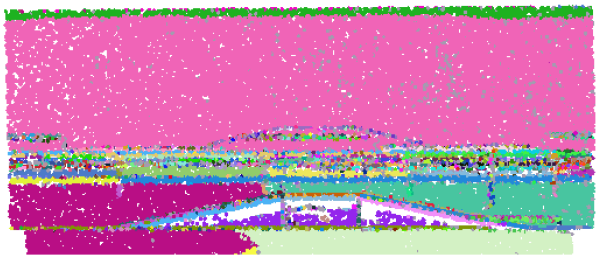

(c)

Segmentation 9

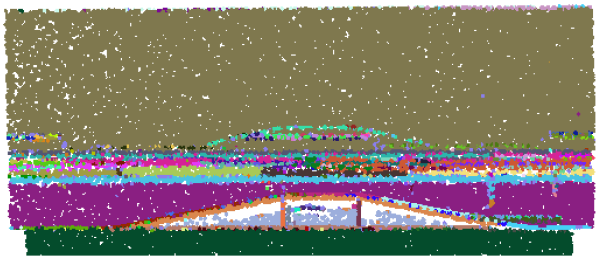

(d)

Figure 5.11: The results of the segmentation process for different parameter values. The parameters that are used are given in Table 5.7.

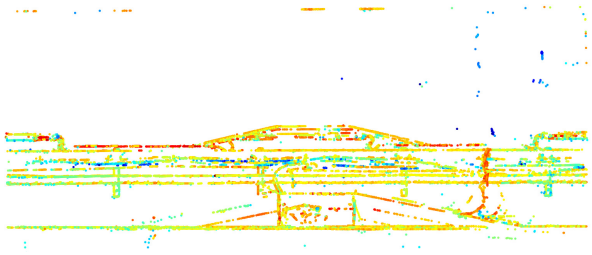

Figure 5.12: Points in the point cloud that did not get a segmentation label, with segmentation parameters $k = 30$, $\alpha_{th} = 30°$ and $\delta_{th} = 3$ cm.

The surface of region B is approximately planar. If the distance threshold is set to 3 cm or higher, it results in one segment. This leaves segmentation 1, 2 and 9 as possible best segmentations. The final decision is based on the region C. Region C also forms a planar surface. Only in segmentation 9 this region results in one segment, see Fig. 5.11d. Therefore, the final segmentation parameters are set to:

$$\begin{aligned} k &= 30 \\ \alpha_{th} &= 30° \\ \delta_{th} &= 3 \text{ cm} \end{aligned}$$

Region D illustrates the effect of edges on the segmentation result. In this region, the surface of the wall is connected to the ceiling with a fillet. Using a larger value for α_{th}, more points of region D are added to the segment of region A, or the other way around, depending on the order of the region growing. In addition, it is seen that δ_{th} affects the result. Points on the fillet are further away from the plane through region A. The larger the distance threshold, the more points are added to the segment of region A. In all cases there is a transition area where points can be assigned to either two of the segments.

5.3.3 Outliers during the segmentation process

There are points that are not assigned with a segmentation label during the segmentation process. These points do not meet the segmentation criteria, for example when their distance to a segmented region is too high. Often these points are located on edges of objects, or the points are single and isolated, see Fig. 5.12. In both cases, many of their neighbouring points do get a segmentation label. The result is that only a small amount of the point cloud is not segmented, in this case 1.4% of the points.

5.4 Identify corresponding segments

During the identification of corresponding segments, two segmented point clouds are compared. For every segment, corresponding segments in the other point cloud are identified. Two conditions are defined in Section 5.4. These conditions are specific for planar segments. If both conditions are fulfilled, the segments are considered to correspond and are used for a deformation analysis. If not, the segment indicates a possible change.

5.4.1 Condition I: segments are in the same plane

The first condition compares the orientation and the distance between two segments from two different point clouds. The first requirement is that the difference in the orientation of the two segments is below the threshold, α_{th}, which is set to 10°. This value of the threshold allows for small differences in the orientation of the segments, e.g. caused by the scanning geometry, whereas larger differences indicate that the segments do not correspond. When the variation in the orientation is too large, there is possibly a change.

The next step is to use a threshold for the distance between the segments. The threshold for the distance is set to 10 cm. The distance threshold is important to distinguish between changes and deformations. If the distance between two segments that represent the same object surface is greater than the distance threshold, a possible change occurred and the segments are not subject to a deformation analysis. The larger the distance threshold, the larger the deformations can be and the larger the changes have to be before they are detected. The expected deformation is up to 5 cm, see Section 2.4.

5.4.2 Condition II: segments must intersect

The second condition is that two potentially corresponding segments have a non-empty intersection. In Section 4.3.2, it is described that the convex hull is used to find this intersection. Only the points that are inside the convex hull form the corresponding segment.

A disadvantage of the convex hull is that concave areas in a segment is not noticed by the convex hull, which is illustrated in Fig. 4.6. To overcome this problem, a maximum distance from a point in S^{II} to the corresponding segment in S^{I} is defined, by means of a threshold. If this distance is greater than the specified threshold, the point is assumed to be located inside a concave area and it does not belong in that corresponding segment. The threshold is set to 5 cm.

Instead of calculating a distance to every point in the corresponding segment, an alternative approach is used. A threshold value of 5 cm results in a small search box of 10×10×10 cm, with the point of interest in its centre. The algorithm tries to find a point in the segment that is located within the box. If there is such a point, the segment is considered close enough and the point of interest is not within a concave area. If there is not a point in the segment that is located within the search box, the point of interest is likely in a concave area and it is not considered for this segment.

5.5 Change detection

All the points that are not assigned to a corresponding segment are considered as a possible change. As explained in Section 3.6, a lack of corresponding segments is caused by either a real change or by occlusion of one of the surfaces. A possible approach to distinguish between changes and occlusions is presented in Section 4.4. However, this approach is not implemented in this thesis.

5.6 Deformation analysis

Per segment of epoch II, for each point the distance to the surface representation of the neighbouring points in epoch I is calculated. Since it is done per segment, it is easy to calculate an average distance per segment. It can be used to identify segments showing a large deformation. These segments can be investigated in more detail.

The algorithm finds for the point of interest the 20 neighbouring point in the corresponding segment, which is done by calculating the distances to all the point in this corresponding segment. If the segment contains many points, this step is time consuming. To reduce the computation time, a search window of +/- 20 cm in each direction is used. Points in the segment from epoch I that are located further away than 20 cm from the point of interest are not considered. If this leads to less than 20 nearest neighbours, less points are used. While the aim of the k-nearest neighbours (kNN) approach is to anticipate for varying point densities in a point cloud, the search window is used to neglect points that are too far away.

Chapter 6

Results and discussion

6.1 Introduction

In this chapter, the results of the application of the change detection and deformation analysis procedure on the available tunnel data are given. Processing laser scan data can be very demanding for computer memory. For the fourth epoch, there are approximately 175 million data points, which results in an ASCII-file of 8 GB. The segmentation software is not designed to work with such large files. Pointwise distance calculations, e.g. for the deformation analysis, are also time consuming if very large point clouds are processed. Therefore three case studies are chosen to demonstrate most aspects of the workflow. All cases consider smaller subsets of the full data set, focussing on parts of the tunnel.

The first case deals with a part of the wall from the old metro station. Two scans from epoch I are used. The case illustrates the registration analysis, which is similar to a deformation analysis, but the distance between two scans is mainly caused by the registration process. Furthermore, occlusions in the data set are identified. The second case study concerns the area that is also used in Chapter 5, called 'the footbridge'. The footbridge is placed between two acquisitions and should be detectable with the proposed method. The third case covers the main area of interest in the tunnel: joint number 4, below the *Nationale Nederlanden* building. In Section 2.4 is shown that deformations of a few cm are expected here. Furthermore, this area is intensively monitored, which enables a validation of the measured deformation. Fig. 6.1 shows the locations of the case studies in the metro station and tunnel.

For each case, a brief description of the data is given, followed by the results of the registration and segmentation process. The focus is put on the change detection and deformation analysis steps. The results are discussed and validated using the available deformation monitoring data, as described in Chapter 2.

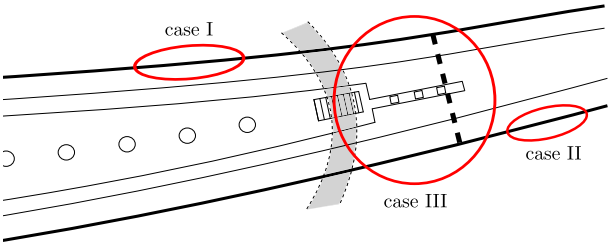

Figure 6.1: Overview of the locations of the case studies.

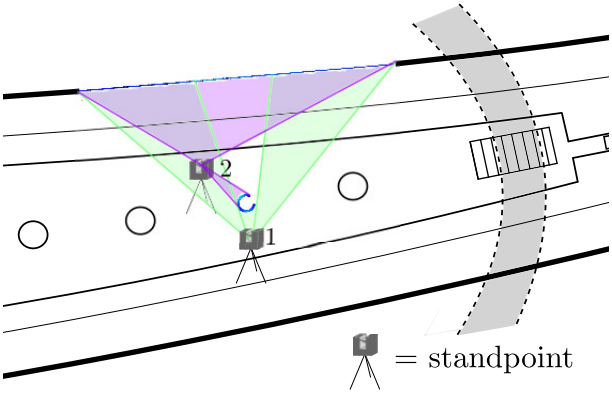

Figure 6.2: Location of the data set of the first case study in the metro station, with the two standpoints. For each standpoint, the visible objects in the data set are shown.

6.2 Case study I: wall old metro station

The first case study demonstrates the use of the proposed method for the registration analysis and occlusion mapping, see also Fig. 4.1. The method of the registration analysis is equal to the deformation analysis, but instead of two point clouds from two different epochs, two scans from the same epoch are used. It is assumed that no deformation occurred between the two acquisitions, so that the distance between the scans is the results of the registration process. Instead of the registration accuracy of the targets, provided by the registration software, an overview of the registration accuracy for the complete data set is available, and areas where the registration is less accurate are identified.

Given that the scans are acquired at the same epoch, there are no changes. Points that are marked as a potential change are not sampled in the other scan, which must be caused by occlusions. Occlusion mapping is a useful tool to identify surfaces or objects that are not sampled in both scans.

6.2.1 The data set

The data set represents a part of the metro station wall, with an area of 17×3 m. The location of the selection is shown in Fig. 6.2.

This data set is acquired at the first epoch. Two scans were made from the standpoints indicated in Fig. 6.2. The two scans of the wall are shown in Fig. 6.3. The number of points in both scans is shown in Table 6.1.

Table 6.1: The total number of points, the number of segments, the number of points that are marked as an outlier during the segmentation process and the number of occluded points for scan 1 and 2.

	Scan 1	**Scan 2**
Points	405,498	868,244
Segments	15	11
Outliers	3,648	2,226
Occluded points	210,010	375,482
Registration analysis	-	309,934

In the data of scan 2, see Fig. 6.3b, there is an area with no data in the middle of the graffiti area. The laser scanner sampled these points with an incidence angle close to 0°, on a distance of a few meters. In combination with the graffiti, the reflected intensity of the laser signal is too strong to accurately determine the range. These points are located a few dm behind the wall and were excluded during the data selection.

6.2.2 Registration

The two scans are registered and georeferenced according to the procedure described in Section 3.4. Since the two scans are taken at the same epoch, georeferencing is actually not required to compare the two scans. However, this process is still performed to incorporate the effect of georeferencing.

6.2.3 Segmentation

The next processing step is the segmentation of the scans as described in Section 3.5.3. The results of the segmentation process are shown in Fig. 6.4, Table 6.1 shows the number of segments. As expected, large parts of the walls result in single segments. Smaller segments are present only near the edges. The pillar results in vertical segments, since the segmentation process groups points in approximately planar segments. These planar segments have the largest extent in the vertical direction of the pillar.

Points that did not receive a segmentation label are shown in Fig. 6.5, indicated by the black circles. Table 6.1 shows the number of outliers for both scans. For scan 1, these points are located on the edge of the walls, on the pillar and on the graffiti. For scan 2, a large amount of the outliers is located on the graffiti. The outline of the graffiti is noticeable and has a dark blue colour, which means a low reflected intensity. Most likely the paint on the surface influences the reflection of the laser signal, resulting in an error in the range measurements. The points are located closer by or further away than their surrounding points and therefore considered as outliers during the segmentation. Moreover, the points coloured in red, which represent high reflected intensity, are located on the graffiti. The light blue points are located on the pillar.

As discussed in Section 4.4, the outliers are expected to be single points that are different from their surrounding points. Changes will influence more than single points. Therefore these points do not indicate changes.

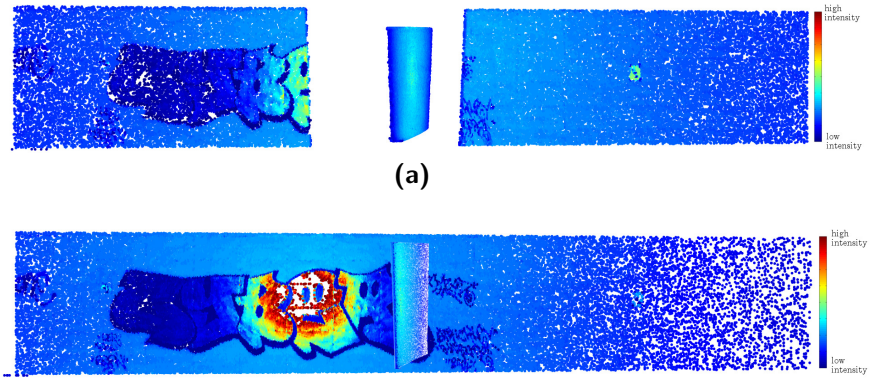

(a)

(b)

Figure 6.3: Two scans coloured with intensity. Both scans are acquired at the same epoch, from a different standpoint. (a) Scan 1, obtained from standpoint 1. The object in the middle is a pillar in the metro station, occluding the wall located behind. (b) Scan 2, obtained from standpoint 2.

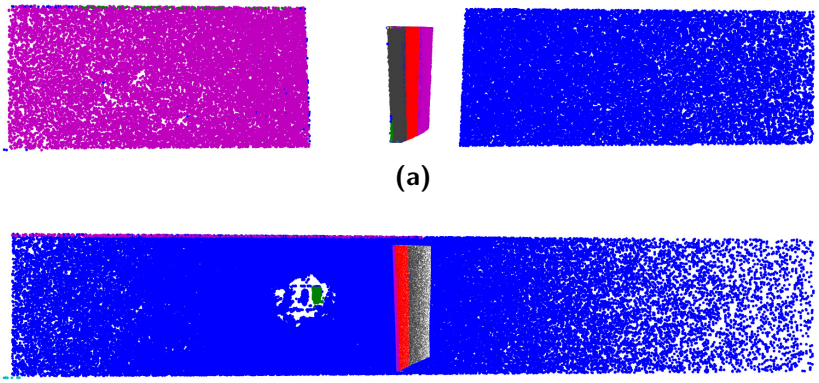

(a)

(b)

Figure 6.4: Segmentation results. (a) Scan 1. The cylindrical pillar is segmented in planar segments, resulting in many vertical segments. (b) Scan 2. Many segments are located on the pillar.

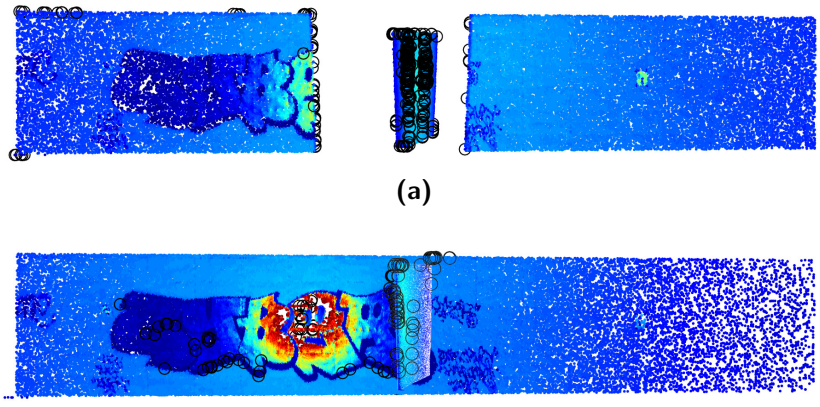

(a)

(b)

Figure 6.5: The outliers during the segmentation process are indicated by the black circles. (a) Scan 1. (b) Scan 2.

6.2.4 Identification of corresponding segments

The segments from the segmentation process are used for the identification of the corresponding segments. The result of this step is shown in Fig. 6.6. There are two segments in scan 1 that have a match in scan 2.

The two sampled parts of the pillar have a small overlap. However, the identification of the corresponding segments did not find matching segments in this overlapping region. As seen from Fig. 6.4a, the segmentation process segments the pillar in elongated vertical planar segments. Since the surface has a curvature in one direction, planar segments are not suitable. Furthermore, the algorithm uses the orientation of the planar segments as one of the measures for the correspondence. When two segments do not represent the same (overlapping) part of the pillar, the orientation will differ too much and there is no match.

6.2.5 Occlusion mapping

A segment in a scan does not necessarily have a corresponding segment in another scan. If a surface is only sampled in one of the scans, there is no correspondence. In this case, this is often due to occlusion, where a part of the surface is not visible from a standpoint, i.e. there is an object in the scene blocking the line-of-sight to the surface. Fig. 6.7 shows the occluded points in both scans.

The possible occlusions in Fig. 6.7 are divided in three groups, based on their location in the data set:

- the big area in the middle of the wall,
- the edges of the segments,
- the pillar.

Occlusions in the middle area of the wall

The most remarkable area identified as a potential occlusion is located in the middle of the considered wall. There is no corresponding segment for these points from scan 2. This occlusion is expected based on the scanning geometry: in the first scan, the pillar blocks the view of the laser scanner towards a part of the wall, see Fig. 6.2.

Occlusions near the edges

The points near the edges are affected by the edge effect, see Section 4.4, and the data set selection. Fig. 6.8 shows for each scan the original segment for the possible occluded points. The points in the top of both scans belong to a narrow segment. Since it is hard to compute the correct orientation for such segments, they are not identified as representing the same surface. However, there is no occlusion in this case. Moreover, the points on the right side of the wall were not occluded. The identification of the corresponding segments algorithm filters points located too far away from a possible corresponding segment. As shown in Fig. 6.3b, the point density for this area in scan 2 is lower than for the same area in scan 1.

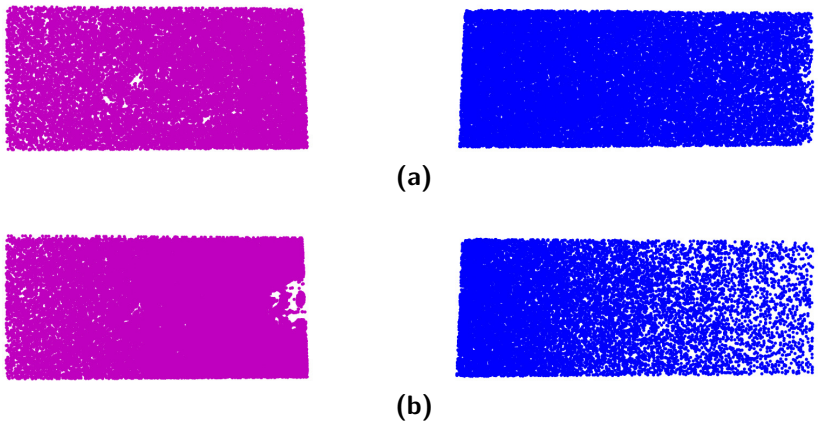

Figure 6.6: The corresponding segments in (a) scan 1 and (b) scan 2.

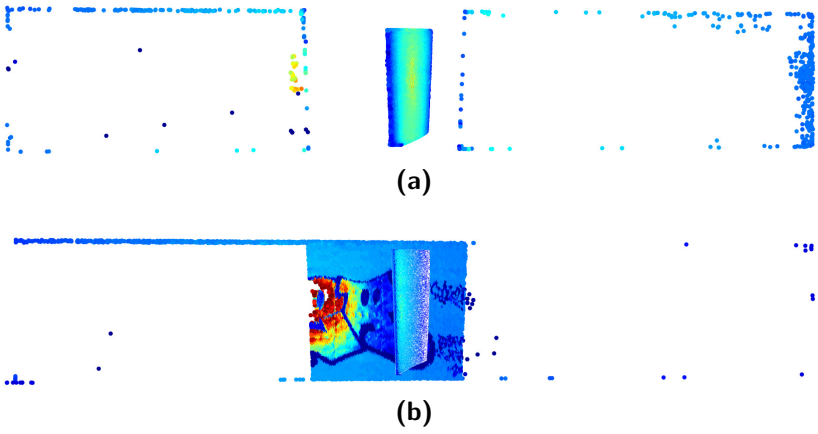

Figure 6.7: Occluded areas in the scans. (a) The occlusions in scan 1. (b) The occlusions in scan 2.

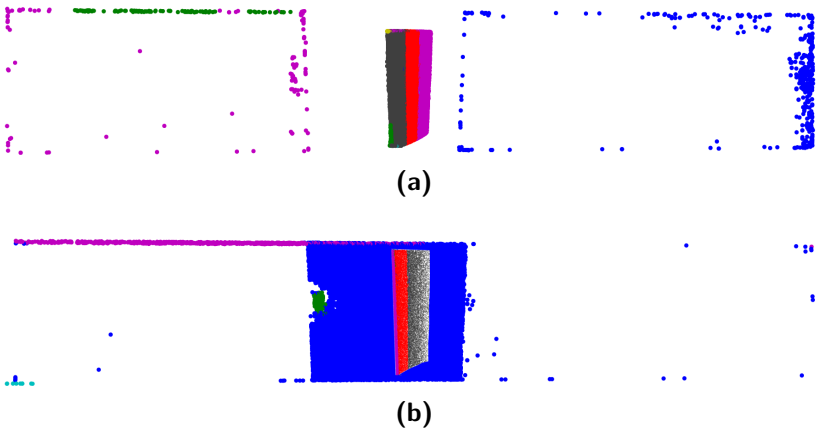

Figure 6.8: Occluded areas in the scans, using the original segmentation labels. (a) The occlusions in scan 1. (b) The occlusions in scan 2.

Occlusions on the pillar

The points on the pillar are identified as an occlusion. A small part of the pillar is sampled in both scans. In Section 6.2.4, it is discussed that the segments of the overlapping areas are only matched if the segments represent the overlapping area. The parts of the pillar that are only sampled in one scan are occluded, in this case by the object itself.

Example: the distinction between changes and occlusions

This data set is suitable to demonstrate the difference between changes and occlusions, discussed in Section 4.4, since the pillar occludes part of the considered wall. The distinction between change and occlusion is difficult to make. If the second scan is acquired at another epoch, it would be difficult to assess whether the possible change is a real change or an occlusion. The proposed solution is to use the scanning geometry. The question is whether the points that are marked as a potential change are sampled in both epochs or only in one epoch.

Scan 2 is transformed to the coordinate system of the standpoint of scan 1, using the transformation parameters from the registration process. Fig. 6.9 shows the 2.5D representations of both scans, as seen from their original standpoint, whereas Fig. 6.10 shows both scans as seen from the standpoint of scan 1. The scans are coloured with the intensities.

The two images of Fig. 6.10 are compared to investigate whether the surface that is identified as a potential change is sampled in both scans. Fig. 6.7 and Fig. 6.8 identify the pillar as a potential change. According to Fig. 6.10, the pillar is present in both scans and located at the same position. Therefore, it is concluded that the pillar is not a change. Points that were sampled in scan 1 were occluded in scan 2, which is due to the different standpoints. Note that in the ideal case the overlapping part on the pillar would be marked as corresponding.

The part of the wall that is located behind the pillar is only sampled in scan 2, see Fig. 6.7. The 2.5D representation of scan 1, see Fig. 6.10a, shows that the pillar blocks the view. This pillar is also present in scan 2, see Fig. 6.10b, and is at the same position. Therefore it is due to the scanning geometry that a part of the wall is not sampled and there is no change, but occlusion. If there would be no pillar in scan 2, the object blocking the line-of-sight is only present in scan 1. In that case, the possible change in scan 2 is indeed the result of a change in the scene.

6.2.6 Registration analysis

The segments that correspond are compared during the registration analysis step. Fig. 6.12 shows the distance between the points in scan 2 and a local surface in scan 1, using the approach described in Section 4.5. Table 6.1 shows the number of points in scan 2 for which the distance is calculated.

The median distance between the two scans is -1 mm. The median is used because it is more robust than the mean in case of outliers in the data. The Median Absolute Deviation (MAD), which is a robust version of the standard deviation, is used to describe the spread of the distances around the median value. The MAD is 1 mm. Furthermore, the distance

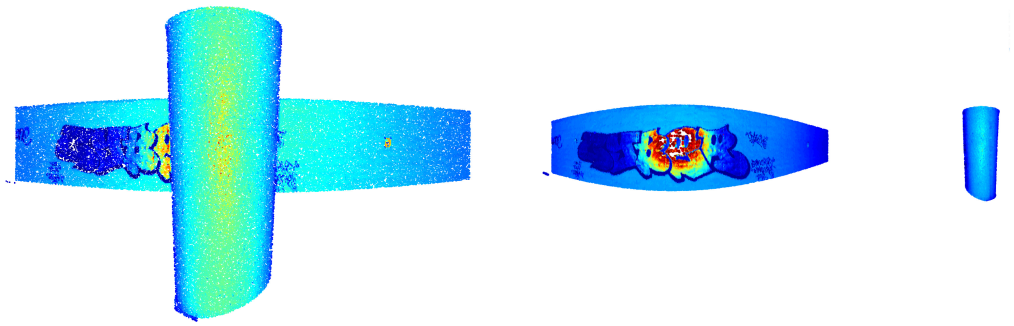

(a) (b)

Figure 6.9: The 2.5D representation of the scans, coloured with intensity. (a) Scan 1. (b) Scan 2.

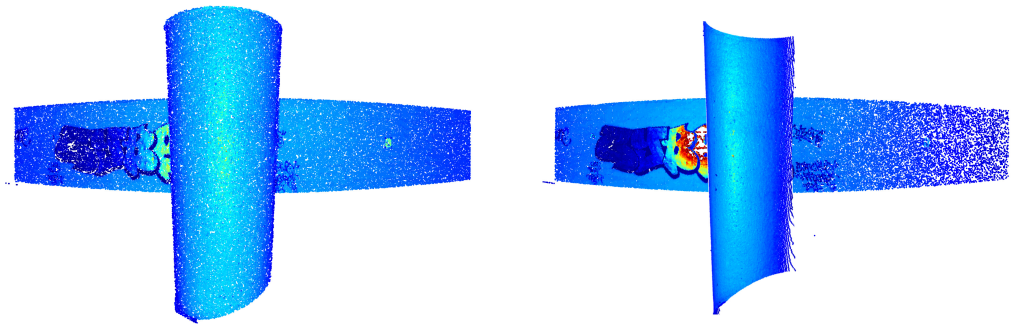

(a) (b)

Figure 6.10: The 2.5D representation of the two scans, as seen from the standpoint of scan 1. (a) Scan 1. (b) Scan 2.

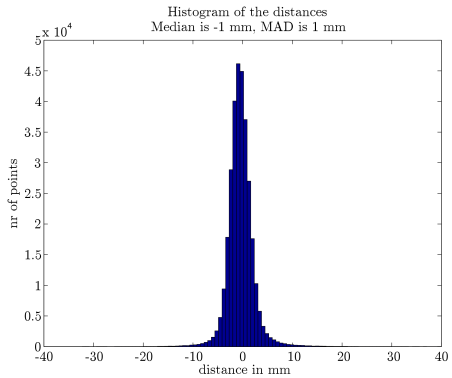

Figure 6.11: The histogram of the computed distances between the points in scan 2 and a local surface representation in scan 1.

distribution is not necessarily symmetric. However, in this case, the histogram of the distances has a symmetric distribution, see Fig. 6.11.

It is concluded that for this part of the metro station, the walls are registered with a high accuracy. The negative distance between the two scans means that the points of scan 2 are on the inside of scan 1, i.e. closer to the scanner. Fig. 6.13 shows whether the distance is positive (red) or negative (blue) for a point in scan 2.

On the left side, the wall is a mix of positive and negative distances. This makes sense, since the median distance is close to zero. In the segment on the right, negative distances are in the majority. Fig. 6.12 and also Fig. 6.14 show that the distances increase towards the right side of the segment. This could mean that the walls are slightly rotated. To verify the rotation, other areas in the full point cloud of epoch 1 should be investigated.

Fig. 6.14 shows the average distance in a regular grid, which is created by rotating the points of each segment to the xy-plane, placing the normal of the segment parallel to the z-axis. The points are binned using a bin size of 10×10 cm. For each grid cell, the average value of the distance to scan 1 is calculated. An advantage of using the average distances is that it reduces the noise. Fig. 6.15 shows per grid cell the standard deviation of the calculated distances.

Influence of the graffiti

In Fig. 6.12 the outline of the graffiti is visible in the distances between the two scans. When the distances are averaged per grid cell this effect disappears. The graffiti results in noisy results. This is explained by the measurement precision. The paint of the graffiti, especially black paint, influences the reflection of the laser signal, decreasing the point precision. The resulting distances for these points are larger than for other points on the wall. The standard deviation of grid cells containing 'graffiti points' is higher, see Fig. 6.15. When the average distance per grid cell is considered, the graffiti results in a slightly higher error compared to areas without graffiti.

Influence of the point density

Fig. 6.16 shows the number of points in each grid cell. The regular grid is based on the points in scan 2 for which a distance is calculated. In the centre of the wall, the point density is the highest. As expected, the point density decreases towards the sides. The incidence angle and the range increase and therefore the distance between two adjacent scan lines increases, reducing the number of points in a grid cell. In the left segment, there is a vertical stripe of grid cells with a high point density, due to an error in the data set. The laser scanner probably sampled this stripe twice during the acquisition and the additional points were not removed from the data set.

Influence of edges

Fig. 6.14 shows that the left edge of the right segment has larger distances. Fig. 6.16 shows that the point density is very low for these grid cells. This is caused by the method that is

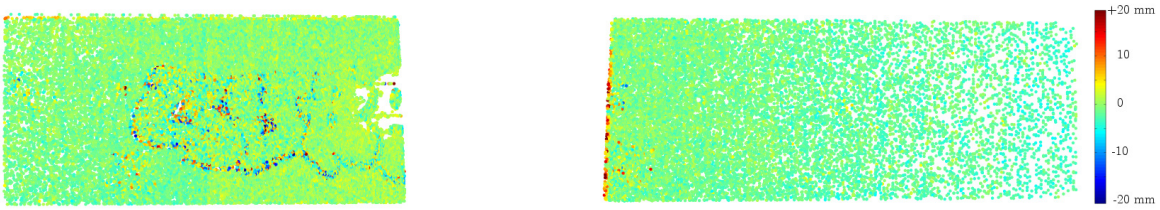

Figure 6.12: The distances between the points in scan 2 and a local surface representation in scan 1. Only the corresponding segments are used for this step.

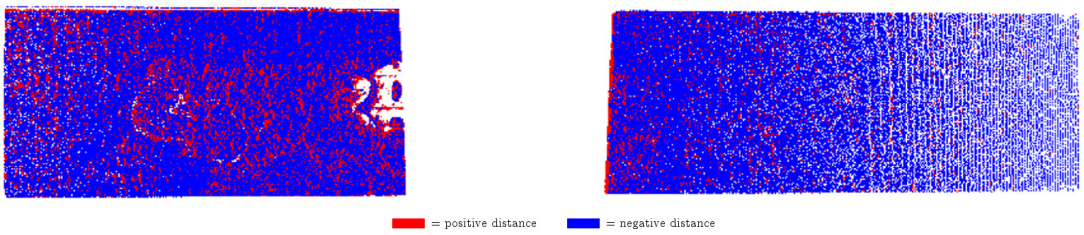

Figure 6.13: The distances between the points in scan 2 and a local surface representation in scan 1. The red points indicate a positive distance, the blue points a negative distance.

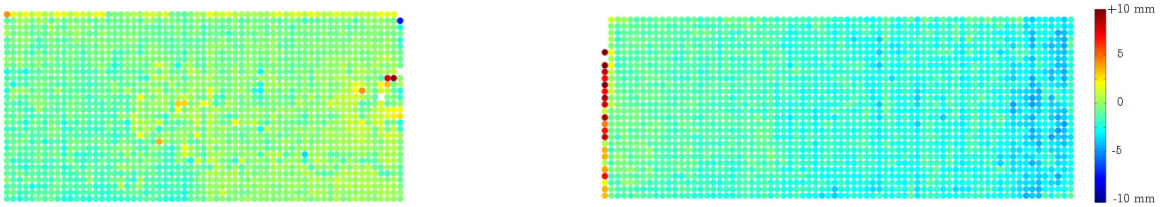

Figure 6.14: The distances averaged per grid cell between the points in scan 2 and a local surface representation in scan 1.

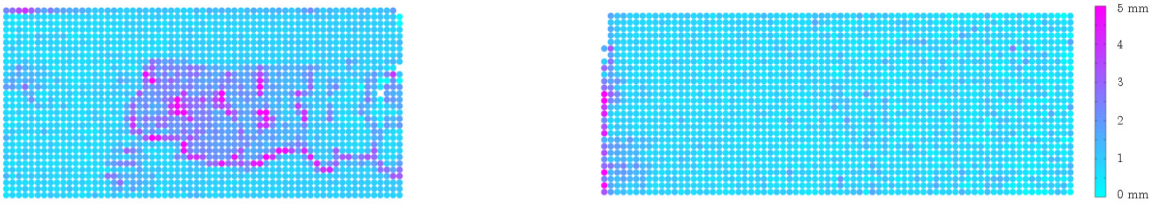

Figure 6.15: The standard deviation per grid cell of the distances between the points in scan 2 and a local surface representation in scan 1.

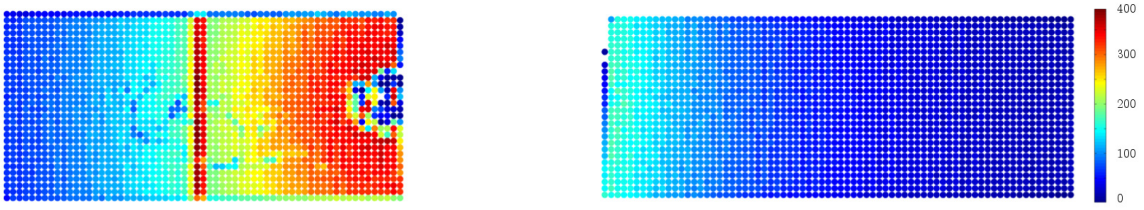

Figure 6.16: The number of points in each grid cell.

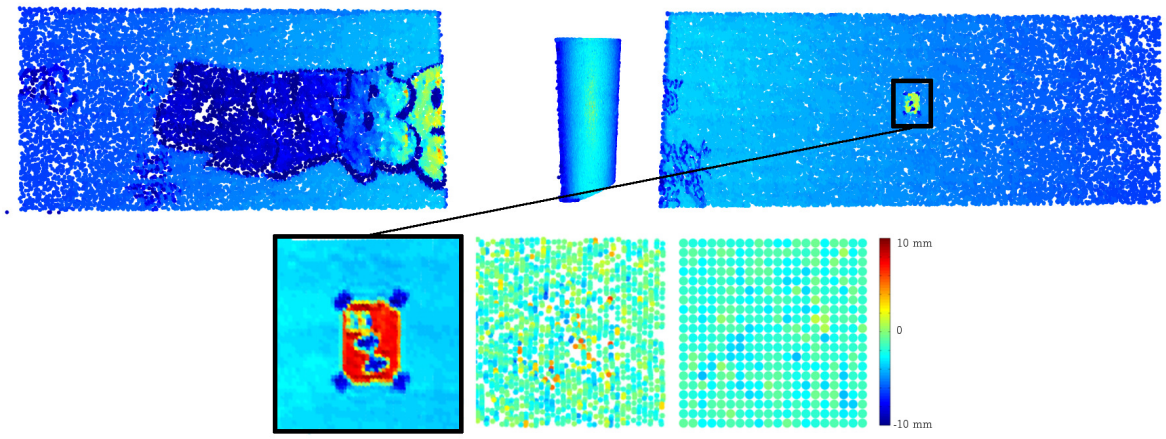

Figure 6.17: The location of the target on the wall. In the bottom row from left to right: a close-up of the target with the intensities measured on the target, the calculated distances, and the calculated distances averaged in regular grid.

used to create the regular grid. The edge of the segment is skew, but the grid is rectangular. Therefore it is expected that the point density in a grid cell is low. However, Fig. 6.12 also shows that there are larger distances for these points. Most likely these are caused by edge effects. In scan 1, these points are just visible and the laser signal travels straight past the pillar. It is not known where the signal reflects exactly. It is well possible that the travel path of the laser signal is affected by the pillar, which could result in a longer range.

6.2.7 Validation of the results

The calculated distances between the two scans should be validated using other measurements. The only possible validation of this case study is to use the registration results from the software Cyclone. The software reports the registration accuracy for the used targets. There is one target present on the wall, which location is shown in Fig. 6.17.

The registration accuracy that Cyclone reports is given by the vector between the target in the first scan and in the second scan after the registration. The length of this vector is 4 mm. The vector has of a x, y and z-direction and the magnitude of the error varies with the dimension. The error is the largest in the x-direction: 4 mm. The x-direction is given in the *Rijksdriehoeksstelsel* and NAP (RDNAP) coordinate system and is approximately along the tunnel direction. The error in the y-direction is 2 mm, which is across tunnel direction. The computed distances during the registration analysis are perpendicular to the local plane and, in the case of the considered wall, across tunnel direction. The error in the z-direction is neglectable.

The absolute error in the y-direction should describe the same error as the computed registration accuracy. From Fig. 6.17 is seen that the signed distance between the scans, at the location of the target, varies between 0 and -5 mm. The absolute average value of all the grid cell values is 2 mm. The used method therefore corresponds with the results from Cyclone.

In the next case studies the method is validated using other measurement techniques as well.

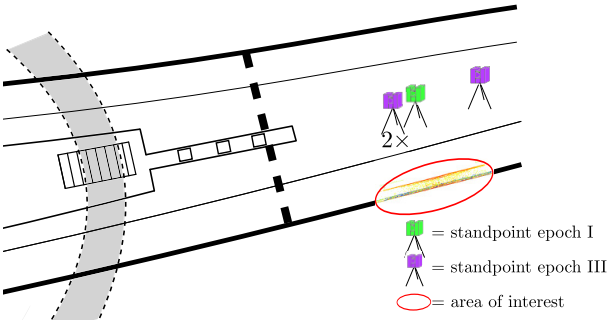

Figure 6.18: Data location and standpoints of the footbridge case study.

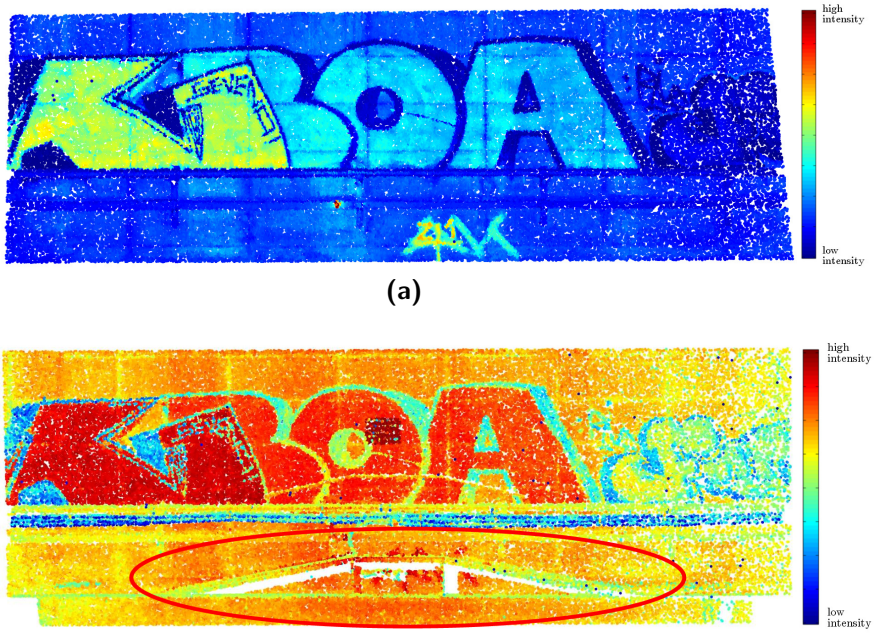

Figure 6.19: The measured intensities for the two point clouds. (a) The point cloud of epoch I. (b) The point cloud of epoch III, with the location of the footbridge indicated by the red ellips.

6.3 Case study II: the footbridge

The second case study demonstrates the change detection possibilities of the proposed method. The data set is selected from point clouds of two different epochs. It is known that a small footbridge was placed between the two acquisitions. Furthermore, this case also shows unexpected deformations.

Figure 6.20: A photograph of the footbridge, taken in January 2010. The situation is not exactly the same as in the point clouds of epoch I and III. For example, the lamps were placed after epoch III. Some features in the photograph are identified, these will be used in this case study. A: the footbridge. B: the hand rail. C: a metal bar. D: a mounting bracket. E: water pipes. F: a metal tube.

6.3.1 The data set

For this case study, the point clouds from the first and third epoch are used. Specifications of these epochs are given in Table 5.2. The selected area covers an area of 8×3 m of the wall on the southern side of the tunnel. During the first epoch, approximately 350 thousand points were sampled at this specific part of the tunnel, from one standpoint. During the third epoch, 3.5 million points were obtained, from two different standpoints. From one of these standpoints, two scans were made, resulting in three available scans in this epoch. Table 6.2 shows the exact number of points per data set. Fig. 6.18 shows the location of the standpoints in the area of interest.

The two point clouds are shown in Fig. 6.19. In both figures, the reflected intensities are shown. The colours of the intensities are different because two different laser scanners were used. The intensity is an uncalibrated product and can therefore differ per instrument. The difference in the point density is not visible in these figures because the visualisation is limited to a maximum of one hundred thousand points.

6.3.2 Registration

The scans from epoch I and III are registered per epoch. To compare the two point clouds, georeferencing is necessary, to transform the point clouds from the two epochs to the same absolute coordinate system. Section 5.2 describes the registration process in detail.

6.3.3 Segmentation

The segmentation process is applied to divide the point clouds in groups of points that belong to the same plane. A plane is a suitable surface representation for this data set, because the wall is approximately planar. Moreover, the largest object present in the data set, a footbridge that is placed in front of the wall, consists of planar parts, see also Fig. 6.20.

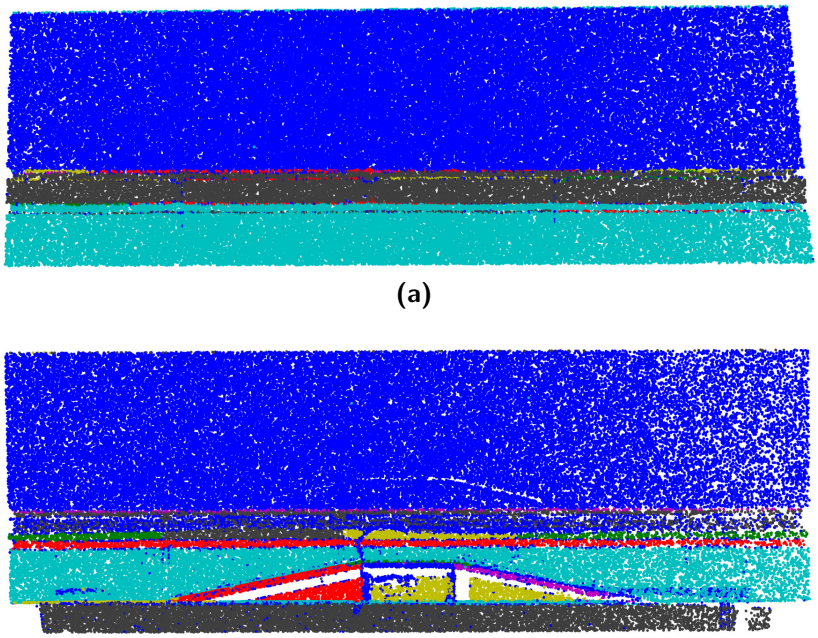

(a)

(b)

Figure 6.21: Segmentation of the two point clouds. (a) The segmented point cloud of epoch I. (b) The segmented point cloud of epoch III.

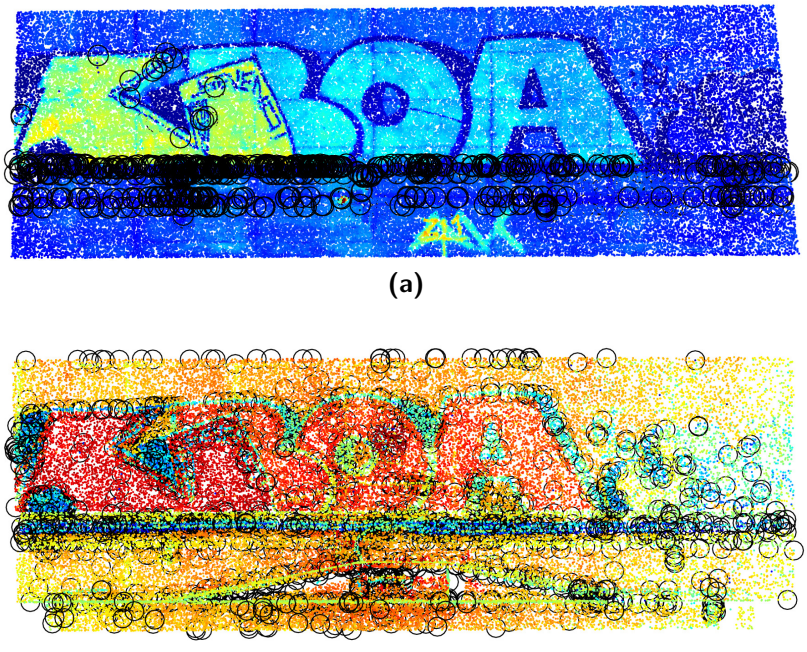

(a)

(b)

Figure 6.22: Outliers during the segmentation process of the two point clouds indicated with the black circles. (a) The outliers in the point cloud of epoch I. (b) The outliers in the point cloud of epoch III.

Table 6.2: The total number of points, the number of segments, the number of points that are marked as an outlier during the segmentation process and the number of potential changes for epoch I and III. For epoch III, the number of points for which the distance to epoch I is calculated is shown as well.

	Epoch I	**Epoch III**
Points	325,516	3,513,291
Segments	20	494
Outliers	3,385	137,684
Potential changes	36,613	1,238,029
Deformation analysis	-	1,350,450

The segmentation results are shown in Fig. 6.21. The number of segments is shown is Table 6.2. In the middle of the wall, there is a horizontal stripe with mainly water pipes. In epoch III, many of the points located on the water pipes are assigned to the upper wall segment, see Fig. 6.21b. In this segmentation, the footbridge is also visible.

The points that are not assigned with a segmentation label during the segmentation process, the outliers, are shown in Fig. 6.22. Points are labelled as an outlier if the angular threshold is exceeded or if the distance to the segment exceeds the threshold value, see also Section 5.3.2. The number of outliers is shown in Table 6.2. Most of the outliers are located at the edges of the data set, on the graffiti and on the water pipes.

Outliers on the edges

In epoch III, there are outliers around the edges. There is a thin segment at the top of the data set, which is hard to see in Fig. 6.21b. For a thin segment it is difficult to calculate the correct orientation of the plane, which will affect the distance of a point to that plane. Another explanation is that some of these points are located on the present fillet. In this case, the distance to the large blue segment, see Fig. 6.21, can also exceed the threshold value.

Outliers on the graffiti

The graffiti influences the interaction of laser signal with the surface, see Section 3.3. If the intensity of the reflected signal is lower, the precision of the range measurement is also lower. With decreasing precision, the chance of an outlier increases. Many of the outliers on the graffiti are located in areas with low reflected intensity, see Fig. 6.22b.

Outliers on the water pipes

The water pipes are non-planar and irregular. For two points, located only a few cm apart, the difference in range to the laser scanner can be up to a few cm. More 'outliers' are expected for non-planar surfaces, since more often the angular or distance threshold will be exceeded. Furthermore, the black colour of the water pipes may influence the amount of reflected energy of the laser signal.

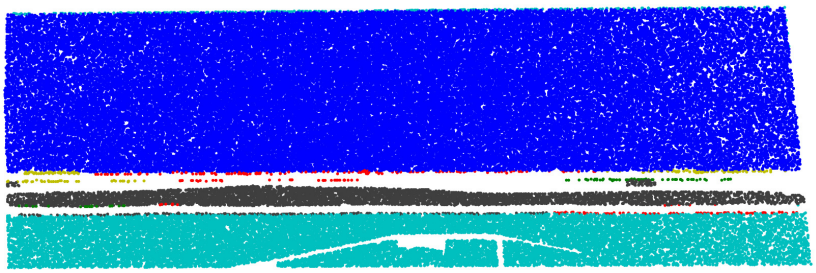

(a)

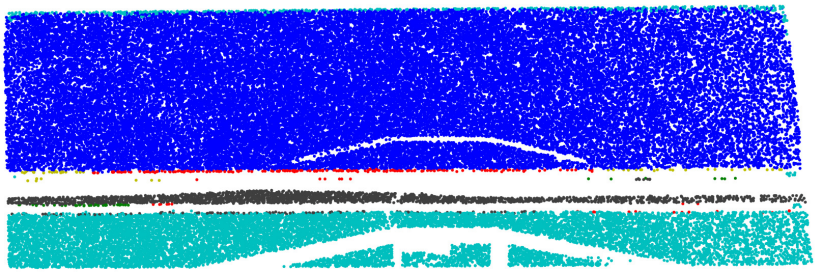

(b)

Figure 6.23: The corresponding segments in the two point clouds. (a) The segments of the point cloud of epoch I with a correspondence in the point cloud of epoch III. (b) The segments of the point cloud of epoch III with a correspondence in the point cloud of epoch I.

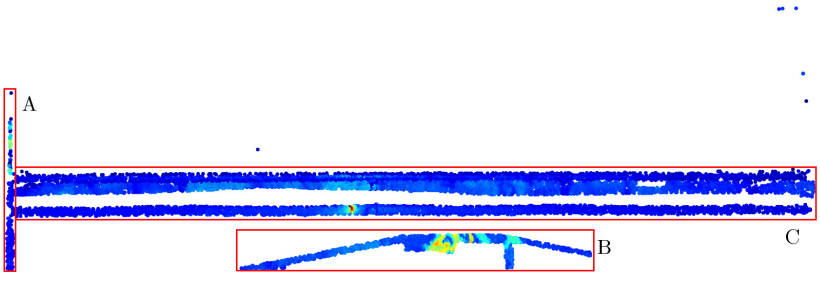

(a)

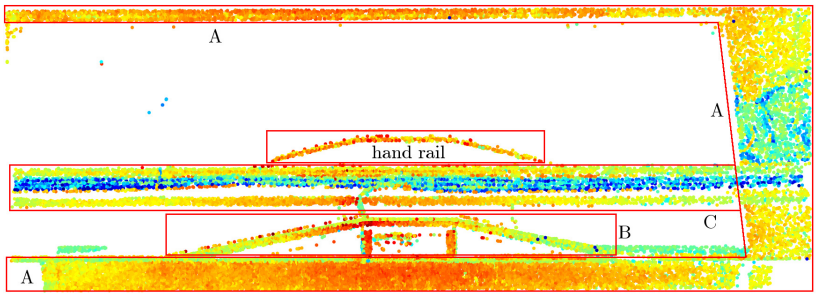

(b)

Figure 6.24: The possible changes between the two point clouds. Indicated in both figures are A: points near the edges, B: points on the footbridge and C: points in the horizontal stripe in the middle. (a) The points that are marked as a possible change in epoch I. (b) The points that are marked as a possible change in epoch III.

Most of the outliers in Fig. 6.22a are located on the metal tube and bar. Most likely edge effects influence the range measurements. As a result, for these points the distance to the planar segment exceeds the threshold value and the points are marked as an outlier.

6.3.4 Identification of corresponding segments

The results of the identification of the corresponding segments are shown in Fig. 6.23. This data set has a cavity, i.e. a region with no data points, caused by the shadowing of the footbridge on the wall behind. This cavity is visible in the segmentation results of epoch III, see Fig. 6.21b. The algorithm for the identification of the corresponding segments tries to identify such a cavity, since there will be no points to compare during a deformation analysis. Fig. 6.23 shows that the algorithm partly succeeds. The cavity is found, but the resulting cavity in epoch I is smaller than its original in epoch III. This is caused by the threshold value that is set in the algorithm. The algorithm calculates, for each point in the convex hull of a segment, the distance to the nearest point in the other point cloud. If this distance to the nearest point is larger than the threshold, the point is assumed to be located in a cavity, otherwise it is in the intersection of the two segments, thus in a corresponding segment. The use of a threshold also explains why the results look like a dilation operation took place. If the threshold is set tight, e.g. 1 cm, the dimensions of the segments correspond even better and the 'dilation effect' is smaller.

6.3.5 Change detection

During the change detection process, changes in the state of an object between two acquisitions are found. Changes are either new objects placed in the scene, or objects that were removed. Points are considered to belong to a possible change if they are sampled in one epoch, but not in the other, see Section 4.4. Fig. 6.24 shows the possible changes in the point clouds of epoch I and III.

The possible changes are divided in three groups, based on their location in the data set:

- around the edges,
- the footbridge,
- the horizontal stripe in the middle.

Changes near the edges

In both epochs, there are possible changes indicated near or at the edge of the data set. In epoch I this is limited to a small stripe of points on the left side, but in epoch III there is a wide stripe on the right side of the wall, and also at the top and the bottom. This data set is a small extract from a larger point cloud, so in this case it is clear that not the exact same region is selected for both epochs.

Without this knowledge, it should be investigated whether these possible changes are real changes or occlusions. Performing the additional processing steps as suggested in Section 4.4, and also illustrated in case study I, see Section 6.2.5, helps to make this distinction. For every

scan in the point cloud, the line-of-sight to the points is investigated. If there is an object blocking the view to the wall, the points were occluded and therefore not sampled in every scan. In these scans, there are no objects hiding these parts of the wall and therefore these points are labelled as changes.

The footbridge

The second group of points that are indicating a potential change are located on the footbridge. In Fig. 6.24b, indicated with B, the points on the footbridge are clearly visible. Moreover, the hand rail that is placed above the footbridge is indicated as a possible change. Additionally in this case, the distinction between changes and occlusions is made using the original scanning geometry. The points on the hand rail are sampled in epoch III but not in epoch I. There are no other objects that could have blocked the view to these specific points in epoch I and the changes are therefore caused by the hand rail.

In epoch I, see Fig. 6.24a, the effect of the occlusion by the footbridge is visible. In epoch III, a part of the wall is not sampled because the footbridge blocks the view from all the standpoints. During the identification of the corresponding segments, no correspondence is found for the points from epoch I. When the scanning geometry is investigated, it will follow that the footbridge blocked the line-of-sight towards the wall in epoch III.

The effect of an object placed in the scene is therefore dual: on the one hand there is a new object detected, and on the other hand this new object creates an occlusion. This should also be the case for the hand rail, which occludes a small part of the wall in epoch III, causing a small cavity in the wall. However, this cavity is too small to be detected during the identification of the corresponding segments. If the threshold is set to a smaller value, this cavity will also be detected.

The horizontal stripe

The third category of indicated possible changes is the wide horizontal stripe in the middle of the wall. This stripe is visible in both epochs, see Fig. 6.24, indicated with C. In epoch I, there are no water pipes present. In the time between the acquisitions, several pipes are placed, which are knotted together. Points located on the water pipes in epoch III do not have a correspondence in epoch I and are marked as a potential change.

Furthermore, Fig. 6.24a shows a long vertical object, which corresponds to the long red vertical segment in Fig. 6.21b. This is a metal bar, see Fig. 6.20, indicated with C. Although the bar was also present during epoch I, it is marked as a potential change. According to Fig. 6.21b, the bar is not segmented as a single object in epoch I, but it is merged with the lower segment. Further investigation learns that the bar is segmented as a single object, but the orientation of the segment is affected by points on the bottom side of the bar, which are also added to the segment. Therefore this segment is not corresponding to any of the segments in epoch III.

6.3.6 Deformation analysis

Segments with a correspondence in the other epoch are compared during the deformation analysis. For every point in epoch III, the distance to a local surface representation of epoch I

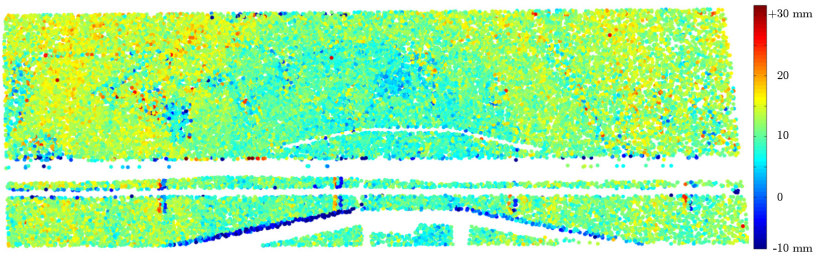

Figure 6.25: Calculated distances between epoch III and epoch I.

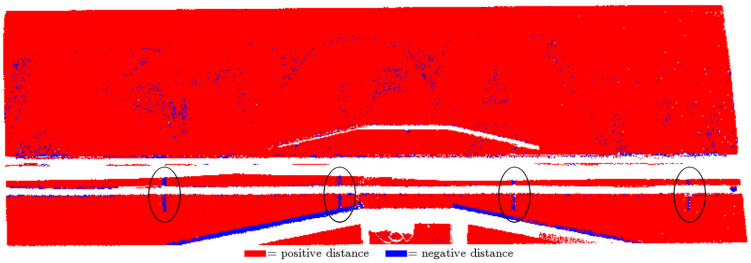

Figure 6.26: Positive (red) or negative (blue) distances. The black ellipses indicate the four construction brackets.

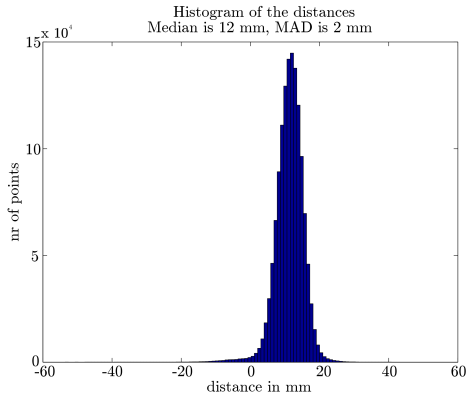

Figure 6.27: Histogram of the calculated distances.

is calculated, see also Section 4.5.

Fig. 6.25 shows the distances between epoch III and epoch I. The number of points in epoch III for which a distance is calculated is shown in Table 6.2.

The median distance between the two points clouds is 12 mm, with a MAD of 2 mm. A positive distance from epoch III to epoch I means that the point cloud of epoch III moved away from the point cloud of epoch I and the centre axis of the tunnel. Fig. 6.26 shows for each point whether the distance is positive (red) or negative (blue). For almost all the points the distance is positive. The histogram of the distances, see Fig. 6.27, shows that the distribution is approximately symmetrical, although the tail on the left side is slightly larger. The overall impression is that the distance have a normal distribution.

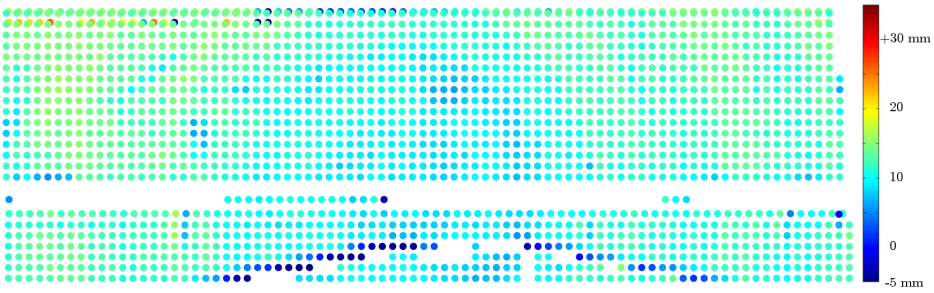

Figure 6.28: Distance between the two point clouds. There is a small hint of a circular deformation pattern, possibly caused by the pressure of water that is injected to the ground around the tunnel.

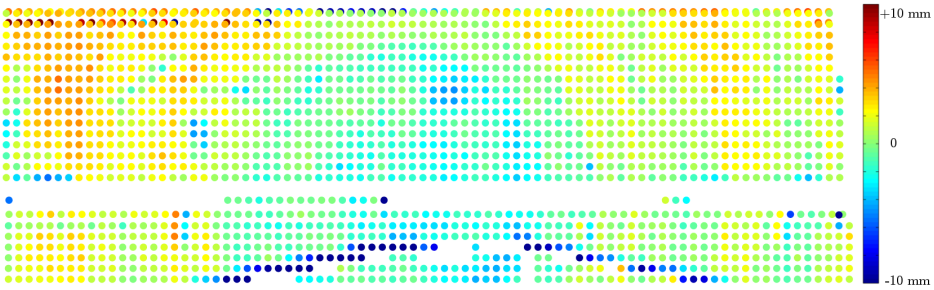

Figure 6.29: Distance between the two point clouds. The mean is removed from the distances. A circular deformation pattern is visible, possibly caused by the pressure of water that is injected to the ground around the tunnel.

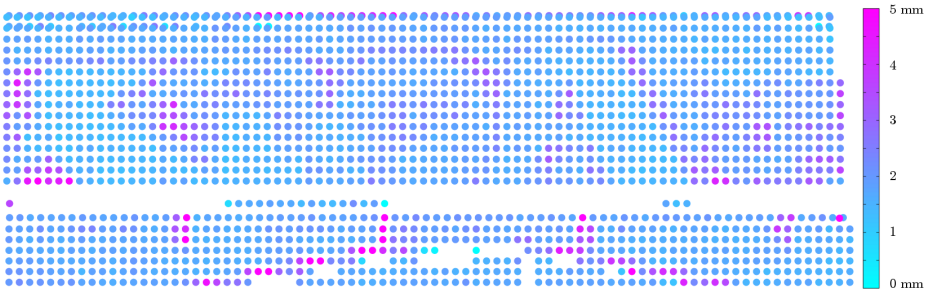

Figure 6.30: For each grid cell, the standard deviation of all the distances in that grid cell is calculated.

Deformation near the edges

Around the edge of the footbridge are negative distances, see also Fig. 6.26. Most of these points are located on the footbridge itself, but nevertheless they are assigned to the wall during the segmentation process. Their distance to the wall is too small to be removed, either during the segmentation process or during the identification of the corresponding segments process. Therefore, extra care should be taken for the interpretation of larger distances located at an

edge.

Deformations on the graffiti

In the upper segment, see Fig. 6.25, there are some of the larger values, i.e. deep red or blue. Many of these points are located on the graffiti. In Fig. 6.26, the outline of the graffiti is visible. Similar as for the outliers during the segmentation, these points have a low reflection, see Fig. 6.19. It is expected that the precision of these points is lower. Furthermore, it is not likely that these points are local deformations, since these points are isolated, i.e. their surrounding points do not show the same behaviour, and deformations are expected to influence a larger area.

Deformations on the construction brackets

There are four vertical small lines of negative distances, starting at the middle stripe, moving downwards, see Fig. 6.26, where the vertical lines are indicated with black ellipses. These are the construction brackets, see Fig. 6.20, indicated with D. These brackets are present in both epochs. The negative distance implies that these brackets moved inwards. The calculated distances are very small, approximately around 5 mm. Perhaps new brackets are installed between the epochs, with a slightly difference shape.

Deformations caused by water injections

From Fig. 6.25, the presumption arises that the deformations follow a circular pattern. The centre of the circle is located in the vicinity the footbridge. As the radius increases, also the distance between the point clouds increases. This can be the result of ground water outside the tunnel (Berkelaar, 2011). The footbridge is placed at this location to protect a water inlet. Below the footbridge, a water tap is constructed to inject water in the ground around the tunnel. The water tap is connected to the water pipes that run through the tunnel. Fig. 6.28 shows the calculated distances in an interpolated regular grid. The circular deformation pattern is visible in this figure as well.

The ground around the tunnel presses on the exterior of the tunnel. When the water is injected in the ground, the pressure on the tunnel increases. The increase is the largest around the injection point, below the footbridge. Further away the pressure decreases, giving the tunnel the opportunity to extend, as the figures show.

Quality of the deformation analysis

In Section 4.5 it is explained that the calculated distance between two point clouds is a combination of the registration, deformations, measurement noise, plane fitting and unmodelled errors. The median calculated distance between the two epochs is 12 mm and only a part of it is caused by deformations.

The registration accuracy of epoch I is 3 mm, the registration accuracy of epoch III is 6 mm. This error is not the same for all the points in the data, but will have a Probability Density

Function (PDF). The reported registration accuracy will also be used for the registration precision.

Using the propagation law of variances, the total registration precision is $\sqrt{(3^2+6^2)} = 6.7$ mm. Assuming a measurement precision of 3 mm, the precision of the range measurement is 7 mm. This means that the median distance of 12 mm has at least a standard deviation of 7 mm, but the plane fitting and unmodelled errors are not included in this number. There are signals of a possible deformation, but the signal is very small and the errors need to be modelled very well.

When the registration accuracy is assumed to be the same for the whole scene, thus a bias, it can be removed from the calculated distances. Then the deformation plays a large role in the remaining total distance. For each grid cell, the median distance of all grid cells is subtracted. The result is shown in Fig. 6.29. The circular deformation pattern due to water injections becomes clearly visible.

Fig. 6.30 shows for each grid cell the standard deviation. The effect of the graffiti on the precision is clearly visible from this figure. The standard deviation is higher on black paint than on white paint, see also Fig. 6.20. It would therefore be wise to incorporate the individual point quality into the deformation analysis. Points surrounded with low reflectance values tend to have a larger standard deviation.

6.3.7 Validation of the deformations

Unfortunately, there are no points in this scene measured with other measurement techniques. However, a few meters aside from the considered wall, there is a planar target that is used during the registration process of both epochs. This target is measured with a total station at the time of the laser scanner acquisitions. The only possible validation is to compare the two coordinates of the target. The target was attached to the wall using duct tape. In the mean time, many metros passed the target.

The comparison of the total station xyz-coordinates shows an absolute movement of 30 mm of the target. This movement is 3D, but the magnitude in the direction perpendicular to the wall is also 30 mm (y-direction). The target moved away from the tunnel axis.

The magnitude of the deformation differs, but the direction is the same for both techniques. However, this target is not very useful. It cannot be compared directly, since it was not sampled in this data set. Furthermore it is not known what happened to the target between the two epochs.

6.4 Case study III: the joint

The third case study concerns the area around joint 4, located below the building of *Nationale Nederlanden*. In Section 2.4, it is described that the biggest deformations are expected in this area, since the joint allows small dilations of the tunnel parts and uplift or subsidence of the tunnel is possible.

Table 6.3: Number of sampled points for each epoch in the joint area.

	Epoch I	Epoch II	Epoch III	Epoch IV
nr of points	413,341	18,896,087	2,399,075	52,227,576

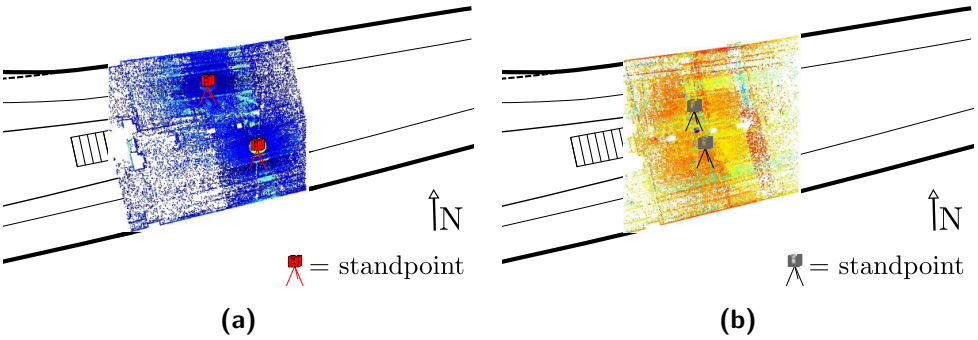

Figure 6.31: Data location and standpoints of the joint 4 case study. (a) The data acquired at epoch II. (b) The data acquired at epoch IV.

6.4.1 The data set

The joint area was sampled during all four available epochs. However, the data used in this case study is from epoch II and IV. During these two epochs, the area is well sampled. The distribution of the standpoints and the scanning geometry, which determine the range accuracy, the incidence angle and the number of points, are better than for the epochs I or III. Table 6.3 shows for each epoch the total number of points. Furthermore, the occlusion in epoch II and IV is minimal. Therefore it is decided to use the data from epoch II and IV. Fig. 6.31 shows the standpoints of the acquisitions and the areas that are sampled. The dimensions of this area are approximately 12×10×4 m.

Epoch II is acquired by the third party hired for this campaign: Fugro. After the registration process, the point cloud is resampled with a fixed interval of 0.8 cm in the x-direction and 3 cm in the y-dimension, resulting in a point cloud with 19 million points. Unfortunately, this resampling process causes problems for the processing. Especially the resampling in the y-direction causes a loss of geometric information. As a comparison, see the samples from the northern wall in Fig. 6.32. On first sight, both samples seem to be as a normal point cloud, see the figures in the top row. When the sample from epoch II is viewed from the top, see Fig. 6.32a, the resampling interval in the y-direction is clearly visible. The geometry of the wall in this sample is completely different than the sample of epoch IV, see Fig. 6.32b.

The assumption is that the data is not interpolated in 3D but points are merged in bins in the x- and y-direction.

Epoch IV is acquired during this graduation project by Delft University of Technology (DUT), in cooperation with Rotterdam Public Works (RPW). Two scans of 26 million points each are used, resulting in a point cloud of 52 million points.

The datasets of epoch II and IV are too large for the segmentation software. Between the

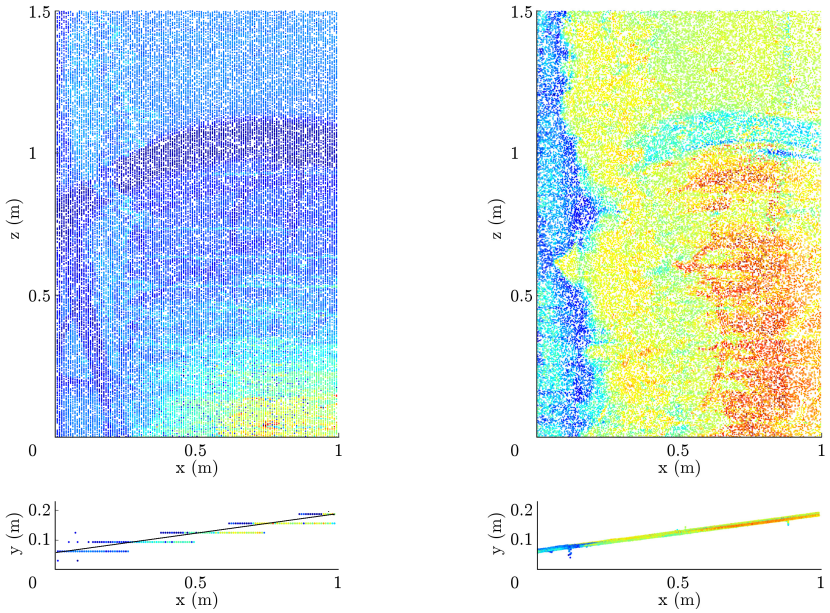

Figure 6.32: Two samples of the point clouds to illustrate the consequence of the resampling. The samples are small extracts from the centre of the northern wall. The top figures show the samples in the xz-plane, the lower figures show the samples from above. (a) The data sample of epoch II. The effect of the resampling is clearly visible in the top view of the point cloud. The black line represents the 'real' wall. (b) The data sample of epoch IV.

registration and the segmentation process, the selected data set is split in four separate data sets per epoch, each containing 1 million points. These data sets represent the ceiling, the northern wall, the southern wall and the floor. The points in the middle of the tunnel are neglected.

The division in four smaller data sets is also convenient for the visualisation of the data, since the visualisation of 3D point clouds is difficult in Matlab. The tunnel is unfolded to a net, see Fig. 6.33 for an illustration. The net results in a perpendicular view to each part of the tunnel and this view is used in the remaining of this case study.

Fig. 6.34 shows for each data set the data coloured with the reflected intensities. The colours of the point clouds differ because different laser scanners were used and the measured intensity is an uncalibrated product.

6.4.2 Registration

The registration of epoch II is done by the company Fugro. The reported accuracy by the software Cyclone is 3 mm, see also Table 5.3 for registration details. The registration of the scans acquired during epoch IV is described in Section 5.2.2. The reported accuracy is 4 mm.

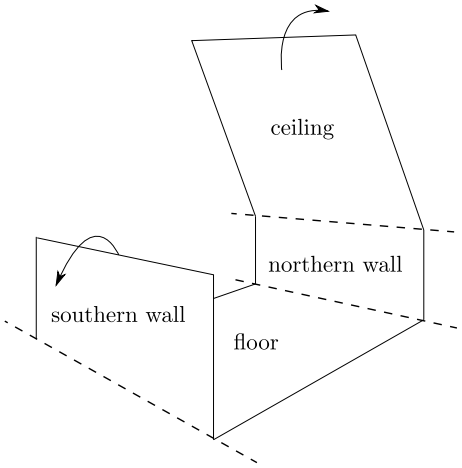

Figure 6.33: Illustration of the visualisation of the tunnel data. The tunnel is unfolded so that the view to each part of the tunnel is perpendicular.

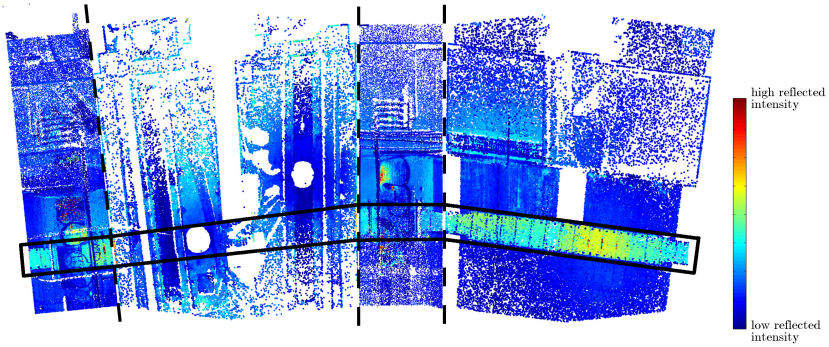

(a)

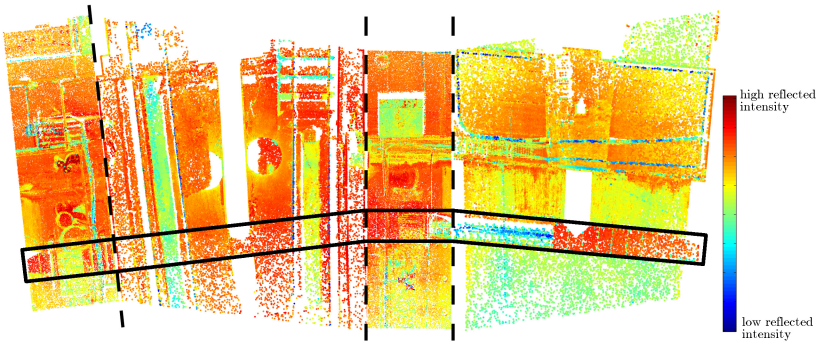

(b)

Figure 6.34: The point clouds of the joint 4 area, coloured with the measured intensities. The representation of each wall is orthogonal, the dashed lines are the fold lines. The joint is outlined by the black rectangle. (a) The data acquired at epoch II. (b) The data acquired at epoch IV.

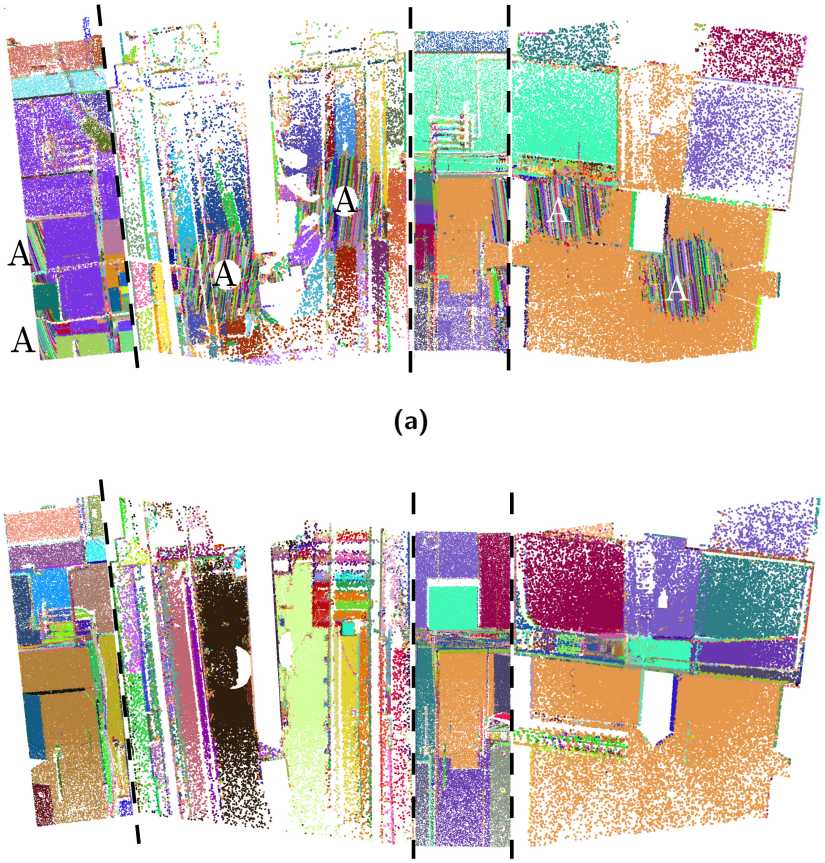

(a)

(b)

Figure 6.35: Results of the segmentation process. Each segment has an arbitrary colour, corresponding colours in two parts of the tunnel does not necessarily mean it is the same segment. (a) Segmentation of epoch II. The regions indicated with A are affected by the resampling of the point cloud. (b) Segmentation of epoch IV.

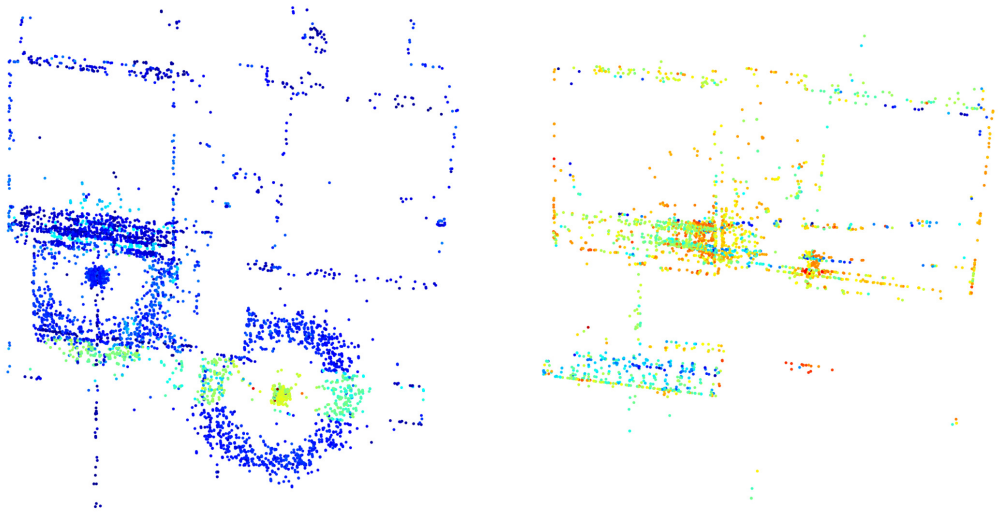

(a) **(b)**

Figure 6.36: Outliers during the segmentation process of the ceiling data set. (a) Outliers of epoch II. (b) Outliers of epoch IV.

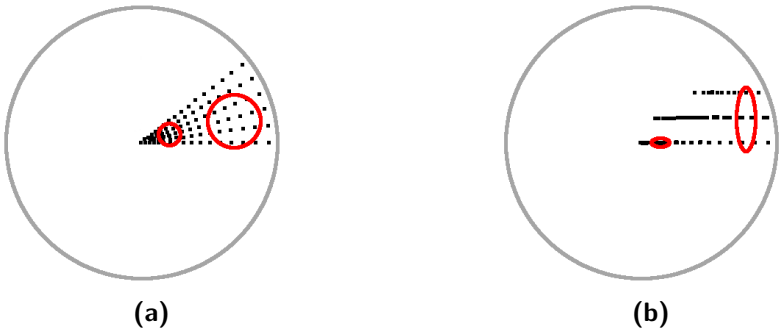

Figure 6.37: Illustration of the effect of the resampling on the nearest neighbours. The points within the red circles/ellipses are the nearest neighbours. (a) The point cloud in the circular area with normal sampling. (b) The point cloud in the circular area after resampling.

6.4.3 Segmentation

The segmentation process is a bottleneck in the processing chain because the used software is not able to cope with data sets larger than 100 MB. For this case study the segmentation parameters are loosened. Using the parameters as given in Section 5.3, gives unsatisfying segmentation results, many areas in the data sets are over segmented. After some trial and error, the distance parameter δ_{th} is set to 5 cm, which seemed to be the most suitable for this data set. The results of the segmentation process are shown in Fig. 6.35. The number of segments for each data set can be found in Table 6.4.

Most of the scene is segmented as expected, except for the regions indicated with A in Fig. 6.35a. The regions on the floor and the ceiling are directly below and above the laser scanner and are segmented into elongated segments. The erroneous segmentation is caused by the resampling of the point cloud, in combination with changing the local point density.

Fig. 6.37 shows an illustration of a sampling with the scanlines, Fig. 6.37a, and the resampled points, Fig. 6.37b, in the circular area around the standpoint. At the centre of the circle, the point density is the highest, since the angle of incidence is minimum. The point density decreases for increasing radius of the circle. In a normal situation, the nearest neighbours of a point near the centre are located on the same and adjacent scanlines. If in the resampled point cloud, for the same point, the nearest neighbours are found, these neighbouring points are all located on the same line. Points from adjacent lines are found as a nearest neighbour after a certain distance, which depends on the number of nearest neighbours and the resampling interval.

The resampling affects the segmentation process in two ways. First, the nearest neighbours are used to calculate the local surface normal. The resampling changes the surface geometry and thus the surface normal. Second, the nearest neighbours are located on the same line. Therefore, during the region growing only points on the same line are added to the growing

Table 6.4: The total number of points, the number of segments, the number of outliers during the segmentation process, the number of potential changes and the number of points for which the distance to the other point cloud is calculated for the ceiling data set of epoch II and IV.

	Epoch II ceiling	**Epoch IV** ceiling
Points	1,000,000	1,000,000
Segments	982	243
Outliers	72,796	28,043
Potential changes	490,612	257,536
Deformation points	-	427,942

segment, which results in the elongated segments. When the radius of the circle is large enough, points on adjacent lines are added.

The problem occurs in areas where the range is relatively small and the angle of incidence is low, i.e. the line-of-sight is almost orthogonal to the surface. Besides the circular areas below and above the standpoint, the effect is also visible on the fillets, see Fig. 6.35a, on the northern and southern wall. The incidence angle for these parts of the wall is lower than for other parts of the wall. Relaxing the segmentation parameters does not remove the small elongated segments.

The northern and southern wall are affected the most by the resampling process. These effects are visible in the segmentation results, see Fig. 6.35, and in the remaining processing steps of the workflow. The data set of the floor contains a lot of small segments, since there are many non-planar objects. The results of this data set are not representative as well. Therefore, these three data sets are not further considered in this section and only the data set of the ceiling is discussed. The results of the walls and floor are shown in Appendix B.

Outliers during the segmentation process

The points that are labelled as an outlier during the segmentation are shown in Fig. 6.36. Table 6.4 shows the number of outliers for each data set. Most remarkable are the two circular patterns in epoch II, see Fig. 6.36a, indicated with A. These points are located on the edge of the elongated segments, as indicated with A in Fig. 6.35a, and the surrounding segments. Probably this is a transition area, where points from adjacent lines are included in the nearest neighbours. When this happens for the first time, the normal of the nearest neighbours differs too much with the normal of the current growing segment and the point is labelled as an outlier. When the range increases even more, the normal of the resampled surface is similar to the normal of the 'real' surface, and the segments are as expected.

In both epochs, part of the outliers are located on edges of an object. This is already explained during the previous case studies.

6.4.4 Identification of corresponding segments

The results of the identification of the corresponding segments are shown in Fig. 6.38. Surfaces which are approximately planar, such as most parts of the walls and the ceiling, are identified

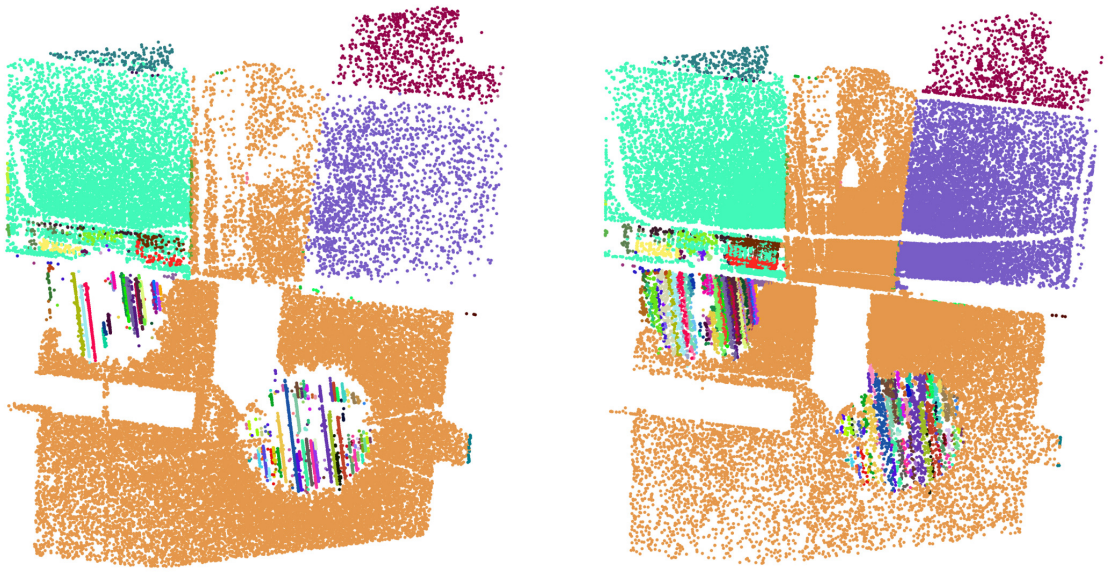

(a) (b)

Figure 6.38: The corresponding segments in the two data sets. (a) The segments in the ceiling data set of epoch II with a correspondence in the data set of epoch IV. (b) The segments in the ceiling data set of epoch IV with a correspondence in the data set of epoch II.

in both epochs. Segments on the small objects are not identified as a corresponding surface.

Again, the elongated segments in the circular area are present. For some of these segments a correspondence is found in epoch IV. This is only possible if these segments in epoch II have an orientation which corresponds with the segment in epoch IV. Furthermore, it should be noted that the results of the identification depends on the reference epoch. When there are many small segments, it is hard to find matching segments.

6.4.5 Change detection

Fig. 6.39 shows the points that are marked as possible change during the identification of the corresponding segments. These points are potential changes that occurred between epoch II and epoch IV. Remarkable areas are discussed in Table 6.5.

The cause of the false changes are divided into three categories:

- false changes due to edge effects,
- false changes due to incorrect segmentation results,
- false changes due to the data selection.

False changes due to edge effects

In Section 6.2.5 is discussed that the edges of the segments cause falsely identified changes. For some objects, the edge effect is generated by the scanning geometry of the epochs, e.g.

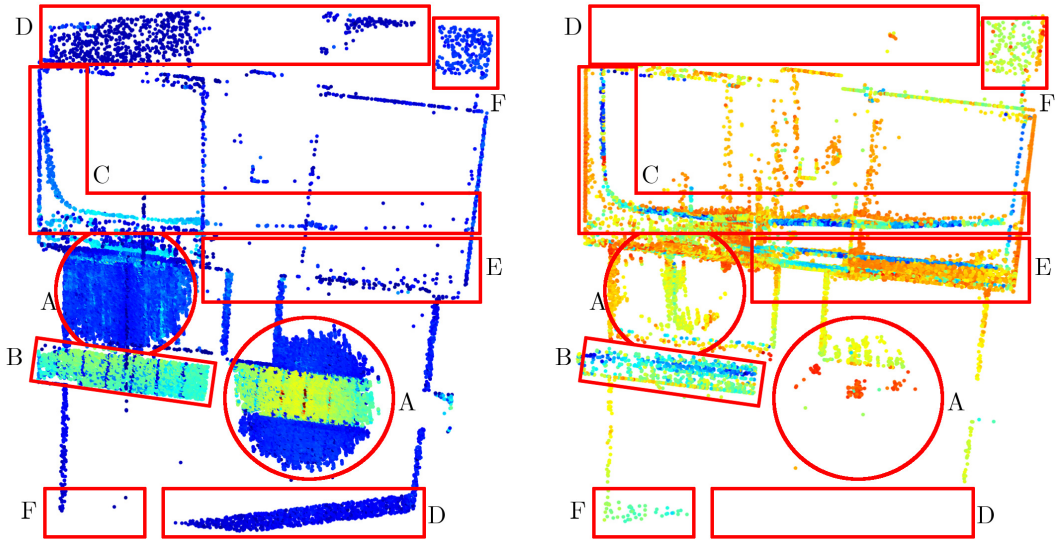

Figure 6.39: The possible changes on the ceiling between epoch II, (a), and epoch IV, (b).

Table 6.5: Description of the possible changes on the ceiling.

Area	Description	Change?
A	These circular areas are the result of the resampling process and the incorrect segmentation results.	N
B	A part of the joint that changed. The flame resistant cover of the joint is removed, but only for the northern half of the tunnel. This is detected during the change detection process.	Y
C	In epoch IV, a long curved pipe is visible, represented by the blue points. The same pattern is also visible in epoch II. This pipe is placed between epoch II and IV.	Y
D	These regions are sampled in one epoch, but not in the other, as a result of the data set selection. The data sets do not fully overlap.	N
E	The points are only marked in epoch IV. A set of wires is mounted to the ceiling at this location. However, the wires are also present in epoch II. Perhaps small changes occurred, but more likely these changes are caused by the incorrect segmentation of the wires.	N
F	A group of points present in both epochs. Closer investigation of these points learns that the surface changed between the two epochs. In epoch II, the surface was covered with an isolation material. This cover was removed before epoch IV. This thickness of this cover is such that the distance between the segments exceeds the distance threshold and the segments are marked as a potential change, see also Section 5.4.	Y

an edge is visible in one epoch and only partially, or not at all, in the other epoch. Moreover, with the large amount of small objects, and thus small segments, present in the data sets, 'changes' due to the edges are also in this case study inevitable. For an illustration, see Fig. 6.39, where the edges of the ceiling are marked as a potential change, whereas no change occurred.

False changes due to incorrect segmentation results

The effects of the resampling are also visible in the change detection, see regions A in Fig. 6.39.

For small objects with a complex shape, planar segments are not suitable. These small objects are often identified as a possible change.

Furthermore, if an object is sampled with a high point density in one epoch, but with a low point density in the other epoch, it can be difficult to match the segments. This can lead to a false change.

False changes due to the data selection

The data set for the case study is a subset of the full point cloud of an epoch. During the selection in the software Cyclone, not the exact same area is exported. Non overlapping areas are marked as a possible change.

Evaluation of the results

It is clear that the segmentation of the objects in the scene plays an important role for the change detection. Large (approximately) planar surfaces are well matched, but when objects have a complex shape, planar segments are not suitable. As a result, these objects are often marked as a potential change, whereas in reality the object is unchanged. Using a segmentation method that is able to deal with these complex objects should improve the results.

6.4.6 Deformation analysis

Segments with a correspondence in the other epoch are compared during the deformation analysis. Fig. 6.40a shows the distances for the points of epoch IV to the local surface representation of epoch II.

Deformations on the ceiling

The ceiling shows a clear distance pattern. There are two main areas, see Fig. 6.40a: the yellow part of the ceiling on the east side of the joint, hereafter named the tunnel side, and the orange part on the west side of the joint, hereafter named the station side. The joint itself is partly analysed, but a large part is distorted by the resampling. In the previous section is explained that the other half of the joint has changed.

It should be noted that it is difficult to draw conclusions from the points that are located in the circular area around the standpoint, since these points are affected by the resampling process.

Fig. 6.40b shows the average distances in a regular grid of 10 cm, see Section 6.2.6 for more details on the construction of the grid. A positive distance means an uplift of the surface with respect to the reference surface. The tunnel side has a median distance of 9 mm, with

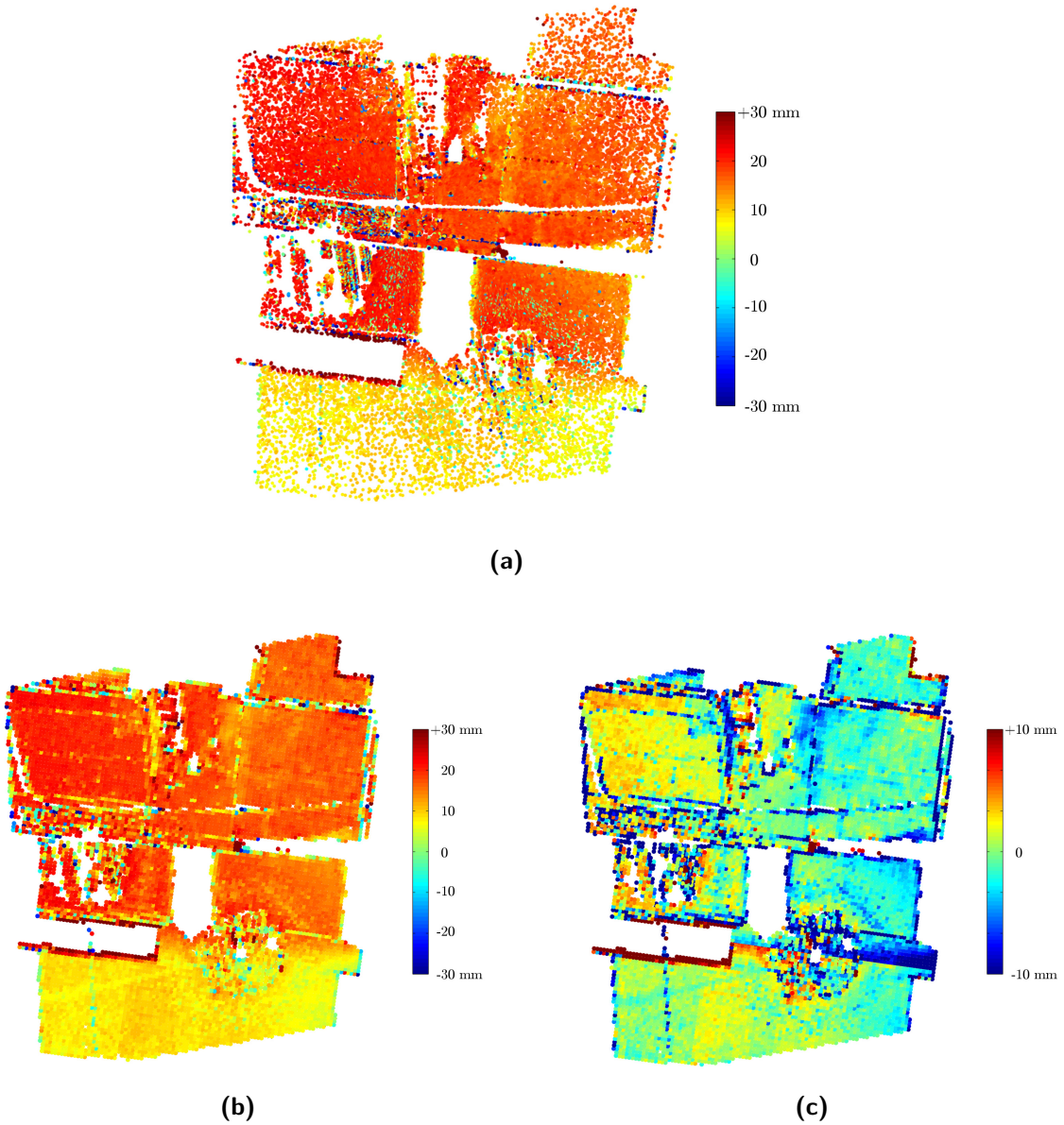

Figure 6.40: (a) Distances between epoch IV and epoch II. (b) Average distance per grid cell. (c) Average distance per grid cell, where for each point on the tunnel side the mean of the tunnel side is subtracted, and for each point on the station side the mean of the station side is subtracted.

a MAD of 2 mm. On the edges, the distance is slightly smaller. The edge with the joint shows a large distance, probably caused by edge effects, but perhaps by the removal of the protection cover.

The ceiling on the station side has a median distance of 18 mm, with a MAD of 2 mm. Again, the circles near the standpoints are affected by the resampling. Furthermore, the edges are visible, including the edge with the joint. The larger distance near the joint can be caused by

the removal of the protection cover.

Rotation of the tunnel

There seems to be a small rotation of the tunnel on the station side around the x-axis, see Fig. 6.40c. This rotation should also be visible on the floor and on the walls, but unfortunately the distances from these areas are not useful due to the resampling process. The figure shows the distances between the point clouds in a regular grid of 10 cm. For each grid point on the tunnel side, the median of the tunnel side is subtracted and for the grid points on the station side, the median of the station side is subtracted. By removing the mean from the data, smaller differences are better visible. Fig. 6.40c shows a bigger uplift of the ceiling on the northern side, but the difference between the northern and southern side does not exceed 10 mm.

The rotation is larger for the station side than for the tunnel side. The tunnel side is fixed to the *Nationale Nederlanden* building. These fixations are on the sides of the tunnel, which might be the reason for the slightly larger deformation in the middle area. The foundation of the station side is not renewed during the construction works. This might cause the rotation of the tunnel. It would be interesting to have a larger data set of the station side, especially for that area the foundation was renewed.

Deformations due to wires on the ceiling

Fig. 6.40a also shows some points in lines that have a different distance than their surrounding. These lines are representing wires and are present in both epochs. However, they are too thin to be detected during the change detection, but they are noticeable in the deformation analysis.

6.4.7 Validation

The joint 4 area is expected to deform during the construction works. An intensive deformation monitoring program was set up, to detect potentially dangerous deformations on time. Data acquired by the joint meters and total stations is used to validate the results of the deformation analysis using Terrestrial Laser Scanning (TLS) data.

From the available validation data, the measurements covering the period between epoch II (February 2007) and IV (January 2010) are used. These measurements describe the deformation in three dimensions. The x-direction is the along tunnel direction. Since there are no walls orthogonal to this direction in this data set, the deformation in this direction cannot be measured with the method proposed in this project. The y-direction is across tunnel direction, thus approximately orthogonal to the northern and southern wall. A deformation analysis of these walls was not possible, as explained in Section 6.4.6. Only the deformation in the z-direction can be validated with the available deformation monitoring data.

The deformation measured with the joint meters is shown in Fig. 6.41. The joint meters are located on the northern and southern wall and measure the relative deformation, see Section 2.3.2 for more details. The deformation measured with total stations is shown in

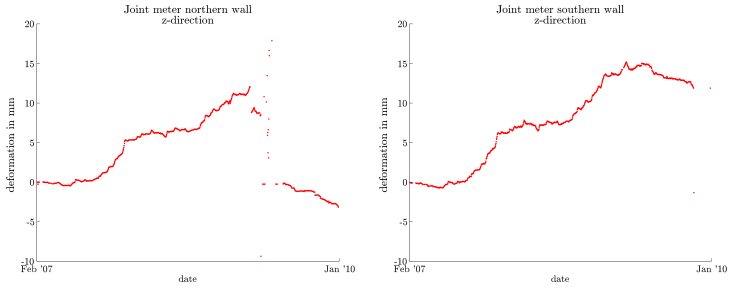

Figure 6.41: The joint meter measurements for the period between epoch II and IV. (a) The joint meter on the northern wall. (b) The joint meter on the southern wall.

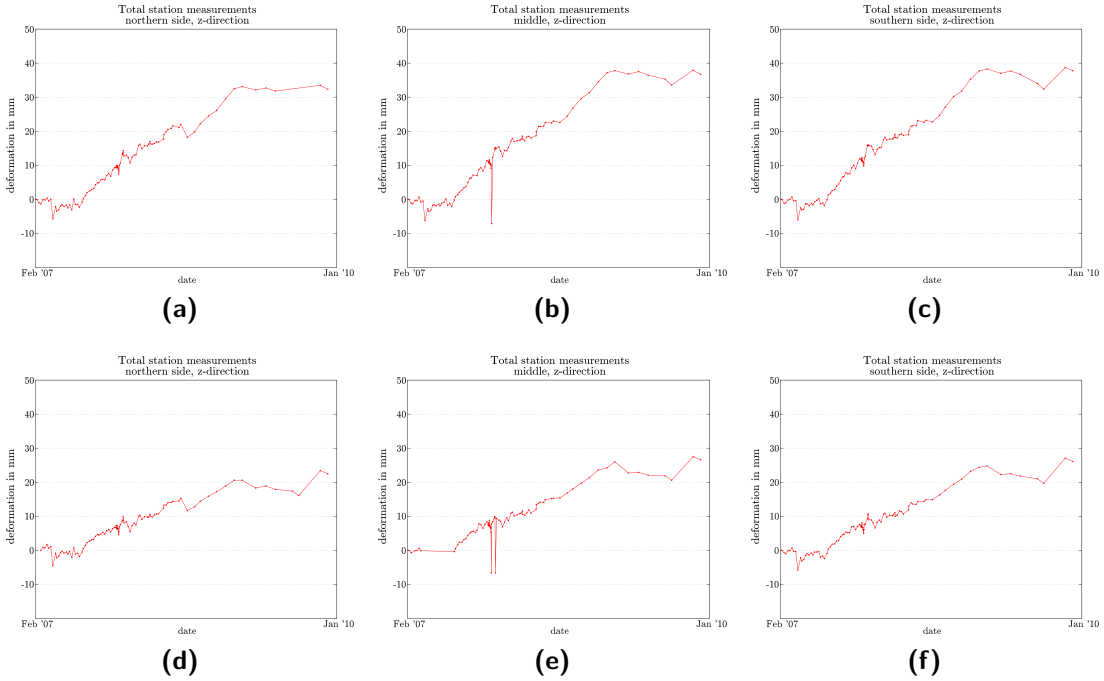

Figure 6.42: The total station measurements for the period between epoch II and Rmnum4.
(a) to (c): measurement points on the station side, from North to South.
(d) to (f): measurement points on the tunnel side, from North to South.

Fig. 6.42. The measurement points are located on the ceiling, three points on each side of the joint. More details on the total station measurements are given in Section 2.3.1.

Relative deformation

The joint meter data shows a relative uplift of the station side of 8 mm on the northern side and 12 mm on the southern side. The total station data shows a relative uplift of approximately 12 mm. The relative deformation as measured with TLS is 9 mm. These numbers correspond very well.

Absolute deformation

The absolute deformation as measured with the total station is approximately 35 mm on the station side and approximately 23 mm on the tunnel side. Furthermore, there is a difference of a few mm between the measurement locations. The absolute deformation of the station side of the ceiling as measured with TLS is 18 mm, the uplift of the tunnel side is 9 mm, which is more or less 15 mm smaller than the results from the total station data.

Remarks

Two important remarks should be made. First, it is important which points are measured. The total station measures three single points located on the ceiling, two of those points are located on the fillets. For an accurate comparison, the total station measurement points should be compared with a scanned neighbourhood of these points.

Second, the measurement frequency of the total station measurements is low near epoch IV. The presented numbers are estimations of the absolute deformation. Better estimates can be given if more total station measurements are available for the last period. The measurements show unexpected jumps near the end for 5 of the 6 measurement points, but it is unknown if these are outliers. If the trend of the period before the last two measurements is used, the difference with the absolute TLS deformation is smaller.

Since the relative deformation of the TLS data corresponds well, the absolute deformation can have an offset. This offset can be caused by the registration process.

Rotation of the tunnel

The joint meter and total station measurements also show a rotation of the tunnel. However, the rotation is in the other direction, i.e. the southern side shows a larger deformation, whereas for the TLS based deformation the northern side shows more deformation. Again, it is important which points are compared. Furthermore, the TLS data points on the station side of the joint, near the northern wall, as distored by the resampling process. The real distances of these points is not known and perhaps these distances are smaller, resulting is a smaller rotation.

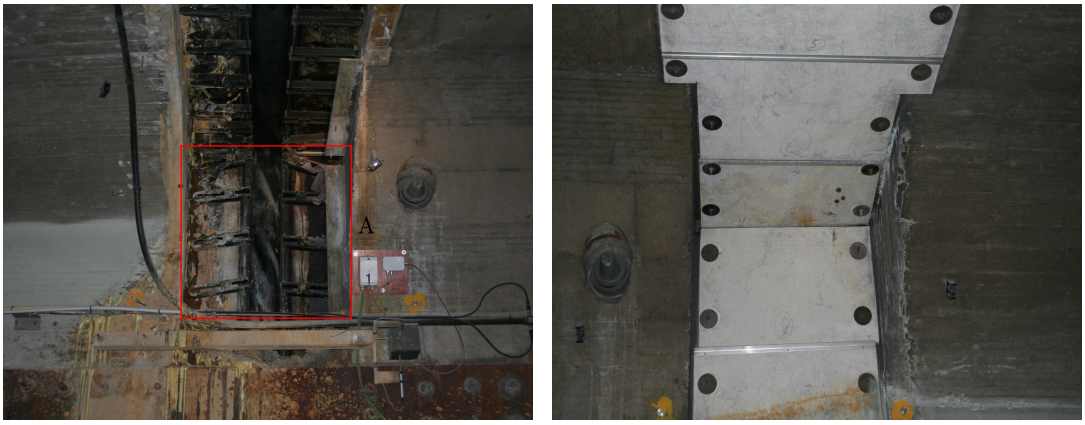

(a) (b)

Figure 6.43: Evidence of deformations of the joint. (a) The joint on the northern side. On this side, the fire resistant protection cover was removed. Indicated are the construction brackets of the joint. (b) The joint on the southern side, the protection cover is still in place.

Evidence of deformations

There are several signs of deformations in the joint area, especially at the joint itself, see Fig. 6.43. These photos are captured during epoch IV.

Fig. 6.43a shows the joint on the northern side. Visible are the construction brackets of the joint. The brackets were horizontally aligned, but due to deformations, they are skewed. Fig. 6.43b shows the joint on the southern side. The foam rubber cover is still in place, where it is removed on the nothern side. The lower two cover patches show a small rotation and an uplift on the right side, which is the station side.

6.4.8 Processing time

Not the full point density was used during the processing of this data set. As described in Section 6.4.1, the data set of the ceiling contains one million points. The total processing time using the proposed method, from acquisition to deformation analysis, takes approximately four days. One day is required for the measurement campaign, probably less than one day for the registration and approximately two days for the other processing steps. Once the data is acquired and registered, less time is needed to process other areas in the data set.

The required time for TLS data is more than the time needed for total station measurements. Of course the number of measurement points differ significantly. However, the processing of the total station measurements is a automated process and a deformation analysis using total stations is real-time. Due to the computational time consuming processing steps of TLS data, a deformation analysis using TLS data is not real-time. TLS measurements are therefore not eligible as a substitution for total station measurements.

Chapter 7

Conclusions and recommendations

The research objective, as defined in Section 1.2, was to *'present a method to detect changes and deformations in repeated TLS point clouds of a complex infrastructural scene'*. In this chapter, the conclusions and recommendations of the research are given.

It is necessary to define the difference between changes and deformations. In this project, changes are considered as differences in the state of an object, whereas deformation are small differences in the shape of an object. However, a large deformation can be regarded as a change, while a small change can be a deformation. Surface changes smaller than 10 cm are regarded as a deformation in this project.

7.1 Conclusions

Segmentation matching

The key step in the proposed method is to distinguish surfaces that have changed significantly, for example objects that are placed in or removed from the tunnel, from surfaces that remained unchanged. The process of identifying corresponding segments proved to be suitable to find these changed and unchanged surfaces. The segmentation matching is based on geometrical comparison. Surfaces that have changed between two acquisitions do not need to be investigated in detail for deformations since the change is larger than the noise level. Surfaces that have a similar geometry are compared in a deformation analysis, especially since the deformation signal is expected to be in the same order of magnitude as the noise.

Change detection and deformation analysis

Using the presented method, a possible change is detected if a surface is sampled in one epoch, but not in the other epoch. It is possible that the surface was occluded in one of the point clouds. The distinction between changes and occlusions can be made using the scanning

geometry. For each possible change, the visibility of the surface should be investigated in both epochs.

Surfaces sampled in two epochs are analysed for deformations. For each point in a segment, the distance to a local surface representation of the matching segment is calculated. The distance computed is the sum of the registration error, deformations, measurement errors, plane fitting error and unmodelled errors. It proved possible to detect deformations in the order of magnitude of the Signal-to-Noise Ratio (SNR).

The deformation analysis using Terrestrial Laser Scanning (TLS) data shows deformations in the same order of magnitude as the ones measured with total stations and joint meters. Differences between the measured deformation are likely caused by the registration process or bad scanning geometry during the acquisition.

Most of the time, two registered point clouds from two different epochs will be processed. However, when two registered scans from one epoch are processed, the presented method is an useful tool to investigate the registration accuracy. Occlusion mapping is possible since it is assumed no changes occurred between the two scans. Non-matching segments are then caused by occlusions during the acquisition.

Limitations of current implementation

The proposed processing steps are implemented for the metro tunnel at Rotterdam central station. Many of the objects in the tunnel are approximately planar and are therefore represented by planar segments. However, for smaller objects with a more complex shape, planar segments are no suitable representation.

The use of planar segments affects the segmentation matching and change detection. The identification of the corresponding segments is implemented for planar surfaces. The planar segments fitted on curved surfaces are incidentally matched correctly.

The implementation of the convex hull is suitable for planar segments, but for curved segments it will lead to incorrect matches.

False changes often occur as a result of non-planar surfaces. Other sources of false changes are due to edge effects, non-overlapping data selections and varying point cloud quality, such as different point density.

The deformation analysis uses a fitted plane as a local surface representation, which is justified for approximately planar surfaces and for areas with a high point density. The distance computed between a point and the plane through its nearest neighbours in the corresponding segment is the shortest distance, so orthogonal to the local surface. Deformations in other directions are not detected.

Computational and processing aspects

Processing the complete point cloud of the tunnel with full point density is not possible yet, due to computational limitations. Two of the three presented case studies use the full point density. The main bottleneck of the presented processing steps is the segmentation software, which can only handle data sets up to three million points. Moreover, one of the

biggest limitations is the computer's RAM, since the data files are very large (up to several GB). However, the presented method subdivides the point cloud into segments, so that smaller pieces are considered at once during the segmentation matching and the deformation analysis, which eases the computations and the required computer memory. Furthermore, first a rough deformation analysis can be conducted, in which deformed surfaces are identified, after which these surfaces can be investigated in more detail.

The complete process for the joint case study, from the acquisition to the deformation analysis with the current implementation, takes approximately four days. With the current state of processing time, deformation monitoring with total stations is still faster than using TLS and TLS cannot substitute total stations yet.

Setting the segmentation parameters is a trade-off between under and over segmentation. The best parameters vary within a scene, depending on the objects present.

The use of convex hulls for concave segments forms a problem during the segmentation matching. Additional computations are required to detect the concave areas. These computations are time consuming, since it involves calculating distances to all the other points to find the closest point.

The deformation analysis requires the nearest neighbours as well, which is a computationally heavy task when the segments contain many points.

7.2 Recommendations and future work

Acquisition

A good distribution of the standpoints is essential for an usable point cloud. It guarantees a good point density for the areas of interest, good scanning geometry (range and incidence angle) and a minimum of occlusions. The raw, unstructured point cloud should be used for the proposed method.

Registration process

The registration is a very important processing step. Therefore it is recommended to perform the registration with great care. The registration process is based on the targets that are placed in the scene. A good registration, preferably with an accuracy of a few mm, requires enough targets that are well distributed in overlapping areas of the scans. Furthermore, the scanning geometry for the targets must be good, so that the point density on the target is high enough. It is shown that the point density on the targets influences the registration error for that target. Targets with a lower accuracy should have a lower weight in the registration process.

The registration using baselines, as demonstrated in Section 5.2.3, is a promising approach for the registration, but only if enough baselines are defined. The redundancy in the data enables a Least Squares (LS) approach for the registration process with quality control, and weights can be assigned to each baseline.

Segmentation

To improve the results of the segmentation process, it is recommended to use smooth surfaces instead of planar surfaces. In that case, objects with a curved surface are segmented in single segments. However, it requires a new approach for the segmentation matching, which is now implemented for planar segments. Possibly, the segmentation matching can follow an object matching process.

Identification of the corresponding segments

During the identification of the corresponding segments, the intersection area of two segments is determined, using the convex hull of the segments. Intensive computations are required to identify the concave areas in the segments. The problem can probably be solved by using alpha shapes.

Change detection

The method for the change detection is not implemented. This should be done in the future.

Deformation analysis

The deformation analysis is only sensitive to deformations perpendicular to the local surface. For deformations in other directions, corresponding points in both point clouds have to be identified.

The deformation analysis is influenced by the measurement errors. Points with a lower precision show often a larger deformation. Implementation of testing theory in the deformation analysis, based on the point quality, will improve the results of the deformation analysis. For areas with a lower point density or high incidence angles, the use of the point quality information is recommended.

Bibliography

Aspert, N., D. Santa-Cruz and T. Ebrahimi (2002). MESH: Measuring errors between surfaces using the Hausdorff distance. In: *IEEE International Conference in Multimedia and Expo*, vol. 1: pag. 705–708.

Barber, C. B., D. P. Dobkin and H. Huhdanpaa (1996). The Quickhull algorithm for convex hulls. In: *ACM Transactions on mathematical software*, vol. 22, nr. 4: pag. 469–483.

Belton, D. and D. Lichti (2006). Classification ans segmentation of terrestrial laser scanner point clouds using local variance information. In: *ISPRS Commission V Symposium Image Engineering and Vision Metrology.*

Berkelaar, R. (2011). Personal communication.

Besl, P. and N. McKay (1992). A Method for Registration of 3-D Shapes. In: *IEEE Transactions on pattern Analyses and Machine Intelligence*, vol. 14: pag. 239–256.

Boehler, W. and A. Marbs (2002). 3D scanning instruments. Tech. rapp., i3mainz, Institute for Spatial Information and Surveying Technology, FH Mainz, University of Applied Sciences, Germany.

Boehler, W. and A. Marbs (2003). Investigating Laser Scanner accuracy. Tech. rapp., i3mainz, Institute for Spatial Information and Surveying Technology, FH Mainz, University of Applied Sciences, Germany.

Cerpentier, B. (2010). Personal communication by email. Leica.

Clark, J. and S. Robson (2004). Accuracy of measurements made with a Cyrax 2500 Laser Scanner against surfaces of known colour. In: *The International Archives of Photogrammetry, Remote Sensing and Spatial Information Sciences, Commission IV, Part B4*, vol. XXXV: pag. 1031–1037.

Edelsbrunner, H. and E. P. Mucke (1994). Three-dimensional Alpha Shapes. In: *ACM Transactions on Graphics*, vol. 13(1): pag. 43–72.

Eggert, D. W., A. Fitzgibbon and R. Fisher (1998). Simultaneous registration of multiple range views satisfying global consistency constraints for use in reverse engineering. In: *Computer Vision and Image Understanding*, vol. 69(3): pag. 253–272.

El-Sheimy, N. (2008). Land mobile mapping systems. In: Z. Li, J. Chen and E. Baltsavias (red.), *Advances in Photogrammetry, Remote Sensing and Spatial Information Sciences: 2008 ISPRS Congress book*.

Faro (2005). Recording reality's digital fingerprint. URL http://www.faro.com/FaroIP/Files/File/Brochures/UK_brochure_FARO_ScannerLS.pdf.

Faro (2009). Laser scanner LS 880 Factsheet. URL http://www.faro.com, last visited: September 8, 2009.

Faro (2010). Faro Scene 4.6. URL www.faro.nl.

Fugro (2006). Algemeen Monitoringsplan verbouwingswerkzaamheden Metrostation CS te Rotterdam. Tech. rapp., Fugro.

Girardeau-Montaut, D., M. Roux, R. Marc and G. Thibault (2005). Change detection on points cloud data acquired with a ground laser scanner. In: *ISPRS WG III/3 III/4, V/3 Workshop Laser Scanning*. Enschede, the Netherlands.

Gittinger, J. (2010). Personal communication by e-mail. Faro.

Gosliga, R. van (2008). Laserscanning: Rotterdamse toepassingen. In: *Geo-Info*, vol. 12: pag. 456–460.

Gosliga, R. van and R. Berkelaar (2008). Laserscanning: in één klap heel veel meten. In: *Stadstimmer nieuws*, vol. 1: pag. 6.

Gosliga, R. van, R. Lindenbergh and N. Pfeifer (2006). Deformation analysis of a bored tunnel by means of Terrestrial Laser Scanning. In: *ISPRS Volume XXXVI, Part 5*. Dresden, Germany.

Gruen, A. and D. Akca (2005a). Fast correspondence search for 3D surface matching. In: *ISPRS WG III/3, III/4, V/3 Workshop Laser scanning*. Enschede, the Netherlands.

Gruen, A. and D. Akca (2005b). Least squares 3D surface and curve matching. In: *ISPRS Journal of Photogrammetry & Remote Sensing*, vol. 59: pag. 151–174.

Hannink, G. and V. Thumann (2007). Existing structures goveern building methods near Rotterdam central station. In: *Geotechniek Special: 14th European Conference on Soils Mechanics and Geotechnical Engineering*. pag. 26–29. URL http://www.vakbladgeotechniek.nl/pdfs/Existing-structures-govern-building-methods-near-Rotterdam-Central-Station.pdf.

Kadaster (2010). Rijksdriehoeksmeting. URL http://www.kadaster.nl/rijksdriehoeksmeting/, in Dutch. Last visited: January 2011.

Kuipers, J. B. (2000). *Geometry, Integrability and Quantization*, Coral Press, hfdst. Quaternions and rotation sequences, pag. 127–143.

Leica (2004). Leica TCA1800, TCA2003, TC2003. URL http://www.leica-geosystems.com/common/shared/downloads/inc/downloader.asp?id=3030, last visited: May 16, 2010.

Leica (2005). Leica HDS4500. URL www.leica-geosystems.com, last visited: September 8, 2009.

Leica (2010a). Cyclone 6.3. URL www.leica-geosystems.com.

Leica (2010b). Leica ScanStation C10. URL www.leica-geosystems.com, last visited: 30 June 2009.

Lichti, D. (2004). A resolution measure for Terrestrial Laser Scanners. In: *The International Archives of the Photogrammetry, Remote Sensing and Spatial Information Sciences, Part XXX*, vol. 34.

Lichti, D. (2007). Error modelling, calibration and analysis of an AM-CW Terrestrial Laser Scanner system. In: *ISPRS Journal of Photogrammetry & Remote Sensing*, vol. 61: pag. 307–324.

Lindenbergh, R. (2010). *Airborne and Terrestrial Laser Scanning*, Whittles Publishing, hfdst. 7, pag. 237–269.

Lindenbergh, R. and N. Pfeifer (2005). A statistical deformation analysis of two epochs of terrestrial laser data of a lock. In: *Proceedings of Optical 3D Measurement Techniques VII, Vienna*, vol. II: pag. 61–70.

Little, M. (2006). Slope monitoring strategy at PPRust open pit operation. In: *Proceedings International Symposium on Stability of Rock Slopes in Open Pit Minig and Civil Engineering.*

Mukundan, R. (2002). Quaternions: from classical mechanics to computer graphics, and beyond. In: *Proceedings of the 7th Asian Technology Conference in Mathematics.*

Pfeifer, N. and J. Böhm (2008). Early stages of LiDAR data processing. In: Z. Li, J. Chen and E. Baltsavias (red.), *Advances in Photogrammetry, Remote Sensing and Spatial Information Sciences: 2008 ISPRS Congress book.*

Qhull (2010). URL www,qhull.org, last visited: May 11, 2010.

Rabbani, T. (2005). *Autmatic reconstruction of industrial installations using images and point clouds.* proefschrift, Delft University of Technology.

Rabbani, T. (2006). QtLaserViewer.

Rabbani, T., F. van den Heuvel and G. Vosselman (2006). Segmentation of point clouds using smoothness constraint. In: *ISPRS Commission V, Symposium Image Engineering and Vision Metrology.*

Ree, J. van (2006). *Determination of the precision and reliability parameters of Terrestrial Laser Scanners.* Master's thesis, Delft University of Technology.

Rees, W. (2001). *Physical principles of remote sensing.* Cambridge University Press.

Remondino, F. (2003). From point cloud to surface: the modeling and visualisation problem. In: *International Archives of Photogrammetry, Remote Sensing and Spatial Information Sciences*, vol. XXXIV-5/W10.

Rijkswaterstaat (2010). Normaal Amsterdams Peil. URL http://www.rws.nl/kenniscentrum/databestanden/normaal_amsterdams_peil/, in Dutch. Last visited: January 2011.

RotterdamCentraal (2010). URL www.rotterdamcentraal.nl, last visited: October 2010.

Salvi, J., C. Matabosch, D. Fofi and J. Forest (2007). A review of recent range image registration methods with accuracy evaluation. In: *Image and Vision Computing*, vol. 25: pag. 578–596.

Schuhmacher, S. and J. Böhm (2005). Geo-referencing of terrestrial laserscanner data for applications in architectional modelling. In: *Proceedings of the ISPRS Working Group V/4 Workshop 3D-ARCH.*

Shakarji, C. (1998). Least-Squares fitting algorithms of the NIST algorithm testing system. In: *Journal of Research of the National Institute of Standards and Technology*, vol. 103: pag. 633–641.

Shan, J. and C. Toth (red.) (2009). *Topographic Laser Ranging and Scanning.* Taylor and Francis Group.

Singh, A. (1989). Digital change detection techniques using remotely-sensed data. In: *International Journal of Remote Sensing*, vol. 10(6): pag. 989–1003.

Soudarissanane, S., R. Lindenbergh and B. Gorte (2008). Reducing the error in terrestrial laser scanning by optimizing the measurement set-up. In: *Proceedings XXII ISPRS Congress.*

Soudarissanane, S., J. van Ree, A. Bucksch and R. Lindenbergh (2007). Error budget of terrestrial laser scanning: influence of the incidence angle on the scan quality. In: *3D-Nordost, Berlin, Germany.*

Stewart, J. (1999). *Calculus - early transcendentals.* Brooks/Cole publishing company.

Teunissen, P. (2000a). *Adjustment Theory, an introduction.* Delft University of Technology.

Teunissen, P. (2000b). *Testing Theory, an introduction.* Delft University of Technology.

Tsakiri, M., D. Lichti and N. Pfeifer (2006). Terrestrial Laser Scanning for deformation monitoring. In: *12th FIG Symposium.* Baden, Germany.

Tsakiri, M., D. Stathas, A. Bithas and A. Valanis (2002). Methodology for testing terrestrial laser scanners. In: *Proceedings of 1st National Conference on Metrology.*

Vosselman, G., B. Gorte, G. Sithole and T. Rabbani (2004). Recognising structure in laser scanner point clouds. In: *The International Archive of Photogrammetry, Remote Sensing and Spatial Information Sciences.*

Wackernagel, H. (2003). *Multivariate Geostatistics*. Springer, 3e druk.

Wehr, A. (2008). LIDAR: Airborne and terrestrial sensors. In: Z. Li, J. Chen and E. Baltsavias (red.), *Advances in Photogrammetry, Remote Sensing and Spatial Information Sciences: 2008 ISPRS Congress book*.

Weisstein, E. W. (2010a). Convex set. From MathWorld - A Wolfram Web Resource. URL http://mathworld.wolfram.com/ConvexSet.html, last visited: May 11, 2010.

Weisstein, E. W. (2010b). Distance. From MathWorld - A Wolfram Web Resource. URL http://mathworld.wolfram.com/Distance.html, last visited: May 25, 2010.

Weisstein, E. W. (2010c). Point-Plane distance. From MathWorld - A Wolfram Web Resource. URL http://mathworld.wolfram.com/Point-PlaneDistance.html, last visited: September 23, 2010.

Zeibak, R. and A. Filin (2007). Change Detection via Terrestrial Laser Scanning. In: *ISPRS Workshop on Laser Scanning*. Espoo, Finland.

Appendix A

Iterative Closest Point algorithm

This appendix presents the Iterative Closest Point (ICP) algorithm in more detail.

Let P^I and P^{II} be two scans of a same scene, taken from two different standpoints. The algorithm finds for every point $\mathbf{p}_i^I$ from P^I the closest point in P^{II}. This closest point is found by minimising the distance between $\mathbf{p}_i^I$ and and the points$\mathbf{p}_i^{II}$ from P^{II}, i.e. find the point $\mathbf{p}_i^{II}$ so that distance between $\mathbf{p}_i^I$ and $\mathbf{p}_i^{II}$ is the minimum distance:

$$d(\mathbf{p}_i^I, P^{II}) = \min_{\mathbf{p}^{II} \in \{P^{II}\}} \|\mathbf{p}^{II} - \mathbf{p}_i^I\|. \tag{A.1}$$

Point $\mathbf{p}_i^I$ and its closest point $\mathbf{p}_i^{II}$ form a correspondence. The goal of the ICP algorithm is to find registration parameters such that the distance between all correspondences is minimised.

The rotation parameters are expressed in quaternions, which are an extension of complex numbers to a 4D space and can be used to express a rotation around any arbitrary axis in 3D space (Mukundan, 2002). In comparison with the 3×3 Euler rotation matrices, quaternions offer computational, operational and/or implementation and data handling advantages (Kuipers, 2000).

The unit quaternion vector $\mathbf{q}_R$ is given by

$$\mathbf{q}_R = [q_0 \ q_1 \ q_2 \ q_3]^T, \tag{A.2}$$

where q_0 is a scalar and $[q_1 \ q_2 \ q_3]$ forms the vector part of the quaternion. The relation between quaternions and the rotation matrix $\mathbf{R}$ is:

$$\mathbf{R} = \begin{bmatrix} q_0^2 + q_1^2 - q_2^2 - q_3^2 & 2(q_1 q_2 - q_0 q_3) & 2(q_1 q_3 + q_0 q_2) \\ 2(q_1 q_2 - q_0 q_3) & q_0^2 - q_1^2 + q_2^2 - q_3^2 & 2(q_2 q_3 - q_0 q_1) \\ 2(q_1 q_3 - q_0 q_2) & 2(q_2 q_3 + q_0 q_1) & q_0^2 - q_1^2 + q_2^2 + q_3^2 \end{bmatrix}. \tag{A.3}$$

Function f gives the distances between the correspondences and is given by

$$f = \frac{1}{N_p} \sum_{i}^{N_p} \|\mathbf{p}_i^{II} - \mathbf{R}(\mathbf{q}_R)\mathbf{p}_i^{I} - \mathbf{t}\|^2, \tag{A.4}$$

where N_p is the number of points in P^I and $\mathbf{t}$ represents the translation vector and is calculated using the two centre of gravities of the point clouds, notated by $\overline{P^I}$ and $\overline{P^{II}}$:

$$\mathbf{t} = \overline{P^I} - \mathbf{R}(\mathbf{q}_R)\overline{P^{II}}. \tag{A.5}$$

The function f must be minimised to find the best registration parameters.

To minimise f, a symmetric 4×4 matrix $Q(\Sigma_{p^I p^{II}})$ is created:

$$Q(\Sigma_{p^I p^{II}}) = \begin{bmatrix} tr(\Sigma_{p^I p^{II}}) & \Delta^T \\ \Delta & \Sigma_{p^I p^{II}} + \Sigma_{p^I p^{II}}^T - tr(\Sigma_{p^I p^{II}})\mathbf{I}_3 \end{bmatrix}, \tag{A.6}$$

where $tr(.)$ is the trace, $\Delta = [A_{23} A_{31} A_{12}]^T$ is computed from the anti-symmetric matrix $A_{ij} = (\Sigma_{p^I p^{II}} - \Sigma_{p^I p^{II}}^T)_{ij}$ and $\Sigma_{p^I p^{II}}$ is the cross-covariance matrix of the points p_i^I and p_i^{II}. The unit vector $\mathbf{q}_R$ corresponding to the maximum eigenvalue of matrix Q is used as the optimal rotation.

The transformation is applied to the first point cloud, P^I. With the updated point cloud, the algorithm follows all the steps again. This process continues until the difference between the mean square distance of the current step and the previous step is smaller than threshold value ϵ or a predefined number of steps is performed.

Appendix B

Results case study III: the joint

The data sets are shown in Chapter 6.

B.1 Segmentation

The results of the segmentation process are shown in Section 6.4.3 and not repeated here.

The outliers during the segmentation process are shown in Fig. B.1. Most remarkable are the four circular patterns in epoch II, see Fig. B.1a, indicated with A. These points are located on the edge of the elongated segments, as indicated with A in Fig 6.35a, and the surrounding segments. Probably this is a transition area, where points in adjacent lines are included in the nearest neighbours. When this happens for the first time, the normal of the nearest neighbours differs too much with the normal of the current segment, and the point is labeled as an outlier. When the range increases even more, the normal of the resampled surface is similar to the normal of the 'real' surface, and the segments are as expected.

Moreover, there are more small objects present in the scene compared to the other case studies. Many of the outliers are located on these small objects, for example bolts that are used to fix the tracks on the floor, see Fig B.1b. Furthermore, many of the objects have a non-zero curvature and planar segments are not the best representation, which explains a part of the outliers on the both walls. Additionally, on the northern wall the resampling causes outliers, see Fig B.1a.

B.2 Identification of the corresponding segments

It is more difficult to find corresponding segments for the floor. Indeed, the area was not so well sampled, especially in epoch II. Probably the laser scanner was placed higher above the floor during epoch IV, which results in a higher point density further away from the standpoint. Furthermore, more points are acquired at each standpoint at epoch IV. The

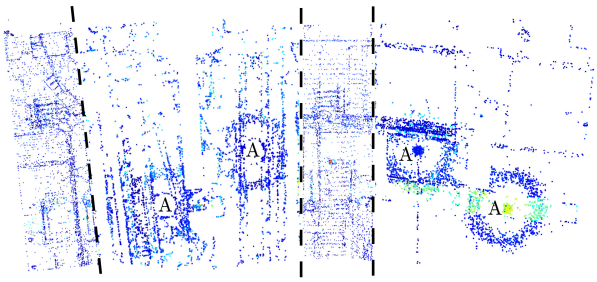

(a)

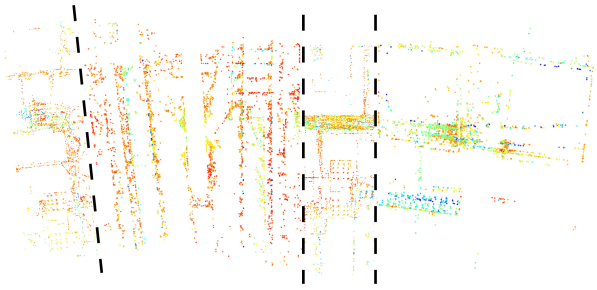

(b)

Figure B.1: The outliers during the segmentation of the two point clouds. (a) The outliers in the point cloud of epoch II. (b) The outliers in the point cloud of epoch IV.

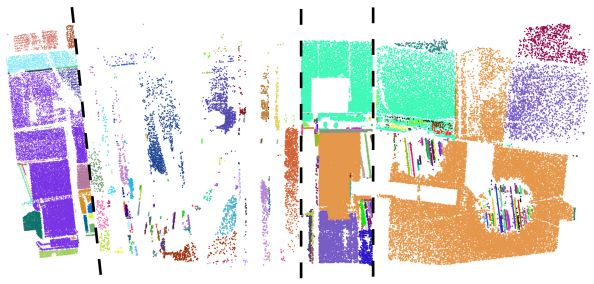

(a)

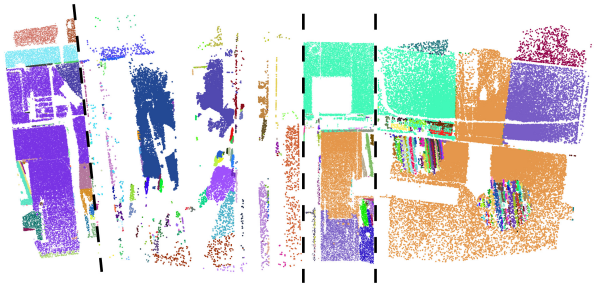

(b)

Figure B.2: The corresponding segments between the two point clouds.

Table B.1: The total number of points, the number of segments, the number of points that are marked as an outlier during the segmentation process, the number of points that are marked as a potential change and the number of points for which the distance to the other point cloud is calculated for the data sets of epoch II and IV.

	Epoch II			
	southern wall	floor	northern wall	ceiling
Points	1,000,000	1,000,000	1,000,000	1,000,000
Segments	519	1,331	462	982
Outliers	58,202	75,878	53,003	72,796
Potential changes	385,033	835,990	446,610	490,612

	Epoch IV			
	southern wall	floor	northern wall	ceiling
Points	1,000,000	1,000,000	1,000,000	1,000,000
Segments	398	477	399	243
Outliers	34,680	49,857	50,075	28,043
Potential changes	262,677	643,350	403,316	257,536
Deformation points	438,978	161,800	337,882	427,942

segmentation of epoch II showed many small segments, see Fig. 6.35a. For a significant part of these segments no correspondence is identified. This also holds for almost all the elongated segments in the two circular areas on the floor.

B.3 Change detection

Fig B.3 to Fig B.6 show the points that are marked as possible change during the identification of the corresponding segments. These points are potential changes that occurred between epoch II and epoch IV in the area around joint 4. For each data set, remarkable areas are discussed.

Furthermore, the effects of the resampling are also visible in the change detection, see the vertical lines in Fig B.5a, below region C and between region C and D. These points belong to a segment, but are labelled as a potential change during the identification of the corresponding segments.

The floor

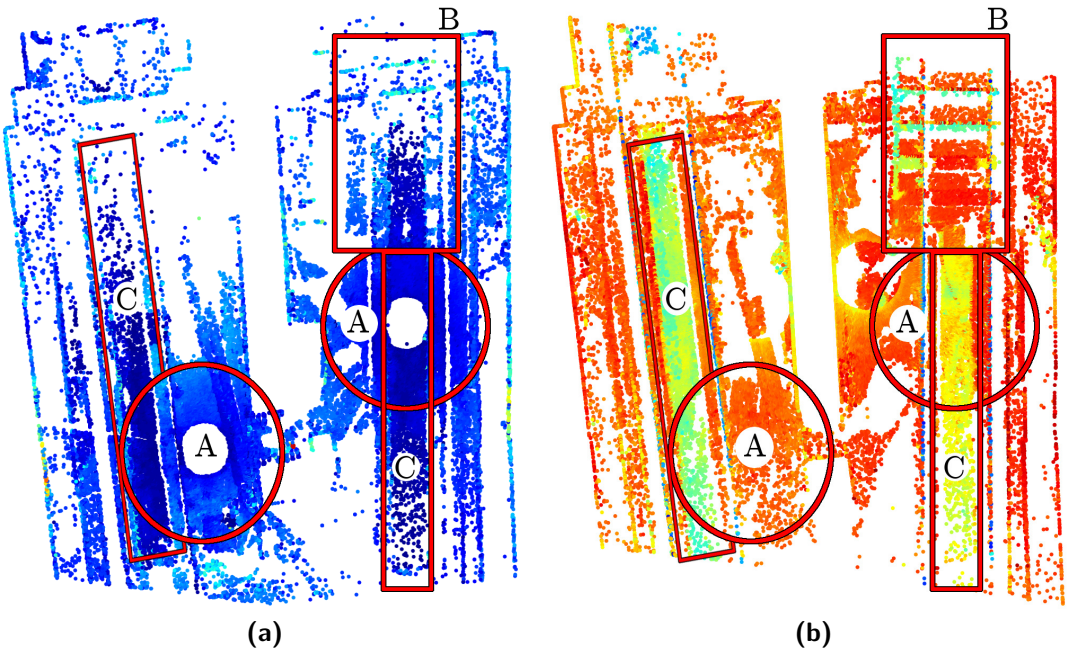

Figure B.3: The possible changes on the floor between epoch II, (a), and epoch IV, (b).

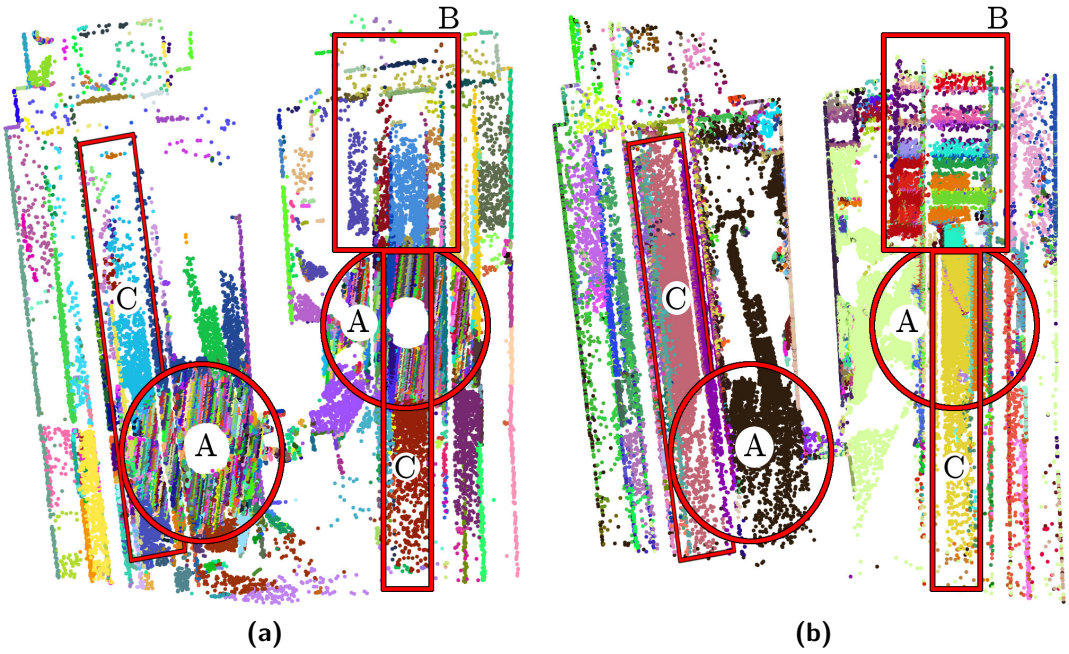

Figure B.4: The possible changes on the floor between epoch II, (a), and epoch IV, (b), using the original segmentation labels.

Table B.2: Description of the possible changes on the floor.

Area	Description	Change?
A	There are many points around the standpoints in epoch II marked as a potential change. The majority of these points is located within the circular area that is affected during the segmentation. Since the orientation of these segments can be different than the orientation of the 'real' surface, no corresponding segment in epoch IV is identified and these points are marked as a change.	N
B	A part of the track. With the construction of the new metro station, this part of the track is moved. Sleepers are placed to fix the new part of the tracks. The sleepers are visible in Fig. B.3b and Fig. B.4b.	Y
C	In the middle of the track, the tunnel floor is sunken, creating a small pit which contains debris and stagnant water. The water causes a weak reflection of the laser signal, which is also visible in Fig. B.3.	N

Many points are marked as a potential change, see Table B.1 for the exact numbers. Moveover, regions are included that are not likely to change. Most of the floor is built of concrete and is expected to be rigid.

In Section 4.4 is explained that potential changes can be caused by occlusions in the scene. Although for both standpoints in each epoch there is a good visibility, objects in the scene can cause occlusions. Objects present in the scene are the rail tracks, the third rail, small boxes and installation units for the switches. However, it is not likely that these objects cause occlusions for all the potentially changed points. More likely these objects cannot be represented by planar segments.

The southern wall

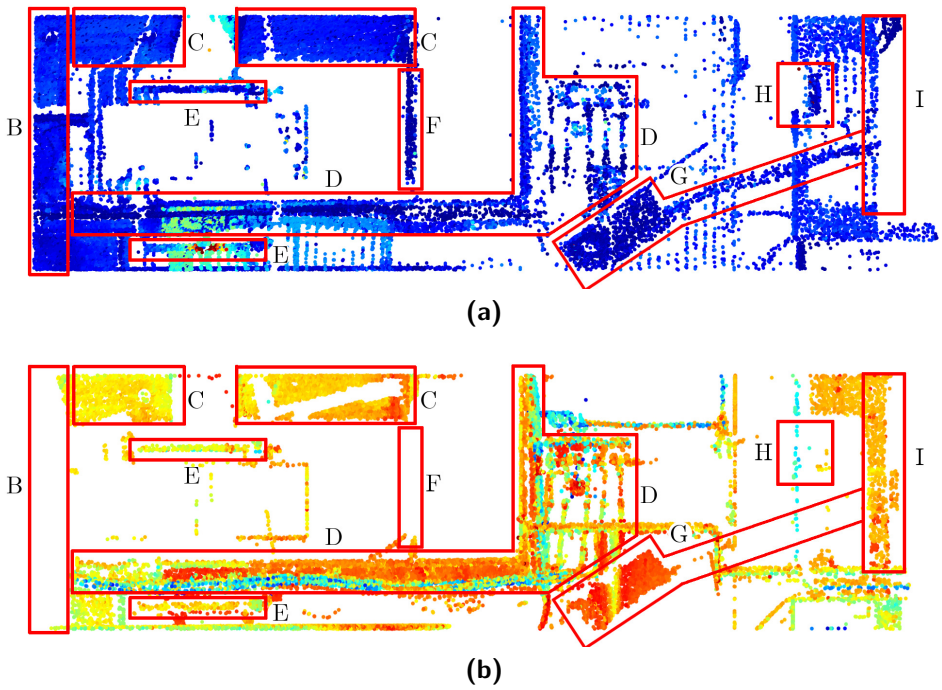

Figure B.5: The possible changes on the southern wall between epoch II, (a), and epoch IV, (b).

Table B.3: Description of the possible changes on the southern wall.

Area	Description	Change?
B	The area is sampled in epoch II, but not in epoch IV. Since this concerns a large surface, it should be investigated whether area A is a change or an occlusion. The proposed procedure to make this distinction is described in detail in Section 4.4 and Section 6.2.5. In this case, the possible change in area A is caused by the selection of the area in the full point cloud.	N
C	The area represents two fillets which are present in both epochs. In epoch II, these fillets are affected by the resampling of the data. This is also visible in the segmentation results, see Fig. 6.35a. As a result of the unexpected segmentation results, these areas are marked as a possible change.	N
D	A horizontal stripe containing water pipes, connected to a control installation for the water injections and larger metal water pipes. Planar segments are not suitable to represent these complex surfaces. Identifying corresponding segments is hard for this area and most of the points are marked as a possible change. Although it is possible that small changes occurred, it is not expected that there is an actual change.	N
E	The joint meters, present in both epochs. In epoch II, the laser scanner was placed close to the joint meter during the acquisition. It is possible that only a small amount of the signal is reflected to the laser scanner, resulting in a poor range measurement, although points on the lower joint meter have a high reflected intensity. In epoch IV, the joint meter was scanned from another standpoint and therefore other points were sampled on the joint meter. Moreover, the resampling of epoch II can influence the results, since the area of the joint meter's surface is small.	N
F	It is a small protruding part of the tunnel wall, of about 10 cm wide. The resampling affected the segmentation and the segments are not correctly matched.	N
G	A metal protection cover and mount for wires that run across the wall. It is present in epoch II, but removed before epoch IV. The points on the metal cover are marked in epoch II, in epoch IV the points on the wall, that were occluded by the metal cover, are marked. Points on the wires are only marked in epoch II.	Y
H	A total station used for the deformation monitoring. It was removed before epoch IV.	Y
I	Sampled in epoch IV, but not in epoch I. This is due to the selection of the data set.	N

The northern wall

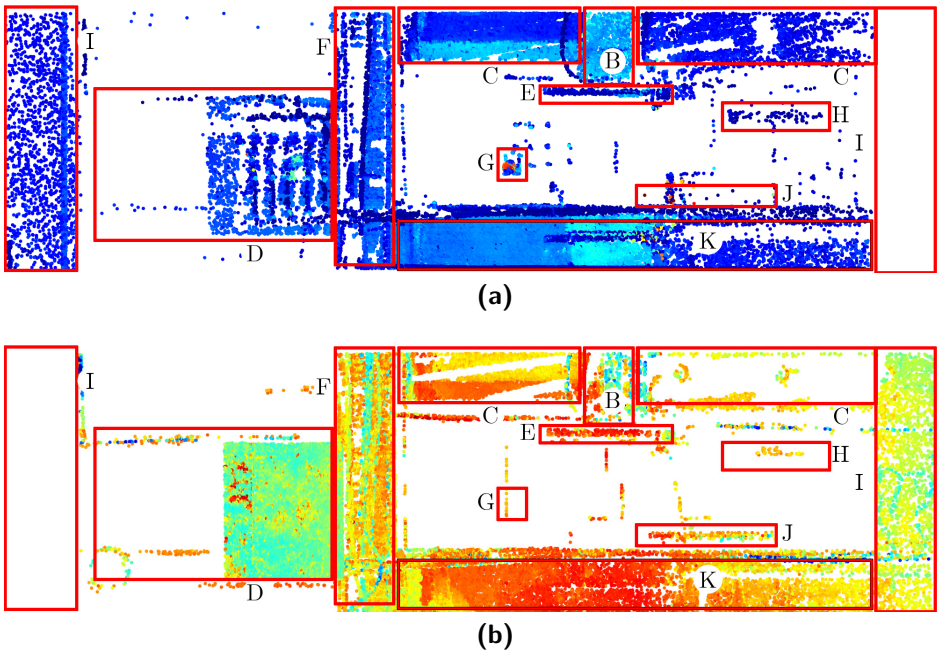

Figure B.6: The possible changes on the northern wall between epoch II, (a), and epoch IV, (b).

Table B.4: Description of the possible changes on the northern wall.

Area	Description	Change?
B	The joint itself. In epoch II, the joint was covered with a foam rubber layer. Before epoch IV, this layer is removed for a part of the joint, which causes a difference in the range measurement and also results in different segments.	Y
C	The fillets. Due to the resampling process, the segmentation results are not as expected, see also Fig. 6.35a. The segments could not be matched and the points are marked as a potential change.	N
D	Installation for the water injection. In epoch II the installation is visible, in epoch IV a wooden plate covers the installation. For this object a segmentation based on planar segments is justified. On the left side of the area, there are a few water pipes. As described for the southern wall, these circular pipes are not correctly segmented. The circular pattern in the lower left corner of area D in Fig. B.6b, lower left corner, are rolled up wires, not present in epoch II.	Y
E	The joint meter. Most likely the joint meter causes an occlusion, due to the different scanning geometry.	N
F	Wires and cables. Planar segments are not suitable for these objects, and although small changes are possible, it cannot be stated with certainty that real changes occurred.	N
G	A target that is used for the registration. It is located approximately 20 cm in front of the wall. It is unknown what type of planar targets are used for the registration process in epoch II. Based on the reflected intensities for these points, it is assumed that the target reflected a large ratio of the incoming signal. This causes saturation of the reflected signal, resulting in a biased range. Therefore the target is located in front of the surface it was located on. It is a change, since it is present in epoch II, but not in epoch IV.	Y
H	Light installation, present in epoch II but not in epoch IV. It causes an occlusion of the wall, which is also visible in epoch IV.	Y
I	Surfaces that are scanned in one epoch, but not in the other. This is caused by the data selection.	N
J	A new placed lamp, present in epoch IV.	Y
K	This area was sampled in both epochs. During the segmentation process, the surface of epoch II was divided in multiple segments, see also Fig. 6.35a. The orientations of these segments differs slightly too much from the orientation of the segment in epoch IV. When the parameters for the identification of the corresponding segments are relaxed, the segments match and they are not marked as a possible change.	N

B.4 Deformation analysis

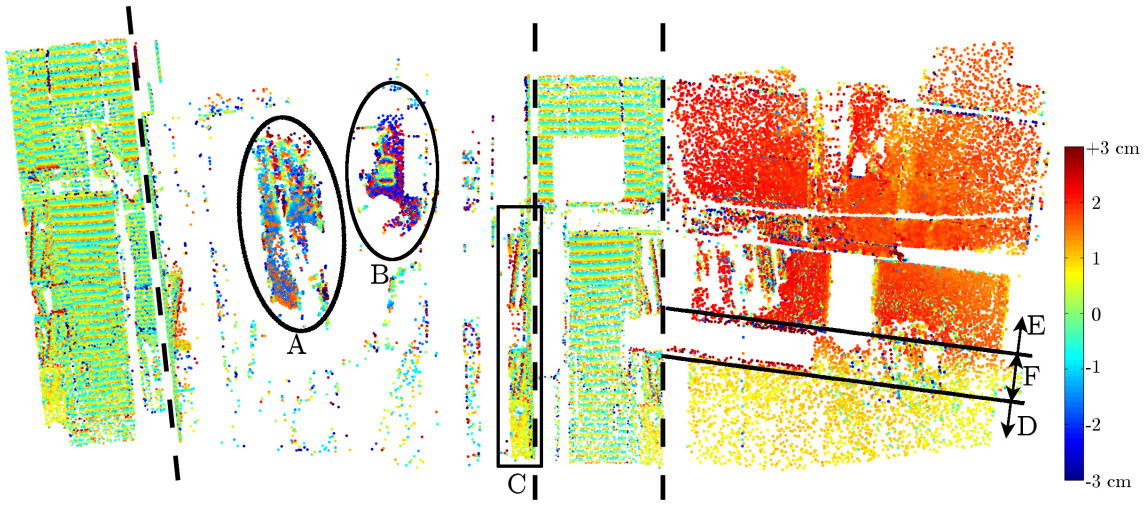

Figure B.7: Distances between epoch IV and epoch II.

The distances on the northern and southern wall are dominated by the resampling effects of epoch II. The distance from epoch IV to epoch II is orthogonal to a local plane in epoch II. Distances are therefore alternating positive and negative values, making the results useless, which can also be suspected based on the figures on the bottom row in Fig. 6.32.

Moreover, the results of the floor are not useful either. Only for a limited number of points, a distance is calculated and often these points are isolated. There are three large groups of points, as indicated in Fig. B.7. Groups A and B are located close to the standpoints of epoch IV. This results in a high point density and for many points is distance is calculated. The point density in epoch II is much lower, compare Fig. 6.34a and (b). The results are very noisy and hard to interpret. The third group of points, C, seems less noisy. There is a small line of larger distances. This line is parallel to the x-axis and probably caused by the resampling of epoch II.